INVESTIGATION AND SUPPRESSION OF MULTIPATH COMMUNICATION SIGNALS WITH APPLICATIONS TO A MARINE ENVIRONMENT

COREY D. BIRD

INVESTIGATION AND SUPPRESSION OF MULTIPATH COMMUNICATION SIGNALS WITH APPLICATIONS TO A MARINE ENVIRONMENT

by

© Corey D. Bird, B.Sc.E.

A thesis submitted to the School of Graduate Studies

in partial fulfilment of the

requirements for the degree of

Master of Engineering

Faculty of Engineering and Applied Science

Memorial University of Newfoundland

July, 1996

St. John's Newfoundland Canada

Abstract

An investigation of multipath communication signals with applications to a marine environment is conducted by examining a typical L-Band satellite-to-ship communication system. In order that this investigation be performed, a numerical stochastic maritime multipath model is constructed. This model has the ability to calculate the average power contained in a multipath communication signal which is reflected off the ocean surface and received by a ship mounted antenna. This allows the model to provide signal-to-noise ratios as well as signal fade characteristics for different degrees of sea surface roughness as well as a variety of receiving antenna patterns. By comparing the results obtained with the stochastic multipath model to those from other models as well as various measurement campaigns, the stochastic maritime multipath model is shown to be a valid and useful tool that can be used in multipath research. Some of the research carried out in this thesis includes an investigation of how various parameters affect the multipath phenomenon. These parameters include sea roughness, elevation angle, antenna position aboard the vessel, and antenna directivity. It was discovered that it may be possible to decrease the amount of multipath fading experienced by a ship mounted receiving system by locating an optimal antenna position aboard the vessel and constructing a low cost antenna stabilization platform that could allow the use of a fairly directive antenna. Suggestions for the continuation of the research reported here are also presented.

Acknowledgements

The author would like to thank Dr. R.K. Donnelly (Memorial University of Newfoundland) for his supervision of this research and his insistence that most things should not be blindly accepted without some investigation first. I would also like to express my gratitude to the Canadian Centre for Marine Communications (CCMC) for their help in carrying out this research and their extremely generous financial support. Other individuals that should be mentioned include Ken Butt (formally CCMC, presently Lotek Marine Technologies) whose enthusiasm convinced me to pursue this project, Keith Elms and David Mitchell (CCMC) who always provided assistance and information when called upon, Norm Arsenault and Dennis Pothier (graduate students at the University of New Brunswick) who kept me informed of events back home on a daily basis through countless useful (or useless) e-mail conversations, my father, Ronald Bird, who always encourages me no matter what decisions I make, and the Faculty of Engineering and Applied Science of the Memorial University of Newfoundland for their assistance and financial support. Finally I would like to express my sincere gratitude to Nita Stairs, who puts up with me while I "stay in school".

Table of Contents

List of Figures

List of Tables

List of Symbols

The following is a list of some of the most extensively used symbols and notations present in this thesis. Other symbols that are more general or less frequently used are well defined within the text of this report.

Symbol	Definition
A	Attenuation coefficient.
$a(\beta)$	Polarization coefficient dependent term.
a_e	Radius of curvature of the earth.
α	Local grazing angle.
β	Reflection angle.
β_l	Local reflection angle.
β_{MIN}	Lower angular limit for power density integration.
β_{MAX}	Upper angular limit for power density integration.
CV	Subscript denoting Concave.
CX	Subscript denoting Convex.
D	Divergence factor.
E	Elevation angle.
E_l	Local elevation angle.

E_R	Antenna polarization ratio.
θ_m	Antenna phase mismatch angle.
θ_p	Antenna pitch angle.
θ_{ss}	Antenna pointing error angle.
$\xi(p)$	p% availability crossing level for a standard normal random process.
$F_{Dp\%}$	Fade depth for a p% availability system.
f_d	Doppler frequency shift.
G_H, G_V	Horizontal and vertical antenna gain functions.
g_a	Antenna gain angle.
Γ_H, Γ_V	Horizontal and vertical surface reflection coefficients.
$H_p(f)$	Antenna pitching motion filter transfer function.
$H_s(f)$	Antenna stabilization filter transfer function.
$H_v(f)$	Antenna vertical translation filter transfer function.
h_R	Horizon range of an antenna.
L	Length of a vessel.
Λ	Average ocean wave component wavelength.
λ_c	Transmitted carrier signal wavelength.
$\lambda(\beta)$	Specular point density function with respect to reflection angle.
$\lambda(x)$	Specular point density function with respect to distance from a vessel.
M_{RC}	Mean radius of curvature at a scattering facet.

$m(x)$	Approximate sea surface slope.
P_D	Direct path signal power .
P_m	Multipath signal power.
σ^2_m	Variance of the multipath signal.
σ_z	RMS surface height.
$\sigma_{z'}$	RMS surface slope.
$\sigma_{z''}$	RMS surface second derivative.
$R(\beta_l, E_l)$	Effective radius of curvature of the sea surface at a specular point.
r_c	Radius of curvature of a scattering facet.
SNR	Signal-to-noise ratio.
$S(\beta)$	Power density function with respect to reflection angle.
$S_r(f_d)$	Doppler (power) spectrum.
$T_{Dp\%}$	Average fade duration for a p% availability system.
$T_{Ip\%}$	Average fade interval for a p% availability system.
t	Time variable.
u	Vessel velocity.
v_x	Horizontal component of antenna velocity.
v_z	Vertical component of antenna velocity.
$w_B(\beta_l, z_l)$	Signal blocking weighting factor.
$w_S(E_l, z_l)$	Signal shadowing weighting factor.
x_a	Instantaneous antenna horizontal position.

x_c	Centre of gravity of a vessel.
x_D	Distance between the antenna mount and the centre of gravity of a vessel.
x_L	Length of the blocking and shadowing search region.
x_o	Initial antenna horizontal position.
x_{START}	Lower distance limit for power density integration.
x_{STOP}	Upper distance limit for power density integration.
$z(x,t)$	Local ocean surface waveheight.
$z_s(x,t)$	Ocean surface waveheight.
z_a	Instantaneous antenna height.
z_o	Nominal antenna height above the waterline.
z_f	Sea surface height at a specular reflection point.
z_{wl}	Vessel waterline height.

Chapter 1

Introduction

Multipath interference in a maritime satellite-to-ship communication system is the phenomenon in which a communication signal propagating from a transmitting satellite reaches a ship mounted receiver via a direct path as well as several scatter paths after being reflected from the rough ocean surface. The scattered, or multipath, signals arriving at the receiver often cause undesirable fluctuations in the overall received signal level as they interfere with the direct path component. This fluctuation is often referred to as *multipath fading*. The fading process can either be rapid or slow, as well as shallow or deep. Lengthy deep fades in the received signal level are often attributed to the presence of a smooth sea surface. In this instance, the reflected signal arises from only a small portion of the sea surface and is very concentrated and coherent. This is what is known as *specular* reflection. Rapid shallow fades are usually the result of signal reflections from a rough sea. With a rough scattering surface, multipath signals can be reflected from a large surface area and arrive at the

receiver from numerous directions. In this situation the scattered signal is less concentrated than for the specular reflection case and is less likely to interfere with the direct path signal component as destructively. This is often called *diffuse* reflection. Both of these situations are depicted in Figures 1-1 and 1-2.

The degree of roughness is not the only factor that governs the extent of multipath fading that a ship-borne communication system may experience. The size and velocity of the vessel, the position of the antenna aboard the ship, as well as the antenna gain and polarization characteristics, and the elevation angle to the transmitter are some of the parameters that have an effect on the amount of multipath interference experienced.

With the growing popularity in low gain, low cost, nondirective ship earth stations, the sea surface multipath phenomenon is becoming increasingly significant. Because of this, investigations into the properties and behaviour of multipath fading as well as methods for fade reduction are well worth the time and effort they require.

1.1 Aim of the Thesis

The use of satellite communication technology aboard sea faring vessels has been increasing dramatically over recent years. This is partly due to the introduction of

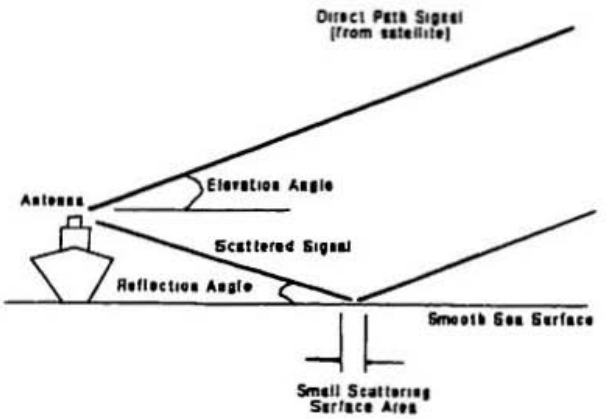

Figure 1-1: Specular multipath reflection scenario.

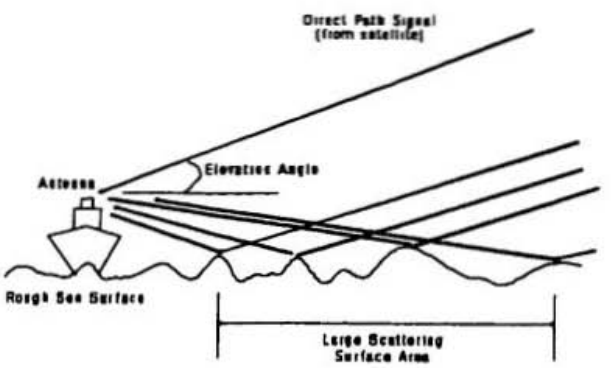

Figure 1-2: Diffuse multipath reflection scenario.

low cost, low gain, nondirective, and often unstabilized receiving systems. An example of this are INMARSAT Standard-C compatible systems which are mostly used for data transmission only, and use small, almost omnidirectional antennas. Such systems operate at L-Band frequencies (approximately 1.5GHz). The low cost of such systems make satellite communication capability available to operators of even the smallest vessels. Some examples of nondirectional antennas used with the INMARSAT Standard-C system are presented in Appendix E.

When the elevation angle between a ship-mounted receiver and a transmitting satellite becomes significantly small (less than about 10°), multipath fading becomes quite prevalent. With nondirectional antennas, the fading becomes even more significant. Since many transmitting satellites are in, or close to being in, an equatorial orbit, low elevation angles are often experienced by vessels sailing off the coast of Canada. Because of this, and due to the above mentioned increase in the use of lower cost receiving systems, a study of the multipath fading phenomenon in a marine environment is warranted.

The aim of this thesis is to provide an in-depth investigation of the maritime multipath phenomenon in order that a greater understanding of the sea scatter problem be established. This is done by examining the effects that certain parameters have on the fading characteristics of a satellite signal, which is corrupted by multipath interference,

arriving at a ship mounted receiver. By attaining a knowledge of the maritime multipath process, one may be able to suppress some of the multipath interference by adjusting certain parameters such as antenna height, antenna placement on the vessel, antenna gain patterns, or by incorporating simple signal processing techniques.

Multipath effects can often be lessened through the use of large, very directional, high gain antennas, or by using complicated antenna stabilizers or signal tracking techniques, as well as some form of adaptive beam forming for antennas. These techniques are usually extremely expensive and void the ideology of a low cost and affordable receiving system for small operators. Therefore by understanding the effects that simple things like antenna location has on reducing the multipath process, an inexpensive solution to the multipath reduction problem may be attainable.

1.2 Accomplishments of the Thesis

In order that an investigation of multipath fading be conducted, an efficient and valid numerical model that allowed easy parameter input and variation had to be developed. Using the models constructed in [1] as a foundation, a numerical *stochastic maritime multipath model* was created. This model uses much the same theory as was used for the aeronautical stochastic sea scatter model contained in [1]. The basis of this model is the formation of the specular point location process into a random curve crossing

problem. Specular reflection points are points on the ocean surface from which the reflected signal will intersect with the receiving antenna coordinates. By considering the ocean surface profile to be a Gaussian random process, one can utilize the random curve crossing solution of [4] to generate a expression for the density of specular reflection points on the ocean surface for a given sea state, elevation angle, and antenna position. The technicalities of this ideology are described in Chapter 3. Applying this technique to the maritime multipath problem requires somewhat more rigorous calculations than it does for the aeronautical case of [1]. The close proximity of the receiving antenna on a ship as compared to an aircraft, as well as the coupling between a boat's motion and that of the ocean surface complicates the solution. The differences and similarities between the two scenarios is discussed in greater detail in Chapter 2.

At the present time, the model developed is a simple DOS application written in the C programming language. It does provide an easy input mechanism by which the user can enter parameters such as sea state, elevation angle, antenna height, vessel velocity, and the length of a simulation. After entering the desired values of these variables, the model can quickly calculate an average signal-to-noise ratio, fade depth, and average fade duration for a given p% availability ([100-p]% outage) system. By varying one parameter while holding all others constant, one can investigate the effect that a particular variable has on the amount of signal fading that occurs at the receiver.

The model is relatively fast and simulations of several minutes long can often be run in almost real time on even some of the slower personal computers. By comparing the results obtained with this model to those calculated by other models as well as those from measurement, it was found that the maritime stochastic multipath model is indeed a valid and useful tool that can be used for the investigation of multipath fading in marine satellite communication systems.

By performing several simulations it was discovered that the most sensitive parameters that influence the degree of multipath fading experienced include the sea state, elevation angle, and antenna polarization. Unfortunately, one cannot change the elevation angle or the roughness of the sea in order to lessen multipath fading. Since satellite transmitters use right-hand-circular polarization, one cannot realistically change the transmitting electromagnetic wave either. The height of the antenna aboard the ship was seen to have a slight effect. The higher the antenna, the greater the multipath interference. This would lead one to conclude that it would be worth the effort to determine an appropriate antenna height on a vessel which is low enough to suppress some multipath fading, but high enough to ensure that the ship's superstructure does not impede the line of sight to the satellite at low elevation angles and in rough sea conditions. The directivity of the antenna was also found to be an adjustable parameter in the receiving system. It was seen that the more directive the antenna is in the direction of the direct path signal, the less the fading that will be

experienced. However this adds increased cost and, if the antenna beam is relatively narrow, movement of the antenna caused both by the ship's own velocity and the movement of the ocean may cause this narrow beam to point away from the direct path signal, and in some cases, point towards the ocean surface leading to the reception of a stronger multipath signal component than the magnitude of the desired direct path signal. This is often referred to as *depointing* and is very significant on small vessels in rough seas if some form of antenna stabilization device is not used. This would also add some expense to the receiving system. The simulation results obtained and a discussion pertaining to them are presented in more detail in Chapters 4 and 5.

It is felt that greatest accomplishment of the thesis is the development of a maritime multipath model which allows for a quick and efficient evaluation of a receiving antenna in various sea conditions and positions on a vessel.

1.3 Organization of the Thesis

This thesis is divided in five chapters as well as several appendices. The first chapter is an introductory chapter. Chapter 2 presents a literature review which describes several other attempts at maritime multipath modelling as well as some of the sources of theory behind the fundamental electromechanical wave scattering from rough

surfaces problem which is the basis of all multipath research. Also contained in the second chapter is a somewhat detailed summary of the models from [1] and how they are related to the model developed in this thesis.

Chapter 3 contains a detailed explanation of the theory and calculations involved in the development of the stochastic maritime multipath model. This includes the solution to the specular point location (random curve crossing) problem, incorporating blocking and shadowing effects, reflected signal divergence, and the calculation of the average scattered signal power. The construction of power (Doppler) spectra of the multipath process and how this is used to extract average fade durations is also explained.

In Chapter 4 a validation of the model that is given in Chapter 3 is carried out by comparing the results obtained with those from other models as well as some from measurement. Chapter 4 also presents results that show how various parameters effect the multipath phenomenon. These parameters include the different results obtained using sea water as well as sea ice, the effects of elevation angle, antenna height, polarization, and directivity, as well as the effects of sea state and vessel velocity. The significance of these simulation results are discussed in the fourth chapter as well as summarized in Chapter 5, which also contains suggestions for future research.

For the most part, the appendices contain detailed explanations of theory that are too lengthy and tedious for the main text. One of the more interesting appendices is Appendix F which provides a somewhat detailed explanation of extracting fade characteristics of the received signal from the simulation results obtained with the stochastic maritime multipath model. This was done as it is often not obvious how fade depths, fade durations, and fade intervals are calculated in much of the literature.

Chapter 2

Literature Review

There have been several attempts made to model accurately the maritime multipath phenomena. One that has been used by the author as a foundation for the current research was made in 1987 by K.W. Moreland at Carleton University [1]. Since we use a similar modelling approach, much of this chapter will focus on describing it.

In [1] two different approaches are developed. The first is what is described as a *propagation model* and the second is termed a *stochastic model*. Both methods assume a two dimensional model: *i.e.* height of the ocean surface z, is assumed to vary only in the x-direction from the receiver to the transmitter. In the perpendicular y-direction the surface is considered to be unchanging. The analysis considers an unmodulated carrier signal only, which at L-Band has a frequency of roughly 1.5GHz and a wavelength of 0.2m. The propagation model was developed for both a maritime situation, in which the receiver is mounted on a vessel travelling in the ocean, and an aeronautical scenario, where the receiver is mounted on an aircraft. The stochastic

model was completed for only the aeronautical case. These two models as well as their applicability to the current research will be discussed in the following sections.

2.1 The Maritime Propagation Model

The propagation model developed in [1] invokes what is even now a very computationally demanding process. Its simplicity however, makes it useful in gaining an understanding of the topic. Moreland's objective was to be able to characterize the ocean scatter signal as a function of physical parameters such as the elevation angle to the satellite, the sea state, the antenna characteristics (gain, polarization and height), as well as the velocity and size of the ship. The details of this model are reviewed in the following sections.

2.1.1 Ocean Surface Modelling

The surface model used in this propagation approach is based on a table of sea states. This table is reproduced in Appendix A. Parameters that determine the shape of the ocean surface are the average sea wavelength Λ, and the RMS waveheight σ_z. Upon choosing these parameters, a surface profile is constructed by adding together a number of random-phase sinusoids and superimposing them on a curved earth as given in (2.1) and (2.2), where z(x,t) is the local waveheight (composed of the sinusoids) at

a specific point x, and $z_s(x,t)$ is the resulting surface height after adding z(x,t) to the curvature of the earth. Figure 2-1 clearly shows how this method is used to construct a profile of the ocean surface with three sinusoidal components.

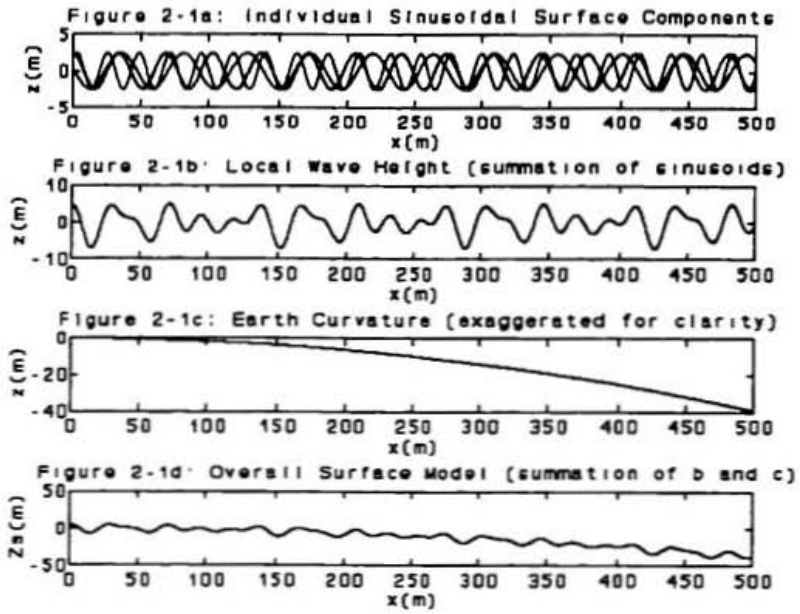

Figure 2-1: Composition of Sinusoids Ocean Surface Model

$$z_s(x,t) = z(x,t) - \frac{x^2}{2a_e} \tag{2.1}$$

$$z(x,t)=\frac{\sqrt{2}\sigma_z}{\sqrt{N_T}}\sum_{k=-N}^{N}\cos\left[\frac{2\pi}{\Lambda_k}(x-v_k t)+\theta_k\right] \qquad (2.2)$$

$$N=\frac{N_T-1}{2}$$

In (2.1) and (2.2) N_T is the desired number of waveforms and a_e is the radius of the earth (6.378×10^3km). The v_k and Λ_k terms are the velocity and wavelength components of the k^{th} sinusoid. The wavelength of each sinusoid is either longer or shorter (depending on the sign of k) than the average sea wavelength. The wavelength of the k^{th} component wave would be $\Lambda_k=\Lambda+k\Delta\Lambda$ where $\Delta\Lambda$ is given by Λ/N_T. The θ_k term is a uniformly distributed random phase for the k^{th} sinusoid. The distance x is assumed positive in the direction towards the satellite. From these equations it is seen that the surface can take on many different profiles for any given sea state depending on the number of random-phase sinusoids incorporated and the differing random phases. It is suggested in [1] that this method can be used to approximate surface conditions ranging from a sine wave to that of a Gaussian distribution if at least 21 waveforms are added.

2.1.2 Specular Point Location

One of the most computationally demanding parts of the propagation model is locating and classifying the specular points on the ocean surface, or the points in which the ray that is reflected off the ocean surface will intersect the pattern of the receiving

antenna. After locating these points both the phase coherent specular scattering and the phase incoherent diffuse scattering can be calculated together through a divergence term which will be discussed later. This situation is portrayed in Figure 2-2.

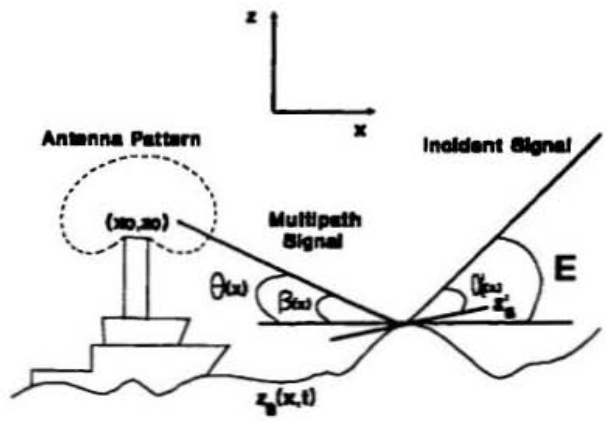

Figure 2-2: Scattering Geometry for the case of $\theta(x)=\beta(x)$.

From Figure 2-2, it can be seen that in order to determine the location of a specular point the solution of equation (2.3) must be found.

$$\theta(x) = \beta(x) \tag{2.3}$$

$$\theta(x) = \tan^{-1}\left(\frac{z_o - z_s(x)}{x - x_o}\right) \tag{2.4}$$

$$\beta(x) = E - 2\tan^{-1}\left(\frac{dz_s}{dx}\right) \tag{2.5}$$

In equations (2.3) to (2.5), $\theta(x)$ is the angle from the reflection point to the receiver, $\beta(x)$ is the reflection angle at the scatter point and E is the elevation angle to the satellite. The pair (x_o,z_o) gives the 2-D coordinates of the antenna. The $\alpha(x)$ in Figure 2-2 is the incident angle relative to the tangent of the surface at the scattering point, this value becomes more important later. It should be noted that for simplicity, we have begun referring to all quantities as functions of position x only. It must be remembered that although not explicitly shown, all values are dependent on time as well.

Specular scatter point locations are found by performing a lengthy numerical search in which one must first look for sign changes in the difference $\theta(x)$-$\beta(x)$. When a sign change is detected then a more exact solution is performed in this area, through the use of Newton's algorithm for solving nonlinear equations. Once found, the specular points are classified as either visible to the receiver, blocked or shadowed (described in section 2.1.2.1), and sub-classified as sensitive or nonsensitive, indicating that the visible, blocked, or shadowed classification is likely to change with time. Only the sensitive points are monitored at the next few time instants but a more comprehensive search must be performed every so often to ensure that a point that was classified as sensitive or non-sensitive does change position in such a way that reverses this classification.

2.1.2.1 Blocking and Shadowing

As mentioned in the previous section, once a specular point is located it is classified as either blocked, shadowed, or visible. The geometry of these scenarios is shown in Figure 2-3.

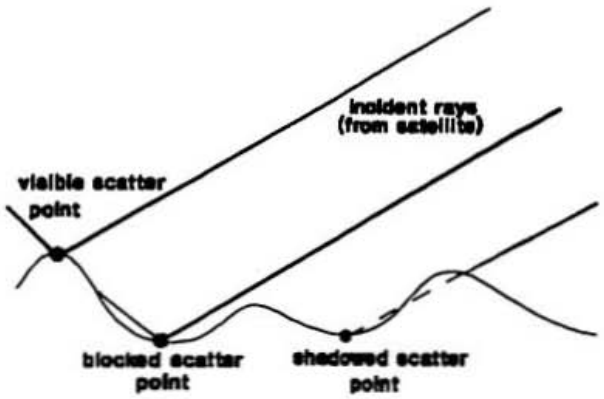

Figure 2-3: Blockage and Shadowing Determination.

To determine if the signal is blocked, 50 evaluation points within 2.5 average sea wavelengths away from the scatter point in the direction of the receiver are considered to see if the reflecting ray is intersected by the ocean surface. If this is the case then that particular point is not considered to contribute to the overall scatter signal. Likewise for shadowing the same process is invoked for 50 evaluation points in the direction away from the scatter point towards the transmitter to determine if the incident signal is obstructed by the ocean surface. If it is found that a point is *just* shadowed, *just* blocked or *just* visible (the difference between the height of the ocean surface and that of the reflected or incident ray is very small) then that point is

labelled as sensitive. If the reflected or incident ray is not obstructed by the ocean surface along the 50 point interval, the point is considered visible to the receiver and contributes to the overall multipath signal.

2.1.3 Multipath Signal Calculation

Once the contributing specular points are determined, the calculation of the multipath signal is rather straightforward. The contribution to this signal from the i^{th} specular point is given by (2.6) and (2.7).

$$s_H(i) = \Gamma_H(\alpha_i)\, e^{-j\phi_i}\, G_H(g_a(i))\, A_i \tag{2.6}$$

$$s_V(i) = \Gamma_V(\alpha_i)\, e^{-j\phi_i}\, G_V(g_a(i))\, A_i \tag{2.7}$$

In the above α is the local grazing angle at the specular point, ϕ is the phase difference relative to the direct path signal, Γ is the complex surface reflection coefficient (given in Appendix B), G is the antenna gain function, g_a is the antenna gain angle and A is the attenuation factor (discussed in the next section). The subscripts H and V represent horizontal and vertical polarization respectively. The overall multipath signal is constructed by adding together all the contributions for each of the N_c specular points that are visible to the receiver, as shown in (2.8) to (2.10). It is suggested in [1] that the number of specular points present in typical North Atlantic sea conditions (around ss4(ii), for which average wavelength is roughly 34.26m and

RMS waveheight is 0.61m) in the region between the ship and the horizon is around 1500 to 2000 with only about 150 to 300 of these points visible to the receiver.

$$s_H = \sum_{i=1}^{N_c} s_H(i) \tag{2.8}$$

$$s_V = \sum_{i=1}^{N_c} s_V(i) \tag{2.9}$$

$$s_{RHC} = \sum_{i=1}^{N_c} \left\{ \frac{s_V(i) + E_R e^{j\theta_m} s_H(i)}{2} \right\} \tag{2.10}$$

A right-hand-circularly polarized signal is constructed by adding the horizontal and vertical components and incorporating the appropriate antenna gain mismatch E_R, and phase mismatch θ_m, as shown in (2.10).

In constructing the multipath signal in this manner the model will generate time indexed samples of the in-phase and quadrature components of the multipath signal. This is convenient as it allows easy investigation of properties and characteristics of the multipath signal through common time or frequency domain analysis techniques.

2.1.3.1 Attenuation Factors

In order to take into account the effect of specular and diffuse reflection, much of the literature [7-10] takes an approach in which these two portions are treated separately.

In such approaches the specular component and the diffuse component are developed and combined using statistical methods. This procedure results in obtaining the probability density function of the multipath signal and not the actual signal approximation that the propagation model provides. This scattered signal is most often assumed to be Rayleigh distributed if the distribution of the ocean profile is assumed to be Gaussian. Since the propagation model of [1] is entirely deterministic, the complexities of a statistical analysis is not a concern. Therefore a simpler approach is used in incorporating divergence into the multipath model.

The attenuation factor was developed so that it would take into account the divergence and phase shift from a scattering portion of the surface, and effectively deals with both specular and diffuse reflection at the same time. In doing so Moreland stresses that there must be a distinction made between the scattering from a convex portion of the surface and a portion which is concave. Furthermore, it is emphasised that special care must be used should the situation arise that the antenna is within two focal lengths of a particular scatter point due to the fact that this may result in energy being focused at the antenna, and so far field assumptions of ray optics are no longer valid. These situations are illustrated in Figures 2-4 and 2-5.

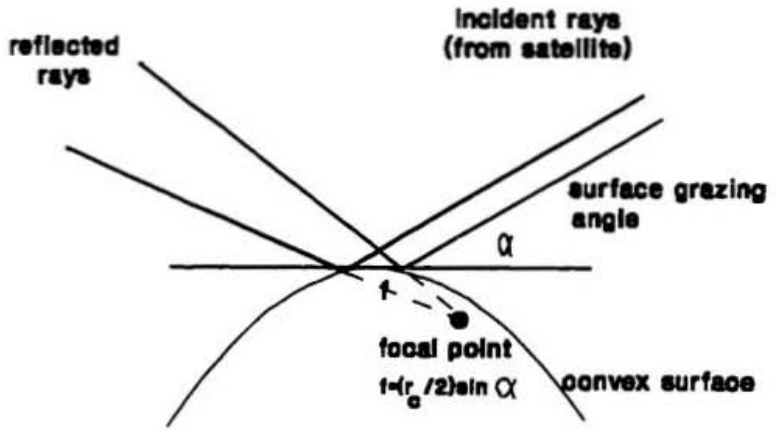

Figure 2-4: Scattering from a Convex Surface.

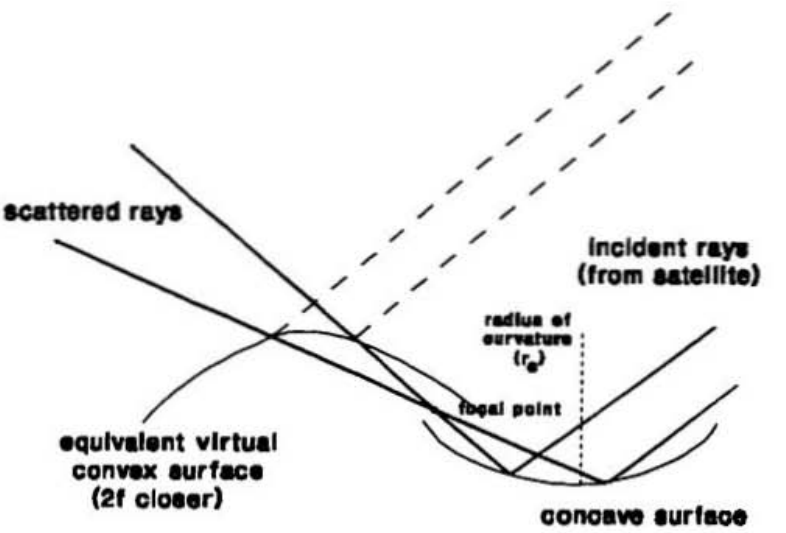

Figure 2-5: Scattering from a Concave Surface.

In determining the attenuation factor from a convex portion of the surface a ray-optics approach is used. Using r as the distance from the scatter point to the receiver and f as the focal length associated with the radius of curvature of the surface at that point, the attenuation factor is given by (2.11).

$$A_{CONVEX}=\frac{1}{\sqrt{1+\frac{r}{f}}} \tag{2.11}$$

For the concave situation shown in Figure 2-5, if the receiving antenna is more than two focal lengths away from the scattering point then Moreland [1] shows that the attenuation factor may be calculated by treating the surface as a convex portion located 2f closer to the antenna with an additional phase shift of 90° as given in (2.12).

$$A_{CONCAVE}=j\frac{1}{\sqrt{\frac{r}{f}-1}}, \qquad [r>2f] \tag{2.12}$$

In the region $0\leq r\leq 2f$, (2.12) is no longer valid. This is especially true if the receiver is located close to the focal point. Such a situation may focus the reflected energy and the far field assumptions involved in the derivation of (2.12) no longer apply. To deal with these complexities a more rigorous Fresnel diffraction approach is used. The region $0\leq r\leq 2f$ is further divided into two separate intervals, one from the scatter point to the focal length, and one from the focal length to twice this distance. By using the Fresnel diffraction approach the following attenuation factors were developed.

$$A_{CONCAVE} = \left(\frac{1}{2B}\right)^{\frac{1}{3}} \int_{-\infty}^{\infty} e^{j\frac{\pi}{2}[V^3 - K_q V^2]}\, dV \qquad r \in [0, f] \tag{2.13}$$

$$A_{CONCAVE} = \left(\frac{1}{2B}\right)^{\frac{1}{3}} \int_{-\infty}^{\infty} e^{j\frac{\pi}{2}[V^3 + K_q V^2]}\, dV \qquad r \in [f, 2f] \tag{2.14}$$

$$K_q^3 = \frac{2\tan\psi \left|\frac{r}{f} - 1\right|^3}{\lambda_c r \left(\frac{1}{r} - \frac{1}{2f}\right)^2} \tag{2.15}$$

$$B = \left[\frac{1}{r} - \frac{1}{2f}\right] \frac{\sqrt{\lambda_c r}}{\tan\alpha} \tag{2.16}$$

In the above λ_c is the carrier wavelength (approximately 0.2m at L-Band) and α is the grazing angle.

2.1.4 Vessel Motion

To update the signal accurately with time the motion of the vessel must be considered. In order to get appropriate antenna coordinates that will be used at each time instant the effects of the ship's velocity and the motion caused by the interaction between the vessel and the ocean must be taken into account. The ocean effects must also be used to calculate the pointing angle error of the receiving antenna. The necessary parameters needed to do this are shown in Figure 2-6. Explanations of these parameters are given below the figure.

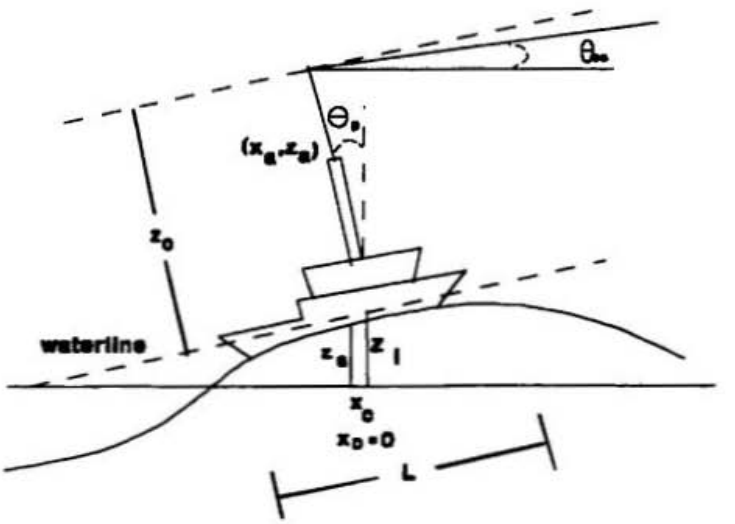

Figure 2-6: Vessel Motion Geometry.

L: vessel length.

z_o: nominal antenna height above the waterline.

x_c: horizontal position of the centre of gravity of the ship. x_c=ut where u is the velocity of the vessel.

x_D: horizontal distance between the centre of gravity and the antenna location.

z_s: instantaneous sea surface height.

z_l: instantaneous waterline height of the ship.

θ_p: pitch angle (ccw assumed positive).

θ_{ss}: antenna pointing angle error.

z_a: instantaneous antenna vertical position.

x_a: instantaneous antenna horizontal position.

To calculate the instantaneous antenna height, first the ocean surface is averaged over the length of the ship. This average height is then put through a vertical translation filter that was developed in [2]. The transfer function of this filter is given by (2-17).

$$H_v(f) = \frac{f_v^2 + j1.4 f_v f}{(f_v^2 - f^2) + j1.4 f_v f} \tag{2.17}$$

$$f_v = \frac{1}{2\pi}\sqrt{\frac{10g}{L}}\,Hz \tag{2.18}$$

The parameter g in the above is the acceleration due to gravity ($g=9.81 m/s^2$). The output of this filter will give the instantaneous waterline height under the point at which the antenna is fixed.

In order to obtain the pitch angle an average incline is calculated by averaging the angles between the horizontal and lines connecting the coordinates of the rear of the vessel (x_c-L/2, $z(x_c$-L/2)), to the ocean surface heights $z_s(x)$ along the length of the ship. Referring to this incline as $\theta_1(t)$, the averaging process takes the form of (2.19).

$$\theta_1(t) = \frac{12}{L^3}\int_{-\frac{L}{2}+ut}^{\frac{L}{2}+ut} z_s(x,t)\,(x-ut)\,dx \tag{2.19}$$

θ_1 is put through a pitching motion filter that was also developed in [2] having the transfer function of (2.20).

$$H_p(f) = \frac{f_p^2 + j0.6 f_p f}{(f_p^2 - f^2) + j0.6 f_p f} \tag{2.20}$$

$$f_p = f_v = \frac{1}{2\pi}\sqrt{\frac{10g}{L}}\,Hz \tag{2.21}$$

The output of this filter will give the pitch angle of the ship at that particular time. If an antenna gravity stabilizer is used then θ_p is put into an antenna stabilization filter with a transfer function of (2.22) which will give the antenna pointing angle error θ_{ss}.

$$H_s(f) = \frac{(f_o^2 - \frac{h}{g}(2\pi f_o)^2 f^2) + j f_o f}{(f_o^2 - f^2) + j f_o f} \tag{2.22}$$

$$f_o = \frac{f_p}{10}\,Hz \tag{2.23}$$

If there is no stabilization present then the antenna pointing error angle is simply equal to the ship's pitch angle.

Once these parameters are known, then from Figure 2-6 and simple trigonometry the antenna coordinates are given by (2.24) and (2.25).

$$x_a(t) = x_c(t) + x_D \cos\theta_p(t) - z_o \sin\theta_p(t) \tag{2.24}$$

$$z_a(t) = z_1(t) + x_D \sin\theta_p(t) + z_o \cos\theta_p(t) \tag{2.25}$$

The θ_{ss} term is used in the gain angle term (g_a) of (2.6) and (2.7). If a reflected signal arrives at the antenna at an angle of $-\beta$ relative to the horizontal then the gain angle

will be $-\beta-\theta_{ss}$.

2.2 The Aeronautical Stochastic Model

Because of the lengthy execution time associated with the propagation model, it is not a practical choice if a quick evaluation is needed of the effects of multipath interference on a satellite-to-ship communication link. In addition to the propagation model Moreland develops a stochastic method of multipath modelling for the aeronautical situation. Although similar to the propagation model there are major differences. The ocean surface is assumed to be a Gaussian random process rather than a superposition of randomly phased sinusoids. This change leads to both benefits and drawbacks. The methodology associated with this approach is described in the following sections.

2.2.1 Specular Point Location

The major time consumer of the propagation model is the search process for locating specular reflection points. This lengthy search and the ensuing blocking and shadowing calculations take up a great deal of cpu time on even fast machines (several hours on a DEC Alpha workstation). Since interested parties that wish to evaluate quickly a potential communication link may not have access to a high speed work

station, it is desirable for a multipath model to run in an acceptable amount of time on a personal computer.

As mentioned, the ocean surface is assumed to be a Gaussian random process superimposed on a curved earth. With such an assumption, the underlying principle of finding the specular points remains the same as in equation (2.3). To find contributing scatter points on the ocean surface one must identify where the angle between that point and the receiver $\theta(x)$, equals the ray reflection angle $\beta(x)$. The difference is that following some manipulation and a Taylor series expansion, $\theta(x)$ can be written in the following form.

$$\theta(x) = \theta_o(x) - \sin(2\theta_o)\frac{z(x)}{2h(x)} \tag{2.26}$$

$$\theta_o(x) = \tan^{-1}\left(\frac{h(x)}{x}\right) \tag{2.27}$$

$$h(x) = z_o + \frac{x^2}{2a_e} \tag{2.28}$$

Instead of the local wave profile z(x) being the superposition of sinusoids as it was in the propagation model, it is now a Gaussian random process. For the aeronautical situation in [1] the aircraft altitude is large in comparison to the local waveheight at the scatter point. Because of this the sine term in (2.26) will be negligible. This leads to a further simplification of (2.26).

$$\theta(x) = \theta_o(x) \tag{2.29}$$

This simplification cannot be made in the maritime case where the antenna will be located much closer to the ocean surface and the local waveheight must be taken into account. This will be discussed in greater detail in the next chapter. However, applying (2.29) to (2.3) for a high altitude aircraft one will obtain (2.30).

$$E - 2\tan^{-1}(z_s'(x)) = \theta_o(x) \tag{2.30}$$

From this it is seen that the objective is to find where the the derivative of the local surface profile with respect to horizontal position x, represented by a Gaussian random process z'(x), crosses the deterministic curve m(x) as given in (2.31) and (2.32).

$$z'(x) = m(x) \tag{2.31}$$

$$m(x) = \tan\left(\frac{E - \theta_o(x)}{2}\right) + \frac{x}{a_e} \tag{2.32}$$

In [1], by calculating that the slope of the process m(x) is extremely small (in the order of 10^{-5}) it is determined that m(x) is constant in the immediate vicinity of a specific point x. Again because of the lower antenna heights associated with a ship mounted antenna, this assumption is not valid for the marine environment. By making it for the aeronautical case, it is found that the density function of curve crossings can be found by using standard methods of finding curve crossings of a fixed level by a stationary random process, as given in [4] and [5]. For this situation the density is given by (2.33), where $\sigma_{z'}$ and $\sigma_{z''}$ are RMS surface slope and RMS surface second

derivative respectively.

$$\lambda(x) = \frac{1}{\pi}\left(\frac{\sigma_{\varepsilon''}}{\sigma_{\varepsilon'}}\right) e^{-\frac{1}{2}\left(\frac{m(x)}{\sigma_{\varepsilon'}}\right)^2} \tag{2.33}$$

Since the previous assumptions cannot be made for the maritime case, a more general solution to the crossing of a function m(t) by a Gaussian process $\varepsilon(t)$ must be used. The following form of this general solution is from Chapter 13 of [4].

$$\lambda(t) = \frac{\gamma(t)}{\sigma(t)}\left(1-\mu^2(t)\right)^{\frac{1}{2}} \phi\left(\frac{m(t)}{\sigma(t)}\right) H(\eta(t)) \tag{2.34}$$

$$H(\eta(t)) = 2\phi(\eta(t)) + \eta(t)\left(2\Phi(\eta(t)) - 1\right) \tag{2.35}$$

$$\sigma^2(t) = VAR\{\varepsilon(t)\} \tag{2.36}$$

$$\gamma^2(t) = VAR\{\varepsilon'(t)\} \tag{2.37}$$

$$\mu(t) = \frac{COV\{\varepsilon(t), \varepsilon'(t)\}}{\sigma(t)\gamma(t)} \tag{2.38}$$

$$\eta(t) = \frac{m'(t) - \gamma(t)\mu(t)m(t)/\sigma(t)}{\gamma(t)\sqrt{1-\mu^2(t)}} \tag{2.39}$$

$$\phi(t) = \frac{1}{\sqrt{2\pi}} e^{\frac{-t^2}{2}} \tag{2.40}$$

$$\Phi(t) = \int_{-\infty}^{t} \phi(v)\, dv \tag{2.41}$$

This solution is applied to the maritime multipath scenario in Chapter 3.

It is desirable at this point to make a change of variables such that the specular point density $\lambda(x)$, will be a function of reflection angle β, rather than horizontal position x. If this change is made then the resulting *power* density that is obtained in Section 2.2.4 is also a function of β. If the power density curve is a function of reflection angle then methods such as those found in [14] and [15] can be used for producing power-spectral densities of the received multipath signal. The methods in [14] and [15] consist of performing a change of variables between the angle of arrival of a multipath signal and the associated doppler frequency shift. If the power density is plotted against the frequency shift, a reasonable estimate of the power spectrum is obtained. The calculations needed for the variable change between x and β are presented in

Chapter 3 where they are applied to the maritime case. At the moment we will assume the exchange has been made and the total number of potential specular points in the contributing region is given by (2.42).

$$N_c = \int_{\beta_{MIN}}^{\beta_{MAX}} \lambda(\beta)\, d(\beta) \tag{2.42}$$

The angular limits of the integration bound the ocean surface region from which the contributing signal will arise. If the integration was performed over x instead of $\beta(x)$ then the limits would be x_{MIN} and x_{MAX}, corresponding to β_{MAX} and β_{MIN} respectively. Generally this region will extend from a few metres in front of the ship to the horizon. The above density solution does not take into account the effects of blocking and

shadowing. The adjustments that must be made for these are presented in the next section.

2.2.2 Blocking and Shadowing

In the propagation model, Moreland had a deterministic ocean surface composed of the summation of a number of sinusoids superimposed on a curved earth. In the stochastic model, the local waveheight profile is considered to be a Gaussian random process. Because of this it is not possible to check for blocking and shadowing at a specular point in the same manner as was done for the propagation model. Rather than being able to conclude that a specular point contributes if it is visible to the receiver, and that it does not contribute if it is not visible as in the propagation model, the method used in the stochastic approach is one of calculating a clearance probability which is used as a weighting factor in the scatter point density function calculation. This weighting factor is a function of the scatter point's local reflection angle β_l for blocking and its local elevation angle E_l for shadowing. These *local* angles are calculated by incorporating the effect of earth curvature on these angles at the scatter point as in (2.43) and (2.44).

$$\beta_l(x) = \beta(x) - \tan^{-1}\left(\frac{x}{a_e}\right) \tag{2.43}$$

$$E_1(x) = E + \tan^{-1}\left(\frac{x}{a_e}\right) \tag{2.44}$$

This is illustrated in Figure 2-7.

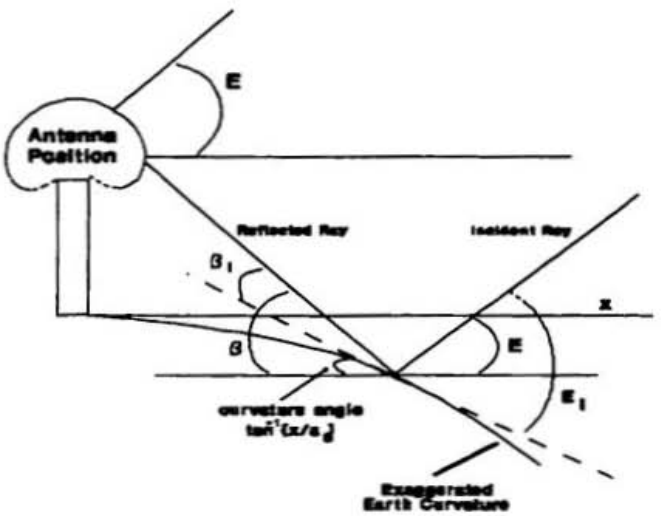

Figure 2-7: Local Elevation and Reflection Angles

It is necessary to mention here that the integration from which the number of specular points is obtained, and later from which the scatter power will be obtained, is carried out with respect to the reflection angle β. However, we still need to know the value of the x-coordinate at the specular point. Knowing that β is a function of x, β(x) can be inverted to get the x-coordinate as given in (2.45).

$$x = a_e \tan\beta \left[1 - \sqrt{1 - \frac{2z_o a_e}{(a_e \tan\beta)^2}}\right] \tag{2.45}$$

Similarly, if the *local* reflection angle is known then the x-coordinate can be approximated by (2.46).

$$x = (a_e + z_o)\tan\beta_1 \left[\sqrt{1 + \frac{2z_o a_e}{((a_e + z_o)\tan\beta_1)^2}} - 1\right] \tag{2.46}$$

Using these relations and Figure 2-8, which shows the geometry for the blocking

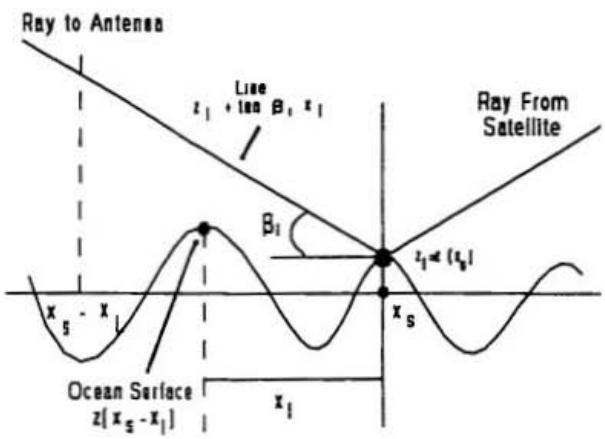

Figure 2-8: Clearance Probability Geometry for Blocking Situation

calculation, a clearance probability can be found. For the blocking situation, this is the probability that the ray to the receiver clears the ocean surface along a length x_L towards the antenna. At distance x_L away from the scatter point, it can be assumed that the reflected ray is no longer at risk of being blocked by the ocean surface. This

distance is a function of the reflection angle and is examined more in Chapter 3.

$$P_c(\beta_1, z_1) = Prob\ \{z(x_s - x_1) < z_1 + \tan(\beta_1) x_1 \mid x_1 \epsilon [0, x_L]\} \quad (2.47)$$

The x-coordinate of the scatter point is given by x_s and z_1 (alternately $z(x_s)$) is the local waveheight at that x-coordinate. In order to compute this probability, a step size Δx is used to divide up the interval $0<x_1<x_L$. This step size is selected to be large enough so that adjacent surface height samples can be assumed to be uncorrelated and therefore independent. With these assumptions, the clearance probability over the interval will be the product of the clearance probabilities at each sample as given in (2.48).

$$P_c(\beta_1, z_1) = \prod_{i=1}^{N_I} [1 - Q(\frac{z_1 + i\tan(\beta_1)\Delta x}{\sigma_z}] \quad (2.48)$$

In (2.48) N_I is the number of independent samples over the interval x_L, and σ_z is the RMS waveheight. The Q-function is given in (2.49) or (2.50).

$$Q(x) = \frac{1}{\sqrt{2\pi}} \int_x e^{-\frac{t^2}{2}} dt \quad (2.49)$$

$$Q(x) = \frac{1}{2} erfc(\frac{x}{\sqrt{2}}) \quad (2.50)$$

$$erfc(x) = 1 - erf(x) \quad (2.51)$$

$$erf(x) = \frac{2}{\sqrt{\pi}} \int_0^x e^{-\frac{t^2}{2}} dt \quad (2.52)$$

Using the same interval length x_L as in the propagation model, where $x_L=2.5\Lambda$, and where Λ is the average sea wavelength, and assuming that (2.54) sufficient to ensure independence of samples (where γ is a Gaussian bandwidth factor of 1.344 corresponding to a noise equivalent bandwidth of the composition of sinusoids surface model of Section 2.1.1 [1]), then after some manipulation and renaming the result w_B for *blocking weighting factor* instead of the clearance probability P_c, (2.53) is obtained.

$$w_B(\beta_1, z_1) = \prod_{i=1}^{9} \left[1 - Q\left(\frac{z_i}{\sigma_z} + i\frac{1.685\tan\beta_i}{\sigma_{z'}}\right)\right] \tag{2.53}$$

$$\Delta x = \frac{\Lambda}{4}\sqrt{1+\frac{\gamma^2}{12}} \tag{2.54}$$

Using the same principles for the case of shadowing but considering a distance x_L from the specular point towards the transmitter, one obtains the *shadowing weighting factor* w_S, given by (2.55).

$$w_S(E_1, z_1) = \prod_{i=1}^{9} \left[1 - Q\left(\frac{z_i}{\sigma_z} + i\frac{1.685\tan E_i}{\sigma_{z'}}\right)\right] \tag{2.55}$$

The behaviour of these weighting factors will be investigated further in the next chapter where they are applied to the maritime case. For the time being it will be mentioned that if (2.42) gives the total number of scatter points that satisfy (2.3), then the number of these points that actually contribute to the multipath signal will be given by (2.56), which incorporates the blocking and shadowing weighting factors.

$$N_c = \int_{\beta_{MIN}}^{\beta_{MAX}} \lambda(\beta)\, w_B(\beta_1, z_1)\, w_S(E_1, z_1)\, d\beta \tag{2.56}$$

2.2.3 Incorporating Divergence

Although the following method for incorporating attenuation caused by divergence of the reflected signal was done only for the aeronautical case in [1], it is worthy of description as we use it as a basis for the maritime situation. Like the aeronautical propagation model in [1], there is assumed to be no difference between scattering from a convex and concave scattering surface area except for the additional 90° phase shift associated with a concave facet. Ignoring the additional concave facet phase shift, the divergence from any scattering point is given by (2.57).

$$D = \sqrt{\frac{1}{1 + \frac{2d}{r_c \sin\alpha}}} \tag{2.57}$$

The radius of curvature at the scattering point is given by r_c, the local grazing angle is given by α, and d is the distance between the scattering point and the antenna as given by (2.58) to (2.60).

$$\alpha(x) = \frac{E + \beta(x)}{2} \tag{2.58}$$

$$d(x) = \frac{h(x)}{\sin\beta(x)} \tag{2.59}$$

$$h(x) = z_o + \frac{x^2}{2a_e} \tag{2.60}$$

These values are portrayed in Figure 2-9.

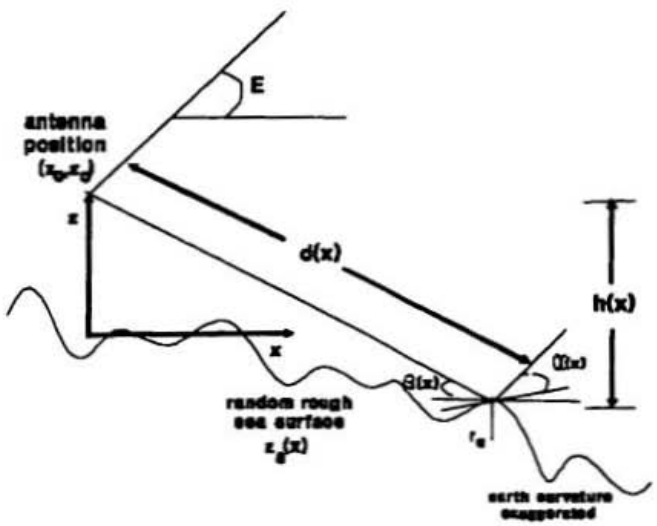

Figure 2-9: Parameters for Divergence Calculation.

The purpose of the stochastic model is to obtain a value for the average power of the signal scattered from the ocean surface. The weighting factor used in the power calculation to incorporate the attenuation resulting from divergence is the square of (2.57). By combining (2.57) with (2.58) to (2.60) we obtain the following more explicit form of the divergence weighting factor.

$$D^2(x) = \frac{r_c \sin\beta(x) \sin\alpha(x)}{2h(x)} \left[\frac{1}{1 + \frac{r_c \sin\beta(x) \sin\alpha(x)}{2h(x)}} \right] \qquad (2.61)$$

For the aeronautical case the aircraft height will be so large that the term in the square brackets in (2.61) can be ignored. This is not the case for the maritime situation.

An important difference between the propagation model and the stochastic model is the calculation of the r_c term in (2.61). The radius of curvature, given by (2.62), is now a function of a random variable. This random variable is the local waveheight second derivative z_1'' at a particular scattering point.

$$r_c = \frac{[1 + (z_s'(x))^2]^{\frac{3}{2}}}{|z_1''|} \qquad (2.62)$$

Using (2.5), $z_s'(x)$ can be written as in (2.63).

$$z_s' = \tan\left(\frac{E - \beta(x)}{2}\right) \qquad (2.63)$$

Substituting (2.63) into (2.61) and assuming that the term confined in the square brackets of (2.61) is negligible, we obtain (2.64).

$$D^2(x) = q(\alpha, \beta, x)\,\hat{R}_c(z_1'') \tag{2.64}$$

where

$$q(\alpha, \beta, x) = \frac{\sin\beta(x)\sin\alpha(x)}{2h(x)}\left(1+\tan^2\left(\frac{E-\beta(x)}{2}\right)\right) \tag{2.65}$$

$$\hat{R}_c(z_1'') = \frac{1}{|z_1''|} \tag{2.66}$$

Because of the assumptions made for the $D^2(x)$ term, these results will not hold for the maritime case. The approximate radius of curvature term in (2.66) will not be valid since it will have to be split into approximations for convex and concave scattering elements. However, with these being valid for the aeronautical case, in order to get a weighting factor for the scatter power calculation a mean radius of curvature, $M_{RC}(z_1)$, at a specular point is needed. This can be calculated by (2.67).

$$M_{RC}(z_1) = \int_{-\infty}^{\infty} \hat{R}_c(z_1'')\, f_{z''}(z_1''|z=z_1)\, dz_1'' \tag{2.67}$$

In (2.67) $f_{z''}(z_1''|z=z_1)$ is the conditional density function of the second derivative of the surface [1] given by (2.68). This assumes that the surface and its second derivative are correlated by the relation of (2.69). Derivations of these relations are contained in Appendix A of [1].

$$f_{z''}(z_1''|z=z_1) = \frac{1}{\sqrt{2\pi}\sigma_{m_2}} e^{-\frac{1}{2\sigma_{m_2}^2}(z_1''-K_2 z_1)^2}$$

$$K_2 = \frac{E\{z''z\}}{\sigma_z^2} = -\left(\frac{\sigma_{z'}}{\sigma_z}\right)^2 \tag{2.68}$$

$$r_2 = \frac{E\{z''z\}}{\sigma_{z''}\sigma_z} = \frac{-\sigma_{z'}^2}{\sigma_{z''}\sigma_z}$$

$$\sigma_{m_2} = \sqrt{1-r_2^2}\,\sigma_{z''}$$

$$E\{z''z\} = -\sigma_{z'} \tag{2.69}$$

Once M_{RC} is known, it is used as a weighting factor to account for the attenuation of the scattered signal caused by divergence. This weighting factor, like the blocking and shadowing weights, is used in the average scatter power calculation which is described in the next section.

2.2.4 Average Scatter Power Calculation

Blocking, shadowing, and the approximate radius of curvature at a particular scatter point can be combined into a one term, $R(\beta_1,E_1)$, which is used to produce an *effective radius of curvature* at that point. This is given by (2.70).

$$R(\beta_1, E_1) = w_B(\beta_1, z_1)\, w_S(E_1, z_1)\, \hat{R}_c(z_1'') \tag{2.70}$$

The expected value of this at any scatter point (x_1,z_1) is given by (2.71).

$$E\{R(\beta_1, E_1)\} = \int_{-\infty}^{\infty} w_B(\beta_1, z_1)\, w_S(E_1, z_1)\, M_{RC}(z_1)\, f_z(z_1)\, dz_1 \qquad (2.71)$$

The term $f_z(z_1)$ is the zero-mean Gaussian density given by (2.72).

$$f_z(z) = \frac{1}{\sqrt{2\pi}\sigma_z} e^{-\frac{z^2}{2\sigma_z^2}} \qquad (2.72)$$

Combining the above results with the specular point density of (2.42), a power density which is a function of reflection angle β, can be defined by (2.73).

$$S(\beta) = |a(\beta)|^2 \lambda(\beta)\, q(\alpha, \beta, x)\, E\{R(\beta_1, E_1)\} \qquad (2.73)$$

The a(β) term in (2.73) takes into account the polarization dependence on the scattered signal. It includes the complex surface reflection coefficient as well as the antenna gain and polarization. The exact composition of this term is given in Chapter 3.

By integrating the power density function over the contributing surface region the total average power is found. This is given by (2.74).

$$P_s = \int_{\beta_{MIN}}^{\beta_{MAX}} S(\beta)\, d\beta \qquad (2.74)$$

The power density function of (2.73) is also useful in determining an approximation for the Doppler spectrum characteristics which can be used for predicting fade durations and depths. Moreland finds that by applying some principles outlined in [14] and [15], and the appropriate change in variables from reflection angle to frequency shift, the power spectral-density or Doppler spectrum can be approximated by the average of several power density curves over a number of time instants. This method and how it may be applied to the maritime case is discussed in greater detail in the next chapter.

2.2.5 Updating with Time

For the aeronautical situation the process of updating the value of the scattered power at a new time instant is quite simple. Since there is no contact between the ocean and the aircraft, only the velocity and direction of the aircraft need to be considered when calculating new antenna coordinates. From (2.26) to (2.29) it is seen that since the aircraft is so much higher than the ocean surface height, the reflection angle changes very slowly with time and the sea surface can be assumed to be stationary. This simplifies the solution to the curve crossing problem as seen in (2.33). However, for the maritime case, the calculation of the antenna coordinates is more complicated. The ocean movement has an effect on the ship's motion so the coupling between the ship and the ocean must be considered when determining new antenna coordinates. It

is suggested in [1] that a method similar to the one used in the maritime propagation model can be used to calculate approximate antenna locations for a maritime stochastic model. This suggestion is investigated in the next chapter.

2.3 Other Attempts at Maritime Multipath Modelling

Although most of the foundation we use for modelling the maritime multipath phenomenon is taken from [1], there are several other methodologies that are worthy of mentioning.

No attempt at multipath signal modelling or any investigation of the process of electromagnetic waves scattering from rough surfaces is complete without mentioning the work of Beckmann and Spizzichino [3], who give a detailed formulation of the scalar Kirchhoff approximation of the field scattered by a rough surface. The Kirchhoff approach is based on the assumption that the curvature of the scattering surface is much greater than the wavelength of the signal and that there are no sharp edges present on the surface. With such a situation the field scattered from any point on the rough surface can be approximated by the field that would be scattered by a tangent plane at that point. If there are sharp edges on the surface, some other form of predicting rough surface scatter must be used. This may involve the different forms of Rician or Rayleigh methods described in Chapter 6 of [3]. For the maritime L-

Band satellite-to-ship situation, the Kirchhoff method is generally appropriate, except for perhaps an extremely rough sea.

The Kirchhoff solution given in [3] is based on the solution to the Helmholtz surface integral. A scattered field strength E_2, received at a point P, located at a distance R′ from a scattering point on a rough surface given by (x,y,z(x,y)), arising from an incident field strength E (note all values are scalars) is given by (2.75).

$$E_2(P) = \frac{1}{4\pi}\int_S \int (E\frac{\partial \psi}{\partial n} - \psi \frac{\partial E}{\partial n})\, dS$$

$$\psi = \frac{e^{jk_2 R'}}{R'} \qquad (2.75)$$

$$k_2 = \frac{2\pi}{\lambda_c}$$

In (2.75) n is the normal to the tangent plane at the scattering point. It should be noted that the simplest solutions to the Helmholtz integral do not take into account the effects of earth curvature, possible time variations of the rough surface, or finite conductivity of the medium of which the surface is composed. All of these need to be included if the surface and receiver are in motion and if the surface is a conductive ocean. Incorporating these effects adds to the complexity of the Helmholtz solution. Another attempt that was made to specifically characterize the maritime multipath phenomenon was by Tseng [6]. His goal was to develop a channel transfer function H(f), that could be used to predict the properties of the received signal in a satellite-to-

ship link in the presence of multipath scattering from the sea surface. Having such a transfer function and knowing the transmitted signal $v_t(t)$, the received signal, composed of the direct path signal from the satellite as well as both specular and diffuse scattered components, could be found by (2.76).

$$v_r(t) = \int_{-\infty}^{\infty} V_t(f) H(f) e^{-j2\pi ft} df \tag{2.76}$$

To develop the transfer function H(f), Tseng bases almost all of his work on the theory of [3]. Some inadequacies in [6] may be caused by the assumption that both the position of the ship and the shape of the ocean surface change very slowly and therefore H(f) is considered time-invariant. This assumption may cause inaccuracies in developing correct power-spectral densities.

Other attempts, such as the works of Karasawa and Shoikawa [8-10], develop what seem to be quick and easy methods for predicting signal fade depth and duration. Often in the attempt to simplify the concepts involved in these approaches, certain assumptions are made, such as considering the ocean surface to be sinusoidal which may lead to error. Even with these simplifications, the fading depths and durations calculated in [8-10] agree well with available measurements, although the sinusoidal model does limit the variety of surface conditions that can be simulated.

Sobieski *et al* [7] present another method of modelling maritime multipath. Expressions for a carrier-to-specular (C/S) power ratio and a carrier-to-multipath (diffuse) (C/M) power ratio are developed by considering the ocean to be a statistically rough surface simulated by what is called a Wallace-Toba-Cox Spectrum (SWTC) which takes into account the effects of wind speed as well as sea state. The results obtained are compared to the measurements in [13], as were the results of [1], and appear to be quite similar.

The above are only theoretical attempts at multipath modelling. The literature also contains attempts of characterizing maritime multipath by measurement. Among these are the results of Fang, Tseng, and Calvit [11] in which a MARISAT maritime L-Band satellite signal is measured with a terminal aboard a vessel that travels from Norfolk, VA, to Texas City, TX. This corresponded to an elevation angle range between approximately 15° and 0°. As with any measurements, the results are very specific to the environment in which the measurement were taken. The warm temperatures in the area where these measurements where taken would not produce the same ocean reflectivity as would the cooler waters off the coast of Newfoundland. It is also difficult to extract the effect of certain parameters such as antenna height or ship motion from such experimental results.

Another attempt at characterizing L-Band communication signals at lower elevation

angles was done by Hicks [12]. This measurement exercise involved using a fairly directive tracking antenna to receive the pilot carrier signal from the INMARSAT MARISAT F-4 satellite. This was done with a terminal on board the Canadian Coast Guard Ship (CCGS) *Sir John Franklin* as it sailed from St. John's, NF, to Thule, Greenland. With this route, the elevation angle varied from around 35° to 5°. With the antenna used, the effects of the multipath scatter are not as predominant as would be seen if a fairly low gain almost omni-directional antenna was used, as is the case for most low cost Standard-C type receivers.

The above attempts of investigating maritime L-Band multipath are informative. Some aspects of these efforts are included in or compared to the model we develop. Although there is a great amount of information on how to simulate maritime multipath in the literature, it was decided that because of the amount of detail presented by Moreland and the possibility of developing a maritime stochastic multipath model, [1] would be an adequate foundation for the current investigation.

Chapter 3

The Stochastic Maritime Multipath Model

The method utilized here to model the ocean scatter multipath phenomenon in a maritime satellite-to-ship communication system is based on an extension of the technique used for the satellite-to-aircraft multipath scenario presented in [1]. This approach is based on the process of using the solution to a random curve crossing problem to find points on the ocean surface that will reflect an incident satellite signal towards a receiving antenna mounted on a moving vessel.

The approach in [1] requires some modification so that it may be applied to the maritime situation. For an aircraft, the movement of the ocean has no effect on the movement of the receiving antenna, and because typical aircraft altitudes are very high, the change in ocean surface height can usually be ignored in multipath power calculations. This is not true for the maritime case. Since a ship-mounted antenna is relatively close to the ocean surface, the effects of the changing surface waveheight at

a specular point must be considered. The movement of the ocean surface has a significant effect on the location and orientation of a ship-mounted antenna. This adds some difficulty to the modelling process. The multipath model we develop by making the necessary adjustments to the model constructed in [1] is presented in the remainder of this chapter.

3.1 Location of Specular Reflection Points

The geometry of identifying specular points on the ocean surface remains the same as shown in Figure 2-2. Specular points are located at points on the random ocean surface where an incident ray from a satellite is reflected at an angle $\beta(x)$, such that it will intercept the gain pattern of a ship mounted antenna. The surface $z_s(x)$ is assumed to be composed of a Gaussian random process z(x), making up the local waveheight, superimposed on a curved earth. This is given by (3.1). The random process z(x) is assumed to have a zero-mean and an RMS deviation in surface height of σ_z. The degree of roughness of the surface is characterized by σ_z as well as an average sea wavelength parameter Λ(values for σ_z and Λ are presented in Appendix A for various sea states).

$$z_s(x) = z(x) - \frac{x^2}{2a_e} \tag{3.1}$$

From the geometry of Figure 2-2, specular points are located at the values of x that satisfy (3.2).

$$\theta(x) = \beta(x) \tag{3.2}$$

It is worth mentioning at this point that, as in Chapter 2, the time dependence of all parameters has been momentarily suppressed. This is done purely for convenience and it must be remembered that all values are functions of time as well as position.

Since the solution of (3.2) involves the random process z(x), it is desirable to expand and manipulate (3.2) into a form that will allow the use of the general solution to a random curve crossing problem from [4] (this solution is presented in the previous chapter). By doing this, the curve crossings will indicate the locations of specular scatter points. The formulation of the curve crossing problem is described in the next section and its solution is presented in Section 3.1.2.

3.1.1 Formulation of the Random Curve Crossing Problem

In order to formulate the appropriate random curve crossing problem, (3.2) must be expanded. In doing so, $\theta(x)$ can be expressed as the following.

$$\theta(x) = \tan^{-1}\left(\frac{h(x) - z(x)}{x}\right) \tag{3.3}$$

$$h(x) = z_o + \frac{x^2}{2a_e} \tag{3.4}$$

By expanding (3.3) through the use of the Taylor series approximation given by (3.5) one will obtain (3.6).

$$\begin{aligned} \tan^{-1}(x+h) &= \tan^{-1}(x) + \frac{h}{1+x^2} \\ &= \tan^{-1}(x) + \cos^2(\tan^{-1}(x))\, h \end{aligned} \tag{3.5}$$

$$\begin{aligned} \theta(x) &= \theta_o(x) - \cos^2(\theta_o(x))\,\frac{z(x)}{x} \\ &= \theta_o(x) - \sin(2\theta_o(x))\,\frac{z(x)}{2h(x)} \end{aligned} \tag{3.6}$$

where,

$$\theta_o(x) = \tan^{-1}\left(\frac{h(x)}{x}\right). \tag{3.7}$$

In Chapter 2 it was seen that for the aeronautical case presented in [1] the aircraft altitude h(x) is much larger than the local waveheight z(x) at a specular point. Because of this the sine term in (3.6) can be considered to have little effect and $\theta(x)$ can be approximated by $\theta_o(x)$. For the much lower antenna heights present in a maritime situation, (3.6) must be used.

Substituting (3.6) into (3.2) and incorporating the fact that $\beta(x)$ is given by (3.8),

$$\beta(x) = E - 2\tan^{-1}\left(\frac{dz_s}{dx}\right), \tag{3.8}$$

where z_s is given by (3.1), it can be shown that the location of specular points is given by the solution of (3.9).

$$z'(x) = \tan\left(\frac{E-\theta_o(x)}{2} + \frac{\sin(2\theta_o(x))}{4h(x)}\right) z(x) + \frac{x}{a_e} \tag{3.9}$$

In order to solve for the specular point locations, (3.9) must be manipulated so that the general solution of a random curve crossing problem given in [4] can be utilized. This requires that (3.9) be arranged so that it can be seen that the location of specular points are given by the curve crossings of a function (*i.e.* curve) m(x) by a Gaussian random process $\varepsilon(x)$. Through a Taylor series expansion of the tangent term in (3.9) the following approximation is realized.

$$z'(x) \approx \frac{\sin(2\theta_o(x))}{4h(x)\cos^2\left(\frac{E-\theta_o(x)}{2}\right)} z(x) + \tan\left(\frac{E-\theta_o(x)}{2}\right) + \frac{x}{a_e} \tag{3.10}$$

By introducing the following notation,

$$\varepsilon(x) = z'(x) - a(x)\, z(x) \tag{3.11}$$

$$m(x) = \tan\left(\frac{E-\theta_o(x)}{2}\right) + \frac{x}{a_o} \tag{3.12}$$

$$a(x) = \frac{\sin(2\theta_o(x))}{4h(x)\cos^2\left(\frac{E-\theta_o(x)}{2}\right)}, \tag{3.13}$$

a random curve crossing problem which can be solved by applying the general solution given in [4] is obtained.

3.1.2 Specular Point Location Solution

The distribution of specular scatter points on the ocean surface is given by the probability density function of the curve crossings of a deterministic function m(x) by a Gaussian random process $\varepsilon(x)$. Using the expressions for m(x) and $\varepsilon(x)$ that were calculated in the previous section and by using the general solution to a random curve crossing problem from [4] we obtain the probability density function of the location of specular points $\lambda(x)$, as given by (3.14).

$$\lambda(x) = \frac{\gamma(x)}{\sigma(x)}\left(1-\mu^2(x)\right)^{\frac{1}{2}}\phi\left(\frac{m(x)}{\sigma(x)}\right)H(\eta(x)) \tag{3.14}$$

In order to obtain expressions for the various parameters in (3.14), the following assumptions relating the correlation between the ocean surface height and its

derivatives as developed in [1] must be mentioned.

$$E\{zz\}=\sigma_z^2 \tag{3.15}$$

$$E\{(z')^2\}=\sigma_{z'}^2=\frac{4\pi^2\sigma_z^2}{\Lambda^2} \tag{3.16}$$

$$E\{(z'')^2\}=\sigma_{z''}^2=\frac{3\sigma_{z'}^4}{\sigma_z^2} \tag{3.17}$$

$$E\{zz''\}=E\{z'z''\}=0 \tag{3.18}$$

$$E\{zz''\}=-\sigma_{z'}^2 \tag{3.19}$$

With the above correlation expressions, the parameters in (3.14) can be found.

$$\begin{aligned}\sigma^2(x) &= E\{e^2(x)\}\\ &=\sigma_{z'}^2+a^2(x)\,\sigma_z^2\end{aligned} \tag{3.20}$$

$$\begin{aligned}\gamma^2(x) &= E\{(e'(x))^2\}\\ &=\sigma_{z''}^2+[a^2(x)+2(a'(x))^2]\,\sigma_{z'}^2+(a'(x))^2\sigma_z^2\end{aligned} \tag{3.21}$$

$$\begin{aligned}\mu(x) &= \frac{E\{e(x)\,e'(x)\}}{\sigma(x)\,\gamma(x)}\\ &=\frac{a(x)\,a'(x)\,\sigma_z^2}{\sigma(x)\,\gamma(x)}\end{aligned} \tag{3.22}$$

$$\eta(x) = \frac{m'(x) - \gamma(x)\,\mu(x)\,m(x)/\sigma(x)}{\gamma(x)\sqrt{1-\mu^2(x)}} \tag{3.23}$$

$$a'(x) = \{2\cos(2\theta_o(x))\,\frac{d\theta_o(x)}{dx} - \sin(2\theta_o(x)) \times \left[\frac{x}{a_e h(x)} + \tan\left(\frac{E-\theta_o(x)}{2}\right)\frac{d\theta_o(x)}{dx}\right]\} \Big/ 4h(x)\cos^2\left(\frac{E-\theta_o(x)}{2}\right) \tag{3.24}$$

$$m'(x) = \frac{-\frac{1}{2}}{\cos^2\left(\frac{E-\theta_o(x)}{2}\right)}\,\frac{d\theta_o(x)}{dx} + \frac{1}{a_e} \tag{3.25}$$

$$\frac{d\theta_o(x)}{dx} = \frac{\sin^2(\theta_o(x))}{h(x)}\left[1 - \frac{h(x)}{a_e\tan^2(\theta_o(x))}\right] \tag{3.26}$$

$$H(\eta(x)) = 2\phi(\eta(x)) + \eta(x)\,[2\Phi(\eta(x)) - 1] \tag{3.27}$$

$$\phi(x) = \frac{1}{\sqrt{2\pi}}\,e^{-\frac{x^2}{2}} \tag{3.28}$$

$$\Phi(x) = \int_{-\infty}^{x} \phi(\tau)\,d\tau \tag{3.29}$$

With the expression for the density function of specular point locations, the overall number of specular scatter points that will potentially contribute to the multipath signal can be found by integrating $\lambda(x)$ over the applicable ocean region. This is given by

(3.30)

$$N_o = \int_{x_{start}}^{h_R} \lambda(x)\, dx \tag{3.30}$$

The contributing region of the ocean is bounded by the distances x_{start} and the horizon h_R, which are in the direction away from the vessel towards the transmitter. If it is assumed that the peak surface height z_p, can be approximated by $4\sigma_z$ and the peak surface slope z_p', by $4\sigma_{z'}$, then by using (3.3) and (3.8), as well as assuming that the specular point at the minimum distance must have the maximum surface slope and the antenna height is reduced by the maximum value of the sea surface height, x_{start} can be found by the following relationship.

$$x_{start} = \frac{z_o - z_p}{\tan(E + 2\tan^{-1}(z_p'))} \tag{3.31}$$

The distance to the horizon, h_R, can be found by calculating the distance between the x-coordinate of the antenna and the x-coordinate of a point on the horizon at which the tangent to the curvature of the earth at that point intersects with an antenna position given by (x_a, z_o+z_p). The maximum antenna height of z_o+z_p is used to find the maximum distance that needs to be considered. Any point beyond this distance will not be visible to the receiver. This distance is given by (3.32).

$$h_R = a_e \cos^{-1}\left(\frac{a_e}{a_e + (z_o + z_p)}\right) \approx \sqrt{2a_e(z_o + z_p)} \tag{3.32}$$

The initial coordinates of the antenna are assumed to be $(0,z_o)$, where z_o is the nominal antenna height above the waterline. With a transmitter, or satellite elevation angle of 10° and sea state 4(ii) (σ_z=0.61m, Λ=34.26m), the search region extends from roughly 10 metres in front of the ship to 16.6km. In order to avoid having to integrate over such a large region, it is desirable at this point to make a change of variable from horizontal distance x to reflection angle $\beta(x)$. The relationships between x, $\beta(x)$, and their derivatives are given by the following equations.

$$\beta = \tan^{-1}\left(\frac{z_o + \frac{x^2}{2a_e}}{x}\right) \tag{3.33}$$

$$x = a_e \tan(\beta)\left[1 - \sqrt{1 - \frac{2z_o}{a_e \tan^2(\beta)}}\right] \tag{3.34}$$

$$\frac{d\beta}{dx} = \frac{\sin^2\beta}{h(x)}\left[1 - \frac{h(x)}{a_e \tan^2\beta}\right] \tag{3.35}$$

Using (3.33) to (3.35) and introducing the following term,

$$c(x,\beta) = \frac{h(x)}{\sin^2\beta}\left[1 - \frac{h(x)}{a_e \tan^2\beta}\right]^{-1}, \tag{3.36}$$

a new specular point location density function can be expressed in terms of scatter point reflection angle β, rather than horizontal position x. The total number of potential scattering points is now given by (3.38).

$$\lambda(\beta) = c(x, \beta)\,\lambda(x) \tag{3.37}$$

$$N_o = \int_{\beta_{MIN}}^{\beta_{MAX}} \lambda(\beta)\, d\beta \tag{3.38}$$

The values for β_{MAX} and β_{MIN} are obtained by substituting (3.31) and (3.32) into (3.33). This produces the following limits.

$$\beta_{MIN} = \tan^{-1}\left(\sqrt{\frac{2(z_o + z_p)}{a_e}}\right) \tag{3.39}$$

$$\beta_{MAX} = E + 2\tan^{-1}(z_p') \tag{3.40}$$

Once again, using sea state 4(ii) with an elevation angle of 10° as an example, the integration for the scatter point location has changed from being carried out over a distance range of approximately 16km to being evaluated over a reflection angle range from about 0.15° to 58°. This change of variables is also useful if an analysis of the power spectrum of the received multipath signal is desired. By making the received power density curve a function a reflection angle, methods similar to those presented in [14] and [15] can be used to obtain approximate power-spectral densities.

Figures 3-1, 3-2, and 3-3 show examples of the behaviour of the specular point distribution for sea states 2(i), 4(ii), and 7(i). The applicable parameters pertaining to

these sea states are listed in Table 3-1 along with the number of specular points obtained. An elevation angle of 5° and an antenna height of 20m was used for all three situations. The integration of (3.38) is performed numerically with a *Simpson's 3/8 Rule* algorithm [16]. Not all specular points will contribute to the multipath signal due the blocking and shadowing effects which are described in Section 3.3. These effects are not included in Figures 3-1 to 3-3. From the figures, it can be seen that the majority of specular scattering points will be located in the region where the reflection angle is less that the elevation angle. This region corresponds to the area close to the horizon. Because of the small reflection angles in this region, many of reflected signals from the specular points will be blocked by the ocean surface, and therefore not contribute to the scatter power.

Table 3-1: Number of Potential Specular Points for Various Sea States.

Sea State (E=5°)	RMS Waveheight σ_z(m)	Average Wavelength Λ(m)	Number of Specular Points
ss2(i)	0.1675	12.2	4171
ss4(ii)	0.61	34.26	1558
ss7(i)	1.981	87.33	628

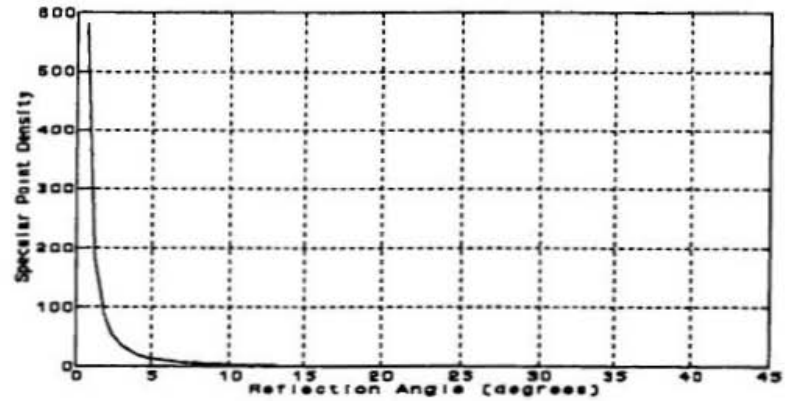

Figure 3-1: Specular Point Distribution for ss2(i), E=5°, z_o=20m.

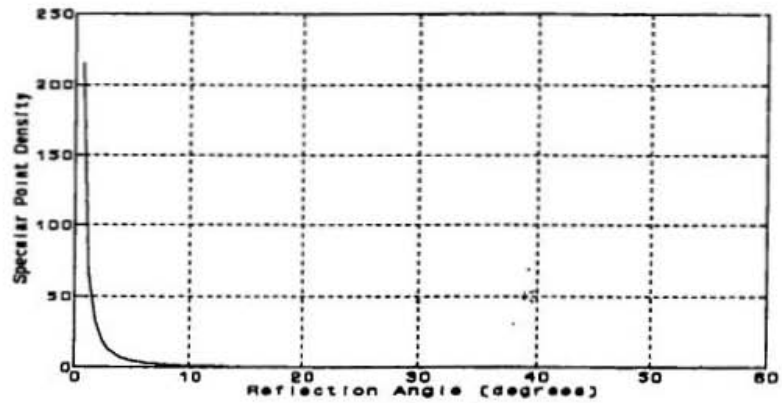

Figure 3-2: Specular Point Distribution for ss4(ii), E=5°, z_o=20m.

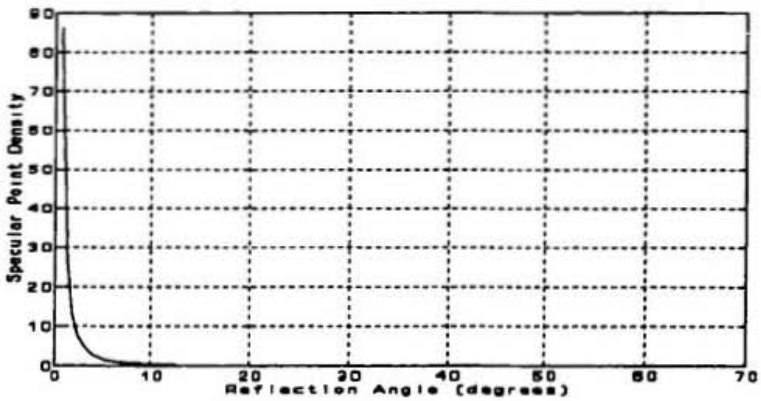

Figure 3-3: Specular Point Distribution for ss7(i), E=5°, z_o=20m.

3.2 Time Varying Antenna Location and Orientation

Before describing the method incorporated for including blocking and shadowing effects, it is necessary to explain the technique used to approximate the variation in antenna location and orientation. The movement of the antenna is caused by the velocity of the vessel as well as the interaction between the vessel and the moving ocean surface. A method that will produce random variations of antenna position and orientation due to the coupling between the ocean and the ship is needed. Since the surface profile is assumed to be a zero-mean Gaussian random process, the antenna movement algorithm should maintain this assumption while calculating realistic antenna locations that incorporate the varying roughness of the ocean. The technique

developed uses some aspects of the vessel motion routine developed in [1] for the maritime propagation model.

The superposition of sinusoids ocean profile presented in the maritime multipath propagation model of [1] is based on the summation of several randomly phased sinusoids. It is suggested that if 21 or more components are added then the resulting surface heights can be considered to have a Gaussian distribution. Therefore, in order to simulate a random Gaussian surface, the ocean profile is assumed to be composed of 21 randomly phased sinusoidal components, given by (3.41).

$$z(x,t)=\sqrt{\frac{2}{21}}\sigma_z\sum_{k=-10}^{k=10}\cos\left[\frac{2\pi}{\Lambda_k}(x-v_k)\,t+\theta_k\right]$$

$$\Lambda_k=\frac{1}{u_k}=\frac{1}{u_o+k\Delta u} \tag{3.41}$$

$$u_o=\frac{1}{1.0726\Lambda},\ \Delta u=\frac{\gamma u_o}{21},\ \gamma=1.344$$

$$v_k=\alpha\sqrt{\Lambda_k},\ \alpha=1.02$$

The parameter u_k in (3.41) represents the spatial frequency of the k^{th} component wave, v_k gives the approximate velocity of that component, Λ_k is the wavelength of the k^{th} wave component (the Λ_k's are distributed around the average sea wavelength, Λ, for a particular sea state), and θ_k is a uniformly distributed random phase component associated with the k^{th} sinusoid. The reader is referred to [1] for the derivation of

expressions for γ, α, and u_o.

By assuming this surface model in the vicinity of the vessel, the antenna position and orientation at any instant in time can be found in a straightforward manner. The geometry of the situation remains the same as shown in Figure 2-6. Values of antenna height z_a, x-coordinate x_a, and pointing error angle θ_{ss}, can be found by using the vertical translation, pitching angle, and stabilization filters whose transfer functions are given by (2.17) to (2.23). By exploiting the sinusoidal nature of the surface, values for waterline height $z_{wl}(t)$, pitch angle $\theta_p(t)$, and pointing error angle $\theta_{ss}(t)$, can be found by using the following expressions.

$$z_{wl}(t) = \sum_{k=-10}^{k=10} A_k |H_v(f_k)| \cos[2\pi f_k t + \theta_k + \angle H_v(f_k)] \tag{3.42}$$

$$\theta_p(t) = \sum_{k=-10}^{k=10} B_k |H_p(f_k)| \sin[2\pi f_k t + \theta_k + \angle H_p(f_k)] \tag{3.43}$$

$$\theta_{ss}(t) = \sum_{k=-10}^{k=10} B_k |H_p(f_k)| |H_s(f_k)| \sin[2\pi f_k t + \theta_k + \angle H_p(f_k) + \angle H_s(f_k)] \tag{3.44}$$

$$A_k = C \frac{\sin\left(\frac{\pi L}{\Lambda_k}\right)}{\frac{\pi L}{\Lambda_k}}$$

$$B_k = \frac{12C}{L^3}\left(\frac{\Lambda_k}{2\pi}\right)^2 \left[L\left(\frac{2\pi}{\Lambda_k}\right)\cos\left(\frac{\pi L}{\Lambda_k}\right) - 2\sin\left(\frac{\pi L}{\Lambda_k}\right)\right]$$

$$f_k = \frac{u - v_k}{\Lambda_k}$$

$$C = \sqrt{\frac{2}{21}}\sigma_z$$

Again, v_k is the velocity of the k^{th} surface component and u is the ship's velocity which is taken to be positive if it is moving with the ocean waves, and negative if it is moving against. The length of the vessel is represented by L.

By using the values for z_{wl}, θ_p, and θ_{ss} from (3.42) to (3.44), the antenna coordinates can be found by using the geometry of Figure 2-6 and simple trigonometric relations.

$$x_a(t) = x_c(t) + x_D\cos\theta_p(t) - z_o\sin\theta_p(t) \tag{3.45}$$

$$z_a(t) = z_{wl}(t) + x_D\sin\theta_p(t) + z_o\cos\theta_p(t) \tag{3.46}$$

The distance between the centre of gravity of the ship x_c (x_c=ut) and the antenna mount is given by x_D. If there is no stabilization present then the pointing error angle will be equal to the pitch angle. Examples of how the antenna height and pointing

error change with time for sea state 4(ii), a vessel velocity of 5m/s in the opposite direction of the ocean waves, and a nominal antenna height of 20m, are presented in Figures 3-4 and 3-5.

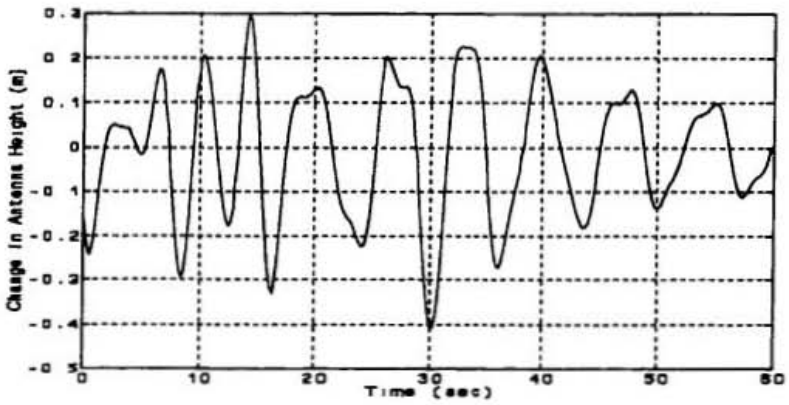

Figure 3-4: Variation in Antenna Height Change, ss4(ii), z_0=20m, u=-5m/s.

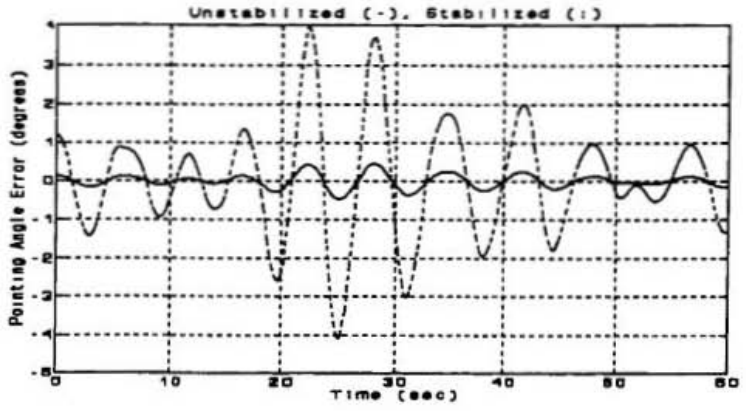

Figure 3-5: Variation in Antenna Pointing Angle Error, ss4(ii), z_0=20m, u=-5m/s.

By incorporating this method of calculating antenna position and orientation, a rather deterministic coordinate location is merged with a statistical analysis of the multipath scatter power in a somewhat *ad-hoc* manner. However, this does provide a reasonable means of simulating the change in antenna position and therefore the received scatter power. Other methods used to incorporate the antenna motion include that used in [7], in which at each instant in time a signal-to-noise ratio is calculated for a randomly chosen antenna pointing angle error between ±10°. The method we adopt seems to agree more with what one might intuitively expect for what is happening to the scatter power as time varies, as it produces changes in antenna pointing errors and height that are more indicative of the roughness of the sea and the motion of the vessel rather than an arbitrarily chosen range of pointing angle errors.

3.3 Blocking and Shadowing

When dealing with the effects of signal blocking and shadowing by the ocean surface for the low antenna heights associated with the maritime situation, one must not only consider the potential obstruction of the multipath signal, but also the possibility that the direct path between the transmitter and receiver is blocked by the surface. Although this may only happen with a combination of a very rough sea, a low antenna height, and a low elevation angle, it is necessary to be able to deal with such a

situation should it arise. If the direct signal is blocked by the sea surface, then it can be safely assumed that there will be no multipath component either. The blocking and shadowing at the specular reflection points of the multipath signal is considered first.

3.3.1 Specular Point Blocking and Shadowing

As was done in the aeronautical model of [1], we adopt a method of calculating a clearance probability at a specific reflection point. The geometry associated with this is similar to the aeronautical case and is presented in Figure 3-6.

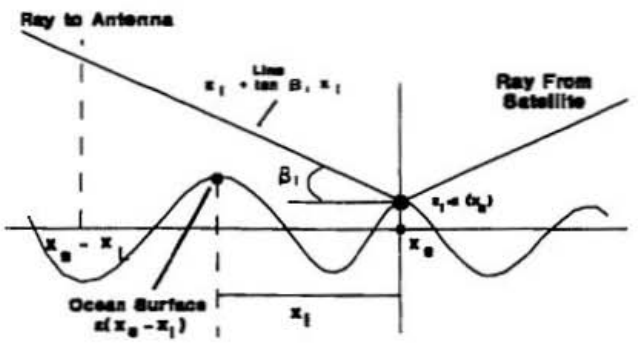

Figure 3-6: Clearance Probability Geometry for Signal Blockage

It is desired to find the probability that the ray reflected from the specular point is not obstructed along a total length x_L from the scattering point towards the receiver. *Local*

reflection angles are used for this calculation rather than the actual reflection angles. These angles are shown in Figure 2-7 and are calculated by the following equations.

$$\beta_1(x) = \beta(x) - \tan^{-1}\left(\frac{x}{a_e}\right) \tag{3.47}$$

$$x = (a_e + z_s)\tan\beta_1\left[\sqrt{1 + \frac{2z_s a_e}{((a_e + z_s)\tan\beta_1)^2}} - 1\right] \tag{3.48}$$

Note that we have begun to use the actual antenna height z_s, rather than the nominal height z_o, in our calculations. This is done to include antenna height variation effects in the scatter power calculations.

Using the geometry of Figure 3-6, the desired probability is given by (3.49).

$$P_c(\beta_1, z_1) = Prob\{ z(x_s - x_1) < z_1 + \tan(\beta_1)x_1 \mid x_1 \varepsilon [0, x_L] \} \tag{3.49}$$

The x coordinate of the scatter point is given by x_s, the surface height at that point is given by z_1 (or $z(x_s)$), and x_1 is a point in the interval $0<x_1<x_L$, at which a comparison between the surface height and the height of the reflected ray is made.

The length of the interval x_L is not fixed. It is calculated as function of sea state and local reflection angle as given by (3.50).

$$x_L = \frac{4\sigma_z - z_1}{\tan\beta_1} \tag{3.50}$$

In (3.50), a maximum surface height is arbitrarily chosen to be $4\sigma_z$ in order that a reasonable search region is obtained. At reflection angles below 1°, x_L will be greater than about 4Λ for most sea states and will reduce to a fraction of the average wavelength for higher reflection angles. In order to ensure that a reasonable region will be considered around a scatter point, a minimum value for x_L has been chosen to be 2Λ. By analogy with Section 2.2.2, the blocking weighting factor $w_B(\beta_i,z_i)$ is defined by (3.51).

$$w_B(\beta_1, z_1) = \prod_{i=1}^{N_i} \left[1 - \frac{1}{2} erfc\left(\frac{z_1 + i\tan(\beta_1)\Delta x}{\sqrt{2}\sigma_z}\right)\right] \tag{3.51}$$

In (3.51), erfc(x) is the complimentary error function (erfc(x) = 1-erf(x)), and Δx is a step size that is chosen to be large enough such that adjacent surface samples can be considered to be independent and uncorrelated. From [1], this step size is given by (3.52).

$$\Delta x = \frac{\Lambda}{4}\sqrt{1 + \frac{\gamma^2}{12}} \tag{3.52}$$

$$\gamma = 1.344$$

The number of sample points taken over the interval $0<x_i<x_L$ is given by N_i, which is determined by evaluating $x_L/\Delta x$.

For shadowing, the same process is implemented in the direction away from the scattering point towards the transmitter but using the local elevation angle E_1, instead of β_1.

$$E_1 = E + \tan^{-1}\left(\frac{x}{a_e}\right) \tag{3.53}$$

The shadowing weighting factor is given by (3.54) evaluated over a region given by (3.55).

$$w_S(E_1, z_1) = \prod_{i=1}^{N_1} \left[1 - \frac{1}{2} erfc\left(\frac{z_1 + i\tan(E_1)\Delta x}{\sqrt{2}\sigma_z}\right)\right] \tag{3.54}$$

$$x_L = \frac{4\sigma_z - z_1}{\tan E_1} \tag{3.55}$$

Figures 3-7 to 3-9 show how these weighting factors vary for elevation angles of 5, 10, and 15 degrees with a sea state of ss4(ii) and an antenna height of 10m. From Figure 3-7, it is interesting to note that the blocking weighting factor seems to be independent of elevation angle. This means that the actual scatter power is a function of elevation angle, but the blocking factor we apply to it is not and is only a function of reflection angle.

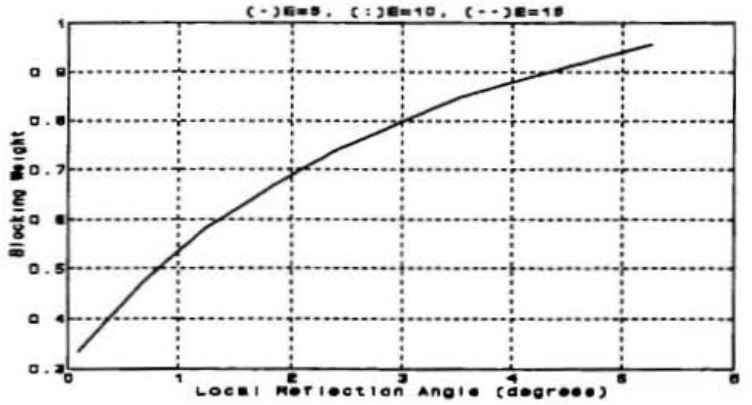

Figure 3-7: Blocking Weighting Factor $w_B(\beta_t,z_t)$, ss4(ii), z_o=10m.

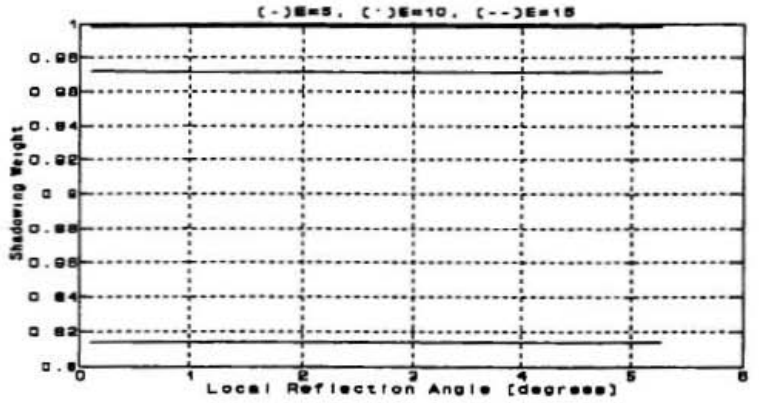

Figure 3-8: Shadowing Weighting Factor $w_S(E_t,z_t)$, ss4(ii), z_o=10m.

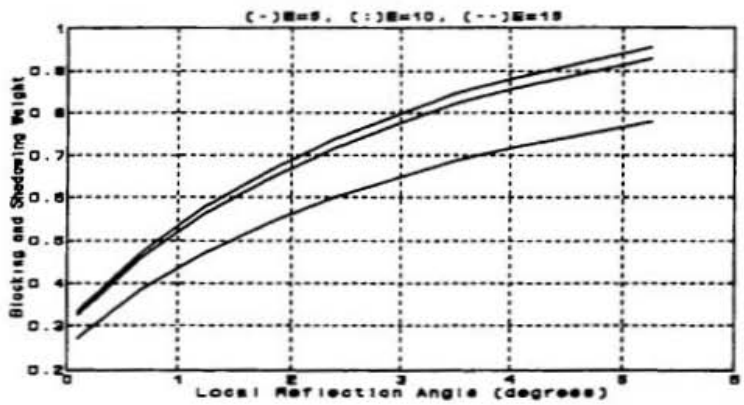

Figure 3-9: Combined $w_B(\beta_1,z_1)w_S(E_1,z_1)$ Weighting Factor, ss4(ii), z_o=10m.

The effect of the blocking and shadowing weights is best appreciated by comparing the number of potential specular points to the number that are actually visible to the receiver in the contributing ocean region. Table 3-2 shows the reduction in the number of specular points from Table 3-1 after the weighting factors are applied.

Table 3-2: Comparison of Potential and Contributing Specular Points.

Sea State (E=5°)	RMS Waveheight σ_z(m)	Average Wavelength Λ(m)	Number of Potential Specular Points	Number of Contributing Specular Points
ss2(i)	0.1675	12.2	4171	210
ss4(ii)	0.61	34.26	1558	76
ss7(i)	1.981	87.33	628	24

3.3.2 Direct Path Signal Blockage

A rough sea in combination with a low elevation angle may result in the possible loss of the line of sight between the ship mounted receiver and the transmitting satellite. A method to realize this situation has been developed as part of the model. Considering the geometry of Figure 3-10, the antenna height may drop significantly in a rough sea. If this happens then the chance of the direct path signal being blocked increases.

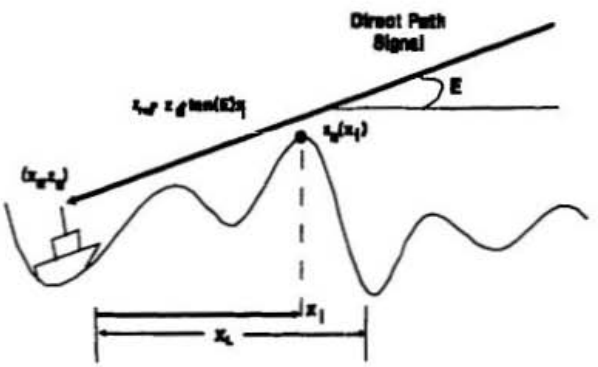

Figure 3-10: Direct Path Signal Blockage Geometry.

The antenna height at a particular time instant is calculated using the method described in Section 3.2. If this height falls below $2\sigma_z$ metres (arbitrarily chosen) then the possibility of the direct path signal being blocked may exist. If the antenna does fall below this value, the sea surface height $z_s(x)$ and the ray between the antenna and the satellite $z_a+x_l\tan E$ (x_l is the distance from the front of the ship to a sample point), must be compared to see if the ocean surface is higher than the ray height in an applicable

length of ocean in front of the vessel. If so, then the direct path is considered blocked. This search region x_L, is given by (3.56). It is divided into 50 evaluation points where the ray heights and the heights of the surface are compared.

$$x_L = \frac{12\sigma_z - z_a}{\tan E} \tag{3.56}$$

The surface $z_s(x)$ at $x=x_l$ is calculated by the method of Section 3.2 or, more specifically using (3.41). Once again, we are combining deterministic and statistical analyses in a rather *ad-hoc* fashion. It was found that the situation where the direct path signal is blocked only occurs in an extremely rough sea in combination with a low antenna height and a low elevation angle. As an example of the number of blockages that may occur, Figure 3-11 depicts the height variation of an antenna for sea state 7(ii) (σ_z=2.82m, Λ=116.27m), an elevation angle of 5°, and an antenna height of 5 metres. For lower sea states, it was found that direct path blockage is not of significant concern even for very low elevation angles and antenna heights.

To properly account for direct path blockage, one should incorporate diffraction effects if the ratio between ray height and the first Fresnel zone radius is sufficiently small (less than 2 [22]). Since the direct path will only be blocked under the worst case scenario (high sea state, low elevation angle, and low antenna height), such an analysis was not included in the model.

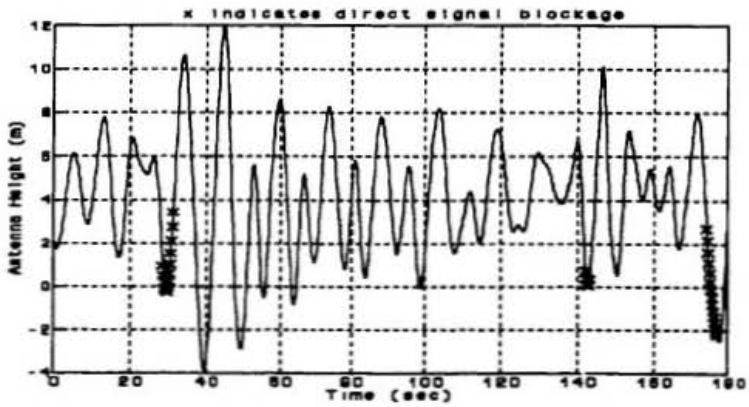

Figure 3-11: Direct Path Signal Blockage for ss7(ii), E=5°, and z_o=5m.

3.4 Attenuation Caused by Divergence

The attenuation caused by the divergence of the reflected signal is incorporated in a similar manner to that done for the aeronautical situation described in Section 2.2.3. A divergence weighting factor is calculated by using ray-optic theory. It was seen in Section 2.1.3.1 that in [1] Moreland stresses that for a concave scattering facet, if the receiving antenna is located near the focal point of the facet, the reflected signal may converge at the antenna and greatly increase the multipath power. Ray-optic approximations are not capable of easily incorporating this phenomenon. To identify such a situation while using our specular point curve crossing solution would be very demanding if possible at all. Since it was seen in [1], as well as in an ad-hoc

propagation model developed by the author, that this situation may only occur about three or four times in a two minute simulation run (with a sample interval on 0.05 seconds this corresponds to less than 5 occurrences out of 2400 sample points), it was decided that the lost accuracy by not using a more exact near field solution would be acceptable. By using ray-optics the divergence factors are given by (3.57) and (3.58) for a convex and a concave surface facet.

$$D^2(x) = \frac{1}{1+\frac{2d(x)}{r_c \sin\alpha(x)}}, \qquad z'' < 0 \ (\textit{convex facet}) \tag{3.57}$$

$$D^2(x) = \frac{1}{\frac{2d(x)}{r_c \sin\alpha(x)} - 1}, \qquad z'' > 0 \ (\textit{concave facet}) \tag{3.58}$$

The distance between the scattering point and the receiver is given by d(x), $\alpha(x)$ is the local grazing angle, and r_c is the surface radius of curvature around the scattering point. z'' is the surface second derivative at the scattering point. These are shown in Figure 3-12.

Using the following expressions,

$$d(x) = \frac{h(x)}{\sin\beta(x)} \tag{3.59}$$

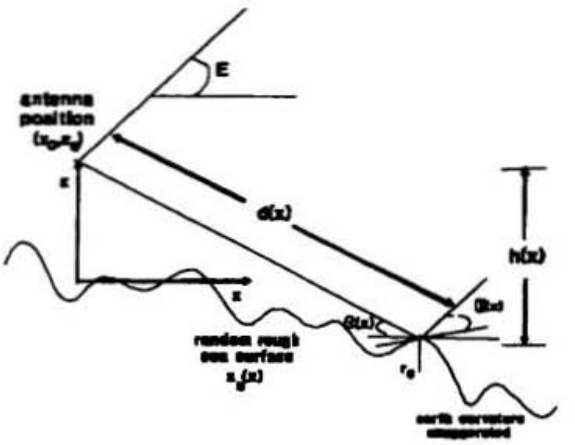

Figure 3-12: Divergence Parameters.

$$h(x) = z_a + \frac{x^2}{2a_e}, \tag{3.60}$$

a more explicit form of the convex divergence factor of (3.57) can be written.

$$D^2(x) = \frac{r_c \sin\beta(x) \sin\alpha(x)}{2h(x)} \left[\frac{1}{1 + \frac{r_c \sin\beta(x) \sin\alpha(x)}{2h(x)}} \right] \tag{3.61}$$

Using the ray-optics approximation for the radius of curvature of a surface as well as the expression for the slope of the surface $z_s'(x)$, we obtain the following.

$$r_c = \frac{[1 + z_s'(x)^2]^{\frac{3}{2}}}{|z_1''|} = \frac{[1 + \tan^2(\frac{E - \beta(x)}{2})]^{\frac{3}{2}}}{|z_1''|} \tag{3.62}$$

$$z_s'(x) = \tan\left(\frac{E-\beta(x)}{2}\right) \tag{3.63}$$

The surface second derivative at the specular point is given by z_1'' (or $z_s''(x_s)$). By introducing the following term,

$$Q(\alpha,\beta,x) = \frac{\left[1+\tan^2\left(\frac{E-\beta(x)}{2}\right)\right]^{\frac{3}{2}}}{2h(x)}, \tag{3.64}$$

and by substituting (3.62) into (3.61), we obtain an expression for the signal attenuation caused by the divergence from a convex surface portion.

$$D_{cx}^2(x) = Q(\alpha,\beta,x)\,\frac{1}{|z_1''|+Q(\alpha,\beta,x)} \tag{3.65}$$

Similarly, the signal attenuation caused by the divergence from a concave surface portion can be given by (3.66).

$$D_{cv}^2(x) = Q(\alpha,\beta,x)\,\frac{1}{|z_1''|-Q(\alpha,\beta,x)} \tag{3.66}$$

To simplify notation in future calculations, the following terms are introduced to represent the approximate radius of curvature at a specular point.

$$\hat{R}_{cx} = \frac{1}{|z_1''| + q(\alpha, \beta, x)} \tag{3.67}$$

$$\hat{R}_{cv} = \frac{1}{|z_1''| - q(\alpha, \beta, x)} \tag{3.68}$$

The subscripts CX and CV refer to convex and concave respectively. Since these radii of curvature are functions of the random variable z_1'', it is desirable to find a *mean radius of curvature*, which we shall refer to as M_{RC}, that includes both convex and concave surface facets. This is given by the following relationships.

$$M_{RC}(h, z_1', z_a) = M_{cx}(h, z_1', z_a) + M_{cv}(h, z_1', z_a) \tag{3.69}$$

$$M_{cx}(h, z_1', z_a) = \int_{-\infty}^{0} \hat{R}_{cx}(z_1', z_1'', z_a)\, f_{c1}(z_1'')\, dz_1'' \tag{3.70}$$

$$M_{cv}(h, z_1', z_a) = \int_{0}^{\infty} \hat{R}_{cv}(z_1', z_1'', z_a)\, f_{c1}(z_1'')\, dz_1'' \tag{3.71}$$

The term $f_{c1}(z'')$ in the above is a conditional density function for the second derivative of the sea surface which includes a constraint that specular points be a minimum distance apart. This is done to ensure that path length differences and reflected signal phases from adjacent specular points can be assumed to be independent. This density function is described in greater detail in Appendix A.

3.5 Average Multipath Power

In order to calculate the average power of the scattered signal, it is necessary to obtain an expression for a power density as a function of reflection angle β, similar to the one calculated for the aeronautical model in [1] given by (2.73). To develop this, we first formulate an expression that incorporates the effects of blocking, shadowing, and divergence into a single term.

3.5.1 Blocking, Shadowing, and Divergence Attenuation

Since the weighting factors for blocking, shadowing, and divergence attenuation all depend on the random ocean surface, it is desirable to combine them into one expression that can be used in the average scatter power calculation. This term is defined as the *effective radius of curvature* and is given by (3.72).

$$R(\beta_1, E_1) = w_B(\beta_1, z_1)\, w_S(E_1, z_1)\, M_{RC}(h, z_1', z_a) \tag{3.72}$$

Knowing the mean radius of curvature expression from (3.69), the expected value of (3.72) can now be written as the following.

$$E\{R(\beta_1, E_1)\} = \int_{-\infty}^{\infty} w_B(\beta_1, z_1)\, w_S(E_1, z_1)\, M_{RC}(h, z_1', z_a)\, f_{c2}(z_1)\, dz_1 \tag{3.73}$$

The $f_{c2}(z_t)$ term in (3.73) is another conditional density function. Like $f_{c1}(z'')$, a more detailed explanation of $f_{c2}(z_t)$ is presented in Appendix A.

3.5.2 Polarization Dependence

Up to this point, the polarization of the signal has not been considered. In order to calculate accurately the scattered power, we introduce a term $a(\beta)$ that incorporates the polarization of the receiving antenna as well as the complex reflection coefficients applicable at a scattering point on the ocean surface.

$$a_H(\beta) = G_H(g_a)\,\Gamma_H\left(\frac{E+\beta}{2}\right) \tag{3.74}$$

$$a_V(\beta) = G_V(g_a)\,\Gamma_V\left(\frac{E+\beta}{2}\right) \tag{3.75}$$

$$a_{RHC}(\beta) = \frac{a_H(\beta) + E_R e^{j\theta_a}\, a_V(\beta)}{2} \tag{3.76}$$

$$g_a = -\beta - \theta_{ss} \tag{3.77}$$

The subscripts H, V, and RHC represent horizontal, vertical, and right-hand-circular polarization respectively. The complex refection coefficient of the ocean surface at a grazing angle of α, is given by $\Gamma(\alpha)$. Expressions for the reflection coefficients are

given in Appendix B. E_R and θ_m represent the mismatch of the antenna gain and phase respectively. $G(g_a)$ is the gain function of the antenna where g_a is the angle at which the multipath signal arrives. Antenna gain patterns and mismatch considerations are presented in Appendix E.

3.5.3 Multipath Scatter Power Calculation

By combining the specular point density function $\lambda(\beta)$ from (3.37), with the effective radius of curvature weighting factor $R(\beta_1,E_1)$ from (3.73), and the polarization term $a(\beta)$, the multipath power density function can be expressed by (3.78).

$$S(\beta) = |a(\beta)|^2 \lambda(\beta) q(\alpha, \beta, x) E\{R(\beta_1, E_1)\} \tag{3.78}$$

Examples of the multipath power distribution are presented in Figures 3-13 to 3-15 for sea state 4(ii) with an omnidirectional antenna at a nominal height of 10 metres and elevation angles of 5° and 15°.

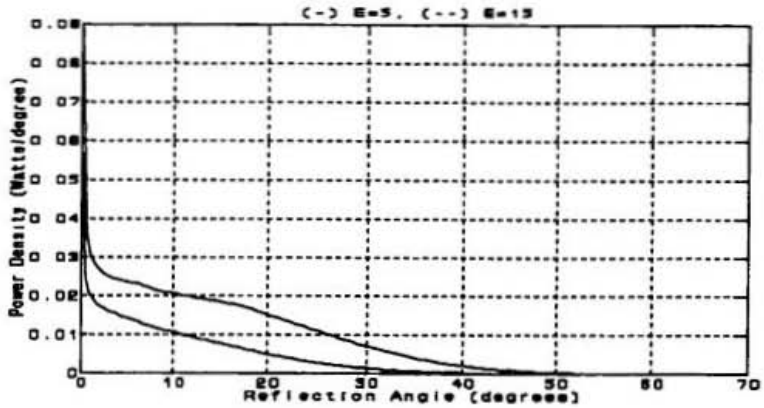

Figure 3-13: Power Density Curves for an Omni Antenna, ss4(ii), z_s=10m, Horizontal Polarization.

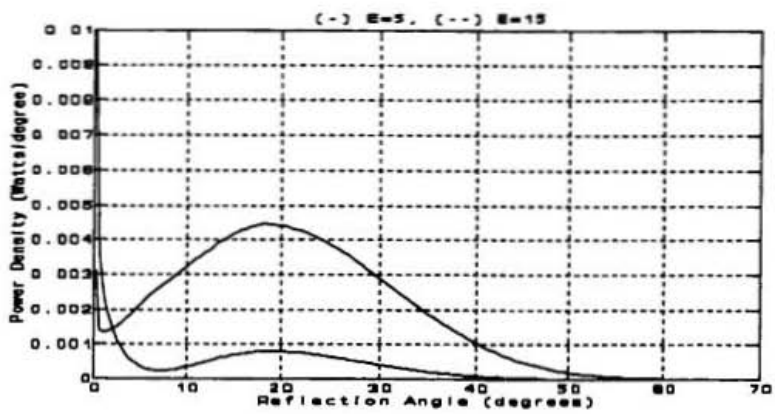

Figure 3-14: Power Density Curves for an Omni Antenna, ss4(ii), z_s=10m, Vertical Polarization.

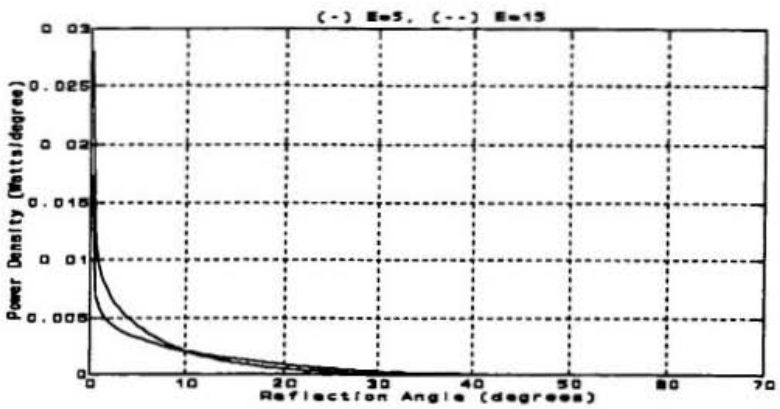

Figure 3-15: Power Density Curves for an Omni Antenna, ss4(ii), z_o=10m, RHC Polarization.

The average scatter power is calculated by integrating over the power density curves. For simplicity it is assumed that the power of the incident signal as it arrives at a specular scattering point is unity. The same applies for the direct path signal as it arrives at the antenna. Path losses in the satellite-to-receiver link as well as the satellite-to-specular point path are not considered. Knowing this, the average multipath scatter power can be written as the following.

$$P_m = \int_{\beta_{MIN}}^{\beta_{MAX}} S(\beta)\, d\beta \tag{3.79}$$

The angular integration limits are given by (3.39) and (3.40). It should be mentioned that most of the above calculations have been evaluated numerically using code

written in *Borland Turbo C V3.0*. In doing so, certain approximations had to be made to perform appropriate integrations. Most of the integrations were done using a *Simpson's 3/8 Rule* algorithm. Some of the necessary approximations for the numerical implementation of the model as well as their justifications are presented in Appendix C. A brief explanation of the code is given in Appendix D.

3.6 Signal Fade Calculations

Some of the most useful information that can be obtained from a multipath model are the signal fade characteristics. These include approximations to signal fade durations (T_D), fade occurrence intervals (T_I), and average fade depth (F_D). Fade duration, T_D, can be described as the amount of time that the received signal falls below some accepted level before it reaches that level again. Fade occurrence interval, T_I, refers to the amount of time from when the signal intensity drops below some specified level to the point in time where it drops below this level again. Fade depth, F_D, is the level the signal intensity will drop below, and remain below for a time of T_D, for a given percentage of the time. These are shown in Figure 3-16.

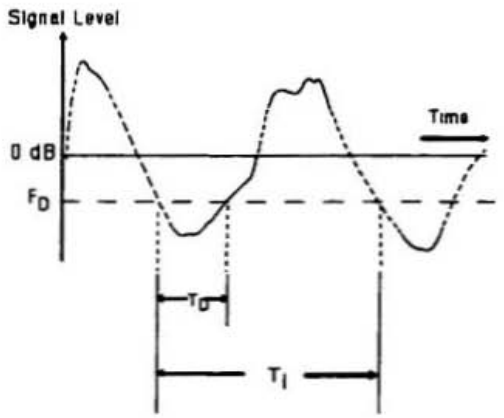

Figure 3-16: Fade Duration (T_D), Fade Occurrence Interval (T_I), and Fade Depth (F_D).

The 0 dB line in the above figure is assumed to be the signal level of the direct path signal, uncorrupted by multipath interference.

Fade durations and fade intervals can often be extracted from the power spectra of a multipath signal. A method to construct approximate power spectra of the scattered signal is presented in the following section and how this can be used to gain fade characteristics is explained in Section 3.6.2. Fade depth can be approximated by the signal-to-multipath noise ratio. This is explained briefly in Section 3.6.3. For a more in depth discussion of determining of fade characteristics, the reader is referred to Appendix F.

3.6.1 Power Spectra Determination

Several sources in the literature, such as [14], [15], [17], and [18], investigate the relationship between the power spectra of multipath signals and the angles of arrival of the various components of the scattered signal. These sources conclude that a reasonable approximation to the power spectrum can be constructed by exploiting the relationship between a doppler frequency shift, caused by the motion of a scatterer and the receiver, and the angle of arrival (or reflection angle). The basic concept is that for each reflection angle region on the ocean surface, there is a corresponding unique frequency shift caused by the movement of the surface and the movement of the receiver. Knowing this, the power spectra value at a particular frequency shift can be approximated by the power density function evaluated at the corresponding reflection angle. The power spectra $S_f(f)$ will take the form of a series of vertical lines distributed around the carrier frequency. If f_d is the doppler shift associated with the reflection angle region around β, then the appropriate power spectrum value is given by (3.80).

$$S_f(f_d(\beta)) = S(\beta) \tag{3.80}$$

In (3.80), $S(\beta)$ is the power density function given by (3.78). For the maritime multipath scenario, the appropriate doppler shift f_d, can be calculated by (3.81) [1].

$$f_d = \frac{v_x}{\lambda}(\cos\beta - \cos E) - \frac{v_z}{\lambda}(\sin\beta + \sin E) \tag{3.81}$$

$$v_x \approx u - DIR\alpha\sqrt{\Lambda} \tag{3.82}$$

$$v_z \approx \frac{z_a(t) - z_a(t-\Delta t)}{\Delta t} \tag{3.83}$$

The velocity of the vessel is given by u, DIR is equal to +1 if the vessel is moving with the ocean waves and -1 if it is moving against the waves, $\alpha\sqrt{\Lambda}$ ($\alpha \approx 1.02$) is an approximation of the average ocean wave velocity, and v_z is the vertical velocity of the antenna caused by the rising and falling of the ocean surface. λ is the carrier wavelength, which is about 0.2m at L-Band. The power spectrum obtained is an average of several power spectra taken at several instances in time.

Figure 3-17 presents examples of the power (or Doppler) spectra that can be obtained using the method described above. The parameters used for this example were ss4(ii), an omni antenna, an elevation angle of 10°, and a vessel velocity of 7m/s in the same direction as the average ocean wave velocity, as well as 5m/s in the opposite direction to the average ocean wave motion. The zero-frequency on the horizontal axis corresponds to the carrier frequency of the satellite-to-ship signal, which is around 1.54GHz at L-Band.

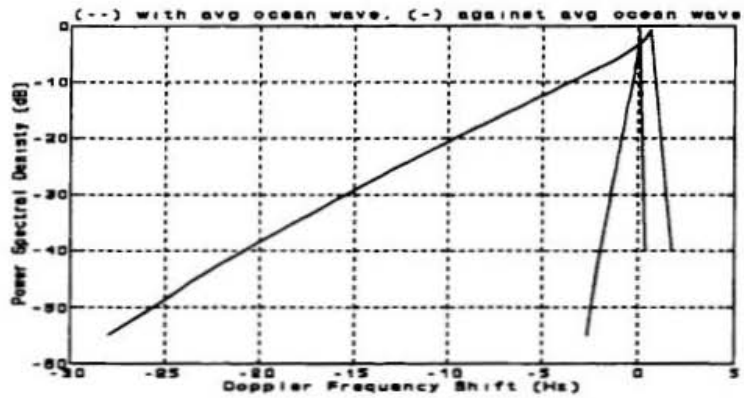

Figure 3-17: Power Spectra Approximations.

From the above figure, it is obvious that the power spectra obtained has inaccuracies. One would expect that the doppler shifts would be less one sided than what is obtained. For this case there should be more positive doppler shifts than are present and the resulting curve should be more bell-shaped, like those constructed as part of the propagation model of [1]. A possible explanation for this is that because we only use the *average* ocean wave velocity in the doppler shift calculation of (3.81), the relative velocity of (3.82) is always positive (for the situation of Figure 3-17) except for reflection angle values that are less than the elevation angle. To obtain a more accurate Doppler spectrum, one should incorporate the doppler shifts from each individual wave component making up the ocean surface and not just the average. With the ocean surface model used here, and our method of power spectra

determination, the author was not able to correct this problem as part of the research. However, the power spectrum obtained should give a close enough approximation from which reasonable signal fade characteristics can be acquired. How these parameters are extracted from the power spectra is described in the following section.

3.6.2 Obtaining Fade Occurrence Interval and Duration from Power Spectra

The average signal fade occurrence interval $\bar{T}_I$ (the average over all time of the fade occurrence intervals like the one depicted in Figure 3-16) can be found by using the power spectrum of the multipath signal (and hence the received signal). This is achieved by utilizing the theory presented in Section 14-4 of [23]. In order to use this approach, it must be assumed that the changing amplitude of received signal has a Gaussian distribution. It is often considered that the variation in received signal intensity due to maritime multipath scatter forms a Rician distribution, but for the purpose of finding the average fade interval in a relatively easy manner, it shall be assumed that a Gaussian distribution provides a close enough approximation. This should be the case given that the direct path signal is overwhelmed by the multipath components. For even moderately rough sea conditions at low elevation angles, this is usually true.

When investigating multipath fading, one is often confronted with terminology such as

a *p% availability* or a *(100-p)% outage*. This means that there is some value $F_{Dp\%}$ for which p% of the time the received signal is above. If a system was designed to handle a fade depth corresponding to $F_{Dp\%}$ then one would expect that, on average, for p% of the time the signal would be detectable. Or alternatively one can expect outages to occur about (100-p)% of the time. Therefore it is beneficial to know average fade depths, occurrence intervals, and fade durations so that one can design a receiving system that will ensure a p% signal availability. Alternatively one could estimate the reliability of a given system by calculating the average outage duration and the expected interval between outages.

Appendix F gives a detailed derivation of average fade occurrence intervals and durations. Using $\bar{T}_{Ip\%}$ for the average fade occurrence interval, $\bar{T}_{Dp\%}$ as the average fade duration, and S(f) as the power (or doppler) spectrum of the multipath signal, we can write the following expressions.

$$\bar{T}_{Ip\%} = \sqrt{\frac{\int_0^{\infty} S(f)\,df}{\int_0^{\infty} f^2 S(f)\,df}}\; e^{\frac{1}{2}\xi^2(p)} \tag{3.84}$$

$$\bar{T}_{Dp\%} = \left(1 - \frac{p}{100}\right)\bar{T}_{Ip\%} \tag{3.85}$$

$\xi(p)$ is extracted from the standard normal distribution curve as described in Appendix F. Common values of ξ are presented in Table 3-3 for several availability percentages.

Table 3-3: Relationship Between p% and ξ

p (%)	$\xi(p)$
1.00	2.33
50.00	0.00
90.00	-1.28
99.00	-2.33
99.90	-3.10
99.99	-3.49

3.6.3 Approximating Fade Depth

In the previous section, the variation in received signal level was assumed to be a Gaussian distribution. This was done so that fade intervals and fade durations could be calculated in a relatively straitforward manner by using the theory of [23]. This assumption is not entirely accurate. In [26] it is shown that the distribution of the

intensity of a signal arriving at a receiver which is a sum of a direct path as well as several scatter paths is Rician. In other sources that are specific to the multipath phenomenon as it relates to marine applications, such as [6] and [10], the received signal intensity, and therefore the fade depth, is said to be a *Rice-Nakagami* distribution. This is describe in more detail in Appendix F. However, it shall be assumed here that the received signal intensity is close enough to a normal distribution so that the Gaussian approximation may be maintained.

The average received signal intensity is assumed to be unity or 0dB. Since we are interested in the fade depth as it relates to the direct path power (*i.e.* the amount the signal increases or decreases due to multipath interference), we can normalize the received signal with respect to the direct path which results in the 0dB average. This makes the assumption that the multipath interference adds to the direct path signal constructively as often as it does destructively. Therefore, using the results of Appendix F, the fade depth, $F_{Dp\%}$, for any p% availability can be calculated using (3.86) and (3.87) where σ_m is the standard deviation of the multipath signal normalized with respect to the direct path level, P_m and P_D represent the average power of the multipath scatter signal and the average power of the direct path signal respectively, and $\xi(p)$ is taken from Table 3-3. From these equations it can be seen that the fade depth is a function of the normalized variance of the multipath signal and hence a function of the signal-to-noise ratio. Once again, the reader is referred to Appendix F

where a more detailed discussion of fade characteristics is presented.

$$F_{Dpk} = 10\log_{10}[\xi(p)\,\sigma_m + 1] \tag{3.86}$$

$$\sigma_m^2 = \frac{1}{2}\left(\frac{P_m}{P_D}\right) \tag{3.87}$$

Chapter 4

Simulation Results

In the previous chapter we developed a stochastic maritime multipath model. In order to establish the validity of this model it needs to be compared to measurement results as well as results from other models. In this chapter the results obtained with the stochastic maritime multipath model are compared to both the propagation model of [1] as well as the measurement results of [12] and [13]. We incorporate two non-directional antennas that were used in [1] and [13]. These are a conical spiral antenna referred to by the mnemonic *DFVLRC3*, and a small backfire antenna called *DFVLRC5*. From [12] we use a very directional adaptive array antenna which we label *CCMCAA*. An omnidirectional reference antenna is also implemented. Antenna patterns and characteristics are presented in Appendix E.

The first part of this chapter deals with proving the validity of the stochastic multipath model by comparing the results obtained with those from other sources. The last part

of the chapter investigates the impact various parameters such as sea state, antenna height and polarization, elevation angle, vessel velocity, and sea water versus sea ice have on the multipath power.

4.1 Validation of the Maritime Stochastic Multipath Model

The validation of the stochastic maritime multipath model shall be investigated by comparing results obtained through incorporating the four antennas mentioned in the previous section. These results are then compared to the results of other sources including [1], [12], and [13], which use these same antennas. The analysis of each antenna is divided into two parts. The first consists of a comparison of signal-to-noise ratios, or first order statistics, and the second part compares fade characteristics, or second order statistics. Since there is not an abundance of fade characteristics for an omni antenna in the literature, this part of the analysis is omitted for the omnidirectional antenna.

4.1.1 Omnidirectional Antenna

In order to compare our model to the propagation model of [1], the vessel is assumed to be 69m long, the nominal antenna height is given to be 20m and a sea state of ss4(ii) (σ_z=0.61m, Λ=34.26m) is present. It is also assumed that for the omni, small

backfire, and conical spiral antennas, the vessel is moving at approximately 5m/s against the ocean waves. Unless otherwise stated, these shall be the default parameters for all simulations presented in this chapter.

4.1.1.1 SNRs for the Omni Antenna

Using the above vessel and sea surface parameters, the following table can be constructed.

Table 4-1: Signal-to-Noise Ratios for the Omni Antenna.

E (°)	Polarization OMNI Antenna	SNR(dB)	
		Stochastic Model	From [1]
5	horizontal vertical RHC	5.24 15.18 10.90	2.3 12.5 9.2
10	horizontal vertical RHC	2.80 12.22 10.65	-0.02 9.6 8.2-10.6
15	horizontal vertical RHC	1.81 8.98 11.62	0.2 6.7-7.8 8.6-10.0
20	horizontal vertical RHC	1.49 6.87 13.19	-0.6-0.1 4.8 11.8

To gain a better understanding of how the signal-to-noise ratios compare between the stochastic model and the model from [1], a plot of elevation angle versus SNR for right-hand-circular polarization is presented in Figure 4-1. The dotted and dashed lines in the figure represent maximum and minimum SNRs found over a two minute simulation. Due to the slight variation in the SNR for the omni antenna, these dotted and dashed lines are not easily seen in Figure 4-1 because of the scale used for the plot. The maximum and minimum SNRs are more distinguishable for the more directional antennas of the following sections. In the cases that two data points from the results presented in [1] are present in Figure 4-1 for a particular elevation angle, these two points indicate a minimum and maximum SNR.

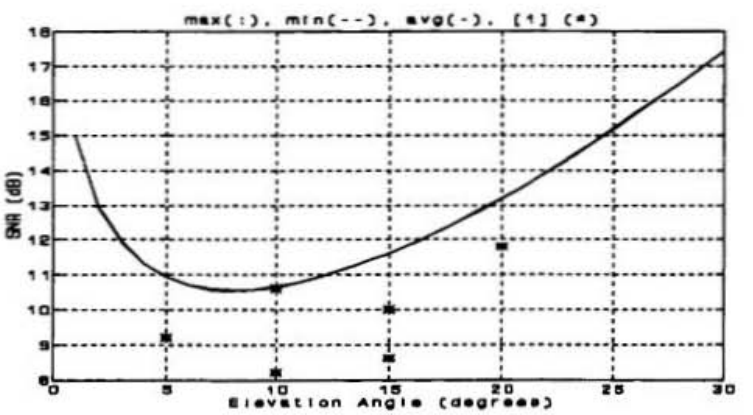

Figure 4-1: Signal-to-Noise Ratio as a Function of Elevation Angle for the Omni Antenna. RHC Polarization.

From Figure 4-1 and Table 4-1, it can be seen that the results from our stochastic model are slightly higher than those from [1]. However, they are in close proximity and both models produce the same trend of increasing SNR with increasing elevation. It is also noticeable that there is very little difference between average, minimum, and maximum SNR values. For an omnidirectional antenna with unity gain, there is almost no change in the observed SNRs at different instances in time. Therefore, the appearance of a constant SNR at a particular elevation angle over time is somewhat justified.

4.1.2 Conical Spiral Antenna

For the conical spiral antenna, or DFVLRC3, we use the same vessel and sea parameters that were given for the omni antenna in the previous section. The antenna gain mismatch E_R is assumed to be -3.0dB and the phase mismatch θ_m is chosen to be -28.6°. These values are consistent with [1] and they appear to produce results in the area of the values obtained with measurement. The experimental results of [13] are presented in Table 4-3 for both the DFVLRC3 and DFVLRC5 antennas. The values in Table 4-3 are for right-hand-circular polarization.

Table 4-2: Signal-to-Noise Ratios for the Conical Spiral and Small Backfire Antennas from [13]. (****) indicates destroyed data.

Elevation Angle (°)	SNR (dB)	
	DFVLRC3	DFVLRC5
3.8 to 4.0	8.6 to 9.1	7.9
7.1 to 7.9	8.6	7.9
9.8 to 10.3	9.7	****
16.3 to 16.8	10.0	10.3
18.8 to 19.3	10.2	12.2
22.2 to 22.4	****	14.4
25.9 to 26.9	10.7	15.0

4.1.2.1 SNRs for the Conical Spiral Antenna

By performing a two minute simulation, as was done for the omni antenna, and finding maximum, minimum, and average SNR values for a range of elevation angles, Table 4-3 and Figure 4-2 can be constructed relating SNR to elevation angle.

Table 4-3: Signal-to-Noise Ratios for the Conical Spiral Antenna.

E (°)	Polarization DFVLRC3 Antenna	SNR(dB)	
		Stochastic Model	From [1]
5	horizontal vertical RHC	6.17 16.43 9.42	4.3 15.3 9.2
10	horizontal vertical RHC	3.90 14.35 8.20	4.1 14.4 9.7
15	horizontal vertical RHC	3.04 14.35 8.16	2.6 10.7 9.2
20	horizontal vertical RHC	2.89 8.99 8.67	2.6-3.0 9.1-9.3 9.8-10.3

From Figure 4-2, it can be seen that the stochastic model produces similar results to those given in [1] as well as [13]. Since the DFVLRC3 antenna is slightly more directive than the omni antenna, a noticeable maximum and minimum SNR is obtained at each elevation angle. For this sea state (ss4(ii)) there is a variation in SNR of roughly ±0.5dB.

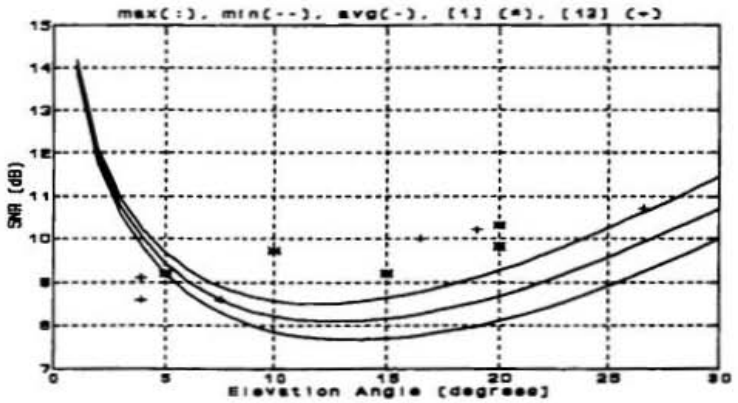

Figure 4-2: Signal-to-Noise Ratio as a Function of Elevation Angle for the Conical Spiral Antenna. RHC Polarization.

4.1.2.2 Fade Characteristics for the Conical Spiral Antenna

Using the methods described in Section 3.6, we can compare the fade depths and durations for the conical spiral antenna using the stochastic maritime multipath model with those obtained with the propagation model of [1]. This comparison is presented in Table 4-4.

Table 4-4: 99% Fade Characteristics for the Conical Spiral Antenna.

E (°)	Ship Velocity (m/s) with waves (+) against waves (-)	Average Fade Duration (99% availability) (sec.)		Approximate Fade Depth (99% availability) (dB)	
		Stochastic Model	From [1]	Stochastic Model	From [1]
5	-5.0	0.0578	0.0851	3.56	5.5
10	+7.0	0.5510	0.8370	4.45	6.5
15	-5.0	0.0473	0.0713	4.49	5.5
20	+7.0	0.4510	0.4850	4.06	5.0

In the above table, it can be seen that the results obtained for both fade duration and fade depth with the stochastic model are slightly smaller than those presented in [1]. It is not clear from [1] how the fade characteristics were calculated, therefore it is hard to compare the theory behind the two methods to see why the discrepancy exists. Although the values differ between the two sources, the general trends seem to be maintained, as SNRs, fade depths, and fade durations seem to increase and decrease in the same manner.

4.1.3 Small Backfire Antenna

Once again, through the use of the same ocean and ship parameters that were used for the previous two antennas, we compare the results obtained with the stochastic model for the DFVLRC5 antenna to those from [1] and [13]. The gain mismatch, E_R, of the antenna is assumed to be -5.5dB and the phase mismatch, θ_m, is chosen to be 0° [1].

4.1.3.1 SNRs for the Small Backfire Antenna

As was done for the previous antenna, a two minute simulation was performed at several elevation angles for the DFVLRC5 antenna. The results are presented in Table 4-5 and Figure 4-3.

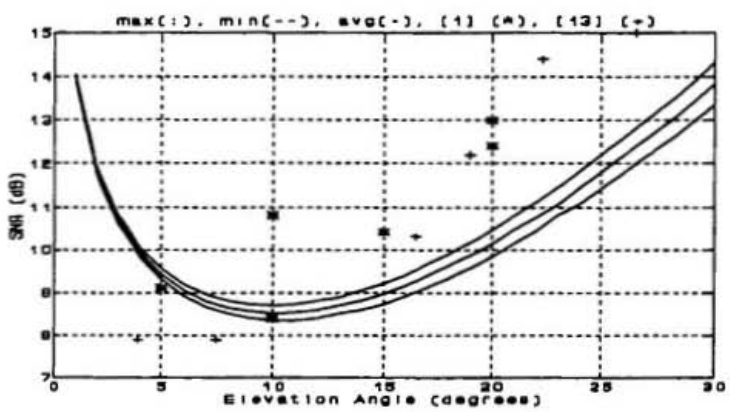

Figure 4-3: Signal-to-Noise Ratio as a Function of Elevation Angle for the Small Backfire Antenna. RHC Polarization.

Table 4-5: Signal-to-Noise Ratios for Small Backfire Antenna.

E (°)	Polarization DFVLRC5 Antenna	SNR(dB)	
		Stochastic Model	From [1]
5	horizontal vertical RHC	7.48 17.78 9.43	5.25 16.31 9.1
10	horizontal vertical RHC	5.98 17.16 8.52	3.8-6.2 14-16.3 8.4-10.8
15	horizontal vertical RHC	6.01 14.66 8.97	5.1 13.5 10.4
20	horizontal vertical RHC	6.83 13.40 10.14	6.3-6.7 12.0-13.0 12.4-13.0

Like the DFVLRC3 antenna, it can be seen that for the DFVLRC5 antenna the SNRs obtained with the stochastic model are in fairly good agreement with both the results from [1] and the experimental results of [13]. However, for both the DFVLRC3 and the DFVLRC5 antennas, the SNRs from the stochastic model and those from [1] are significantly higher than values from [13] at very low elevation angles (below 5 degrees). From Figure 4-3, it can be seen that over the two minute simulation the

SNR for the small backfire antenna fluctuated around the average value by about ±0.4dB.

4.1.3.2 Fade Characteristics for the Small Backfire Antenna

Like the previous two antennas, a comparison between average signal fade duration and fade depth can be made. This is presented in Table 4-6.

Table 4-6: 99% Fade Characteristics for the Small Backfire Antenna.

E (°)	Ship Velocity (m/s) with waves (+) against waves (-)	Average Fade Duration (99% availability) (sec.)		Approximate Fade Depth (99% availability) (dB)	
		Stochastic Model	From [1]	Stochastic Model	From [1]
5	-5.0	0.0616	0.0851	3.54	5.5
10	+7.0	0.6970	1.1100	4.21	8.0
15	-5.0	0.0533	0.0790	3.85	7.3
20	+7.0	0.4940	0.4240	3.14	6.5

As was the case with the conical spiral antenna, the fade characteristics obtained for the small backfire antenna are somewhat lower than those found in [1]. However, like the conical spiral, the trends in the data due to changing elevation and velocities seems to be consistent.

4.1.4 Adaptive Array Antenna

The conditions under which the experiments of [12] were conducted were much different than the ones present in [13]. From conversations with individuals at the Canadian Centre for Marine Communications who were involved with this exercise, it was discovered that during almost the entire time data was recorded, the sea was extremely smooth. In order to approximate this, a very low sea state is assumed. The lowest sea state in Table A.1 of Appendix A is ss1. Even with an RMS waveheight of only 0.0762m and an average sea wavelength of 6.1m, it was found that results obtained using ss1 were not in very good agreement with those presented in [12]. Therefore, a simulation was performed with an RMS waveheight of 0.01m and an average sea wavelength of about 2m. This seemed to provide values of SNR and fade characteristics that were in close proximity to [12]. The length of the ship is assumed to be 70m and the height of the antenna was approximately 10m. Since the sea was so calm, the velocity is assumed to be about 7m/s in the same direction of the ocean waves. The only information about the CCMCAA antenna given in [12] is the equation for the gain as given in Appendix E. It should be noted that this formula is given for elevation angle between 5° and 35°. The value it produces for amplifying the multipath power arriving at very low or even negative angles (with respect to the horizontal) may be questionable.

4.1.4.1 SNRs for the Adaptive Array Antenna

Using the sea and vessel parameters presented in the previous section, a comparison between the SNRs obtained with the stochastic model and those given in [12] can be made. It was found that the best agreement to the measured values of [12] was obtained by assuming an antenna gain mismatch of -5.5dB with a phase mismatch of 0°. Comparisons between the stochastic model results and those from [12] are presented in Table 4-7 and Figure 4-4. All values are for right-hand-circular polarization.

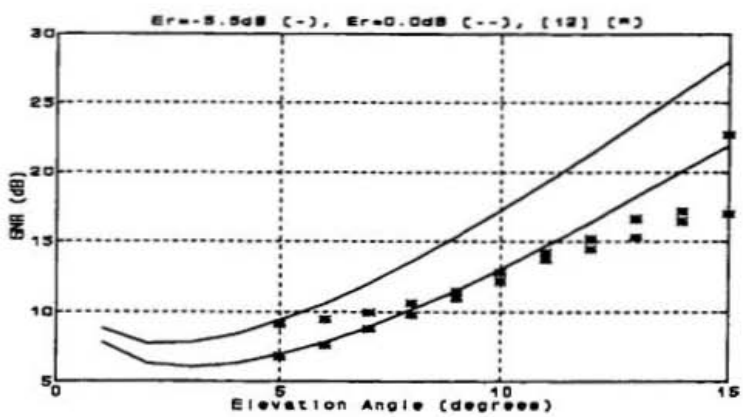

Figure 4-4: Signal-to-Noise Ratio as a Function of Elevation Angle for the Adaptive Array Antenna. RHC Polarization

Table 4-7: Signal-to-Noise Ratios for the Adaptive Array Antenna.

E (°)	SNR (dB) CCMCAA Antenna			
	Stochastic Model E_R=-5.5dB θ_m=0°	Stochastic Model E_R=0dB θ_m=0°	From [12] Minimum SNRs	From [12] Maximum SNRs
5	6.93	9.37	6.79	9.10
6	7.81	10.60	7.58	9.42
7	8.89	12.03	8.76	9.94
8	10.12	13.61	9.78	10.61
9	11.52	15.36	10.94	11.46
10	13.05	17.25	12.18	12.79
11	14.66	19.23	13.72	14.17
12	16.40	21.34	14.48	15.21
13	18.18	23.50	15.32	16.62
14	20.03	25.74	16.47	17.18
15	21.92	28.03	17.02	22.71

From the above results, it can be concluded that the stochastic model provides realistic values for signal-to-noise ratios for the adaptive array antenna used in the measurement exercises of [12].

4.1.4.2 Fade Characteristics for the Adaptive Array Antenna

Using the methods of Section 3.6 along with the vessel and sea parameters listed in Section 4.1.4, a comparison between signal fade depths and durations calculated with the stochastic model and those given in [12] can be made. This is presented in Table 4-9 for various elevation angles.

Table 4-8: 99% Fade Characteristics for the Adaptive Array Antenna.

E (°)	Ship Velocity (m/s) with waves (+) against waves (-)	Average Fade Duration (99% availability) (sec.)		Approximate Fade Depth (99% availability) (dB)	
		Stochastic Model	From [1]	Stochastic Model	From [12]
5	+7.0	0.892	Not Avail.	5.84	6.90-9.25
8	+7.0	0.624	Not Avail.	3.12	5.50-6.20
12	+7.0	0.337	Not Avail.	1.25	2.80-3.20
15	+7.0	0.233	Not Avail.	0.615	1.40-2.05

In [12], values for fade durations are not explicitly given. It is mentioned that fades of "several seconds" were experienced. The stochastic model was not able to simulate these long fades. This could be due to the fact that during the data gathering exercise of [12], the sea was *extremely* calm. A perfectly calm sea would lead to only one specular reflection point on the ocean surface where the reflection angle equalled the

elevation. This would result in a Doppler spectrum very closely resembling a spike at the carrier frequency. Because of this, it can be seen from (3.84) and (3.85) that, in theory for a one-dimensional rough surface (which is what we have used for this study), this could result in an constant fade of infinite duration. The stochastic model developed in this thesis is not able to deal with such a calm sea, since a very calm sea would have short wavelengths (shoter than the carrier signal) with small waveheights, and this would violate Kirchoff rough surface scatter theory. However, since it can be seen that the stochastic maritime multipath model developed produces results that are in *fairly* good agreement with the results obtained from [1], [12], and [13], it does not seem unreasonable to assume that the stochastic model is valid and we can proceed to the next section and investigate the effects of various satellite-to-ship system parameters on the multipath phenomenon.

4.2 Investigation of the Effects of Various Ocean and Receiver Parameters

In this section, we explore the effects that various ocean and receiver parameters have on the multipath phenomenon, and therefore the effect they have on the performance on a receiving system in a satellite-to-ship communication link. The parameters investigated include elevation angle, antenna height, antenna polarization, vessel velocity, sea state, as well as sea water versus sea ice. Each of these is examined

separately in the following sections. Since we are more interested in the change in the model output as we vary parameters than we are in actual values, we shall incorporate an omnidirectional antenna throughout the following investigations. Unless otherwise mentioned, the polarization throughout the following sections is assumed to be right-hand-circular.

4.2.1 Effects of Antenna Height

In order to investigate the effects of varying the antenna height, the elevation angle is kept constant at 10°, a vessel velocity of 5m/s in the opposite direction of the average ocean wave component velocity is used, sea state ss4(ii), and a signal availability of 99% (1% outage) is assumed. Using these parameters and by varying the antenna height, the following table can be constructed.

Table 4-9: Effects of Antenna Height.

Antenna Height (m)	SNR (dB)	$T_{D99\%}$ (sec.)	$F_{D99\%}$ (dB)
5	10.76	0.0477	2.76
10	10.65	0.0467	2.82
15	10.63	0.0519	2.86
20	10.63	0.0532	2.88

From Table 4-9, it can be seen that varying the antenna height results in only small changes in the model output. Changes of only a few tenths of a dB are achieved from moving the antenna from a height of 20m down to 5m. This would lead one to believe that the height of the antenna on a moving vessel is very insignificant in attempting to combat the effects of multipath interference. One could try positioning the antenna as low as possible on the vessel. Even though this may decrease the amount of multipath noise received, it would increase the risk of loosing the direct path signal due to blockage by the ship's hull.

4.2.2 Effects of Antenna Polarization

Although for most marine satellite communication systems the signal is circularly polarized, it is still interesting to observe the effects on multipath interference for different polarizations. Table 4-10 presents results obtained for an omni antenna, sea state ss4(ii), a nominal antenna height of 20m, and a vessel velocity of 5m/s against the average ocean wave component motion.

From the Table 4-10, it can be seen that vertical polarization discriminates against multipath interference more at low elevation angles than do either horizontal or right-

Table 4-10: Effects of Antenna Polarization.

E (°)	Horizontal			Vertical			RHC		
	SNR (dB)	$T_{D99\%}$ (sec.)	$F_{D99\%}$ (dB)	SNR (dB)	$T_{D99\%}$ (sec.)	$F_{D99\%}$ (dB)	SNR (dB)	$T_{D99\%}$ (sec.)	$F_{D99\%}$ (dB)
5	5.23	0.0377	10.08	15.18	0.0260	1.47	10.92	0.0604	2.75
10	2.81	0.0342	20.00	12.22	0.0248	2.25	10.64	0.0532	2.88
15	1.81	0.0309	95%	8.98	0.0246	3.84	11.60	0.0464	2.47
20	1.49	0.0279	94.5%	6.87	0.0235	5.97	13.18	0.0406	1.95

hand-circular due to the small value of the surface reflection coefficient for vertical polarization at grazing angles near the Brewster angle [1] (around 7° for sea water and L-Band frequencies). Above an elevation of 10° it is clearly seen that circular polarization is far superior over either horizontal or vertical. A 99% fade depth could not be calculated for an elevation of 15° and 20° with horizontal polarization. With such small SNRs, by inverting (3.86) it can be found that the best one can hope for is that one will have a detectable signal between 94% and 95% of the time for these two situations. The rest of the time, it disappears completely.

4.2.3 Effects of Sea State

As one might expect, the rougher the sea becomes, the more diffusely the multipath signal scatters. Because of this, it is less concentrated, and therefore less likely to

cause a great deal of interference at the receiver. A rough sea will result in shallow rapid fades. The smoother the sea becomes, then the more concentrated the multipath signal is, and one will experience much deeper and longer fades than for the rougher sea. This is seen in Table 4-11. In this table, the vessel is assumed to be moving at 5m/s against the ocean waves, and a constant elevation of 10° is present.

Table 4-11: Effects of Sea State.

Sea State	RMS Waveheight (m)	Average Sea Wavelength (m)	SNR (dB)	$T_{D99\%}$ (sec.)	$F_{D99\%}$ (sec.)
ss2(i)	0.1675	12.20	8.75	0.0976	4.00
ss4(i)	0.5250	30.75	10.34	0.0582	3.02
ss6(i)	1.1430	57.25	12.20	0.0386	2.25
ss7(ii)	2.8200	116.27	14.68	0.0278	1.57

4.2.4 Effects of Vessel Velocity

Using parameters similar to the following sections, Table 4-12 gives the effects that changing the velocity of a vessel have on the multipath phenomenon. A vessel velocity in same direction as the velocity of the average ocean wave component is indicated by a plus sign and a velocity in the opposite direction than that of the average ocean wave component is indicated by a minus sign.

Table 4-12: Effects of Vessel Velocity.

Vessel Velocity	SNR (dB)	$T_{D99\%}$ (sec.)	$F_{D99\%}$ (dB)
-10.0	10.64	0.0365	2.88
-5.0	10.63	0.0532	2.88
+5.0	10.64	0.0601	2.88
+10.0	10.64	0.0147	2.88

From this analysis, it can be inferred that changes in vessel velocity make very little difference in the multipath power. The significant aspect of vessel motion is whether or not it is moving with or against the ocean waves. The smaller the absolute value of the relative velocity between the velocity of the vessel and that of the average ocean wave component (in this case, the average ocean wave component velocity for ss4(ii) is about 6m/s) the longer the fade durations. This would suggest that fade duration is a somewhat even function of relative velocity.

4.2.5 Effects of Elevation Angle

In the presentation of polarization effects of Section 4.2.2, the elevation angle was varied. It would be redundant to reproduce a table here describing the effects of elevation angle. From Table 4.10, it can be seen that, in general, for right-hand-

circular polarization as elevation angle increases, so does the signal-to-noise ratio therefore decreasing the fade depth as well as the average fade duration. For vertical and horizontal polarization, the trend seems to be a drastically decreasing SNR with increasing elevation. This indicates that circular polarization is more robust and not as sensitive to changes in elevation angle as either horizontal or vertical polarization, which makes it a suitable choice for maritime satellite communication systems.

4.2.6 Sea Water Versus Sea Ice

During winter months in the north Atlantic ocean, ice is often commonplace. Because of this, it is interesting to examine the differences in the results obtained with a vessel travelling in sea water and one travelling in sea ice. To make the change between water and ice one need only change the dielectric constant and conductivity in the ocean surface reflection coefficients which are listed in Appendix B. It is suggested that for first year sea ice at L-Band the dielectric constant is about 3.48 and the conductivity is approximately 0.02 mho/m. Table 4-13 presents a comparison between results obtained with a sea state of ss4(ii) and a ship velocity of 5 m/s against the average ocean wave component for both sea ice and sea water. It must be mentioned that when dealing with ice, one may encounter sharp edges and steep slopes on the surface. This may cause a breakdown in the stochastic model as much of its foundation is based on the Kirchhoff approximation which is invalid in the presence of

sharp edges. At the present time, a frozen ocean surface is modelled in the same manner as a liquid surface with only a change in the reflection coefficient. Because of the simplistic nature of this modelling, the results obtained may be somewhat inadequate but they should provide an idea of how the multipath process changes between a frozen and a liquid ocean surface. Clearly there should be more effort put into modelling the countless forms of sea ice, but due to time constraints, this was not accomplished with this model.

Table 4-13: Differences in Multipath Scatter from Sea Water and Sea Ice.

E (°)	SNR (dB)		$T_{D99\%}$ (sec.)		$F_{D99\%}$ (dB)	
	Water	Ice	Water	Ice	Water	Ice
5	10.92	7.69	0.0604	0.0511	2.75	4.95
10	10.64	6.38	0.0532	0.0478	2.88	6.79
15	11.60	6.61	0.0464	0.0436	2.47	6.38
20	13.18	7.66	0.0406	0.0392	1.95	4.98

From the above table, it can be seen, that in general, sea ice will produce much deeper fades but with shorter duration than sea water. Assuming that ice will be moving slower than water, there will be a rather large relative velocity between the ship and the surface, which would account for the shorter fade durations.

4.2.7 Effects of Antenna Directivity

Since the stochastic model implements four antenna patterns with varying degrees of directivity, it is interesting to investigate how the multipath phenomenon effects the received signal obtained using each of these antennas. Table 4-14 presents the signal-to-noise ratios and fade characteristics for the four different antennas for sea state ss4(ii), an elevation angle of 10°, a vessel velocity of 5m/s against the average ocean wave, and using the gain and phase mismatch values given in Section 4.1.

Table 4-14: Effects of Antenna Directivity.

Antenna	SNR	$T_{D99\%}$	$F_{D99\%}$
Omni	10.63	0.053	2.88
DFVLRC3	8.19	0.052	4.46
DFVLRC5	8.50	0.057	4.20
CCMCAA	17.53	0.200	1.07

From the patterns presented in Appendix E, the conical spiral antenna (DFVLRC3) and the small backfire antenna (DFVLRC5) have somewhat similar patterns and therefore produce much the same results. The very directive array antenna (CCMCAA) discriminates against the multipath interference considerably. Even though the fade duration is significantly longer than it is for the other antennas, the

fade depth is quite small. The values in Table 4-14 would lead one to believe that a highly directive antenna, such as the CCMCAA antenna, is very desirable. This may not be the case. Besides the added cost that would be associated with a very directional antenna, there are also depointing effects introduced by such a narrow beam. This may cause a great deal of signal fluctuation in rough seas, especially on small vessels. If the narrow beam of the antenna is steered away from the direct path and points toward the ocean surface the multipath components may be amplified more than the direct path signal. Even though the multipath effects may be lessened if the main beam of the antenna pointed toward the transmitter, depointing effects may still cause problems if a rough sea introduces a great deal of antenna motion. One must be prepared to make a trade off between reducing multipath interference, cost, and depointing effects when choosing a receiver, especially for small vessels whose motion is effected by the ocean movement more than larger ones.

Figure 4-5 shows the variation of the signal-to-noise ratios for the four antennas over time with an elevation angle of 10° and ss4(ii). It is clearly seen that the narrow beam array antenna experiences the most fluctuation over time. The vessel is assumed to be 69m long for this simulation.

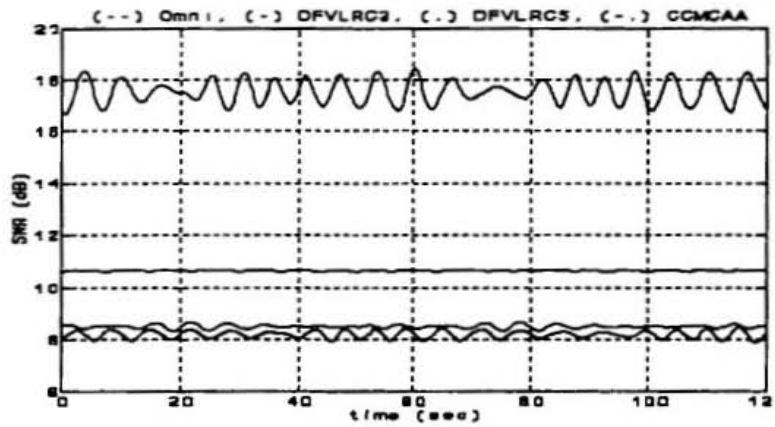

Figure 4-5: Antenna Directivity Comparison

Chapter 5

Conclusions and Recommendations for Future Work

5.1 Conclusions

An intense investigation of multipath communication signals with applications to a marine environment has been performed. To achieve this, a numerical stochastic maritime multipath model was developed. This model has been proven to be a valid and useful tool that can be used to study the multipath interference effects in a satellite-to-ship L-Band communication system. Although in its present form it is, on the surface, a somewhat simple application which can be run on even the most modest personal computers, it has been seen that it can be used to provide quick evaluations of a ship mounted receiving system which is characterized by its antenna gain pattern as well as its position on a ship which is travelling on an ocean surface of any given degree of roughness (as long as it satifies the Kirchoff critera).

It was found that several factors influence the amount of signal fading that a receiving system may experience due to multipath interference. Among these include the elevation angle to the transmitting satellite, the sea state, the polarization of the propagating signal, the position of the receiving antenna aboard a vessel, the velocity of that vessel, as well as the directivity of the antenna pattern.

By performing several simulations which investigated how each of these parameters effected the degree of multipath fading encountered, it was found that the most influential variables included sea state, elevation angle, and signal polarization. Unfortunately these factors are not controllable and nothing can realistically be done to lessen the effect they have on the multipath phenomenon. It is, however, interesting to examine how changes in these parameters effect the amount of multipath fading a ship mounted receiving system encounters.

It was seen that as the elevation angle to the transmitter increased, the general trend tended to be an increase in the signal-to-noise ratio and therefore a decrease in the amplitudes of signal fades. This is an interesting observation, but the operator of a vessel cannot choose the elevation angle between the vessel's receiver and the transmitting satellite. It was also observed that as the sea state increased (ocean became rougher) and the scattered signal become less coherent, the depth of signal fades lessened. For a smooth sea surface along with a relatively low elevation, signal

of a dB for height differences of 15 metres. Although not a significant improvement, it would lead one to believe that it would be worth the effort to place an antenna aboard a vessel as low as possible without risking the possibility that the direct signal path is impeded by the superstructure of the vessel at low elevation angles and in rough sea conditions. As one would expect, it was seen that the more directive the receiving antenna is, the better the performance of the receiver will be. Of course an antenna with a narrow beam in the direction of the direct path signal will be more costly than an omnidirectional one, and if no form of antenna stabilization is implemented, one may risk depointing effects on small vessels travelling in rough seas as the main beam of the antenna moves away from the direct path due to the ocean movement effects on the ship. This depointing effect could be lessened through the use of a stabilizer, or through the use of an adaptive beam forming or mechanically steered antenna which could adapt its gain characteristics by using the satellite beacon signal to determine in what direction its maximum gain should be pointing.

Fading could also be suppressed by implementing more than one antenna, each mounted in different positions aboard the vessel, and using signal comparison techniques to determine which antenna the receiver should take its signal from at any instant in time. Ideally the receiver would choose the antenna which is obtaining a signal with the least amount of multipath corruption. This is often referred to as antenna site diversity. Although these methods may be effective, they do add cost to

the receiving system which is in contrast to the idealogy of a low cost satellite communication receiving system that is affordable to small scale vessel operators.

From the simulations performed as part of this thesis and the results they produced, it may be concluded that the only realistically simple and low cost techniques that could be implemented would be the determination of an optimal antenna position aboard the vessel and developing an antenna pattern that consists of a compromise between being directive enough such that it is resistant to the multipath signal components coming from the sea surface, and has a wide enough main lobe such that depointing effects are not a problem in rough seas while allowing for adequate amplification of the direct path signal form a wide range of elevation angles. Another alternative may be the construction of a low cost antenna stabilizer, such as the mobile antenna stabilization platform mentioned in [34], that would decrease the depointing effects if a relatively directive antenna is implemented.

5.2 Recommendations for Future Work

Although a useful multipath model has been developed and some intriguing results have been obtained, there is still a great deal of work that could be undertaken using the accomplishments of this thesis as a foundation. This includes improvements to the model as well as more in-depth investigations into the multipath phenomenon.

At the time being, the actual numerical model is, on the surface, quite basic. A simple input screen allows the user to input the desired ocean, vessel, and antenna characteristics. One possibility of future work could include improvements to the actual source code of the model to make it more efficient or to develop some form of graphical user interface that allows easy parameter input and even perhaps incorporating some graphical capabilities so that the user would not have to rely on using other software packages to produce plots (most of the graphs presented in this thesis have been constructed using Matlab). To incorporate equations for new antenna patterns, at the present time, would require changing the antenna gain subroutines and recompiling the model code. A simple input mechanism for including additional antenna patterns would be very useful. The refinement of the user friendliness of the model may be appropriate for a small undergraduate project for an aspiring engineering or computer science student.

The actual theory of the model could be improved upon as well. It was seen in Chapter 3 that the power spectra produced were somewhat different than what one might expect from an ocean scattered multipath signal. This was caused by the assumptions used in the ocean surface modelling process. The model only considers the velocity of the *average* ocean wave component of a given sea state when calculating the Doppler frequency shift from a particular reflection angle region. A method that takes into account *all* of the velocities of the various surface components

making up the ocean wave profile when constructing the power spectrum would be extremely beneficial and may result in the calculation of more precise fade characteristics.

Improvements could be made to the model so that very low elevation angle scenarios could be investigated. The model developed seems to be valid at elevation angles above about 5°. Improving the stochastic model or developing a new model for very low and even grazing incidence angles would be extremely beneficial.

The way in which the model accounts for direct path blockage could also be improved upon. At the time being, the model determines if the direct path signal is blocked by the ocean surface and if so, it considers the signal to be lost for that instant in time. To be more precise, diffraction effects should be taken into account which would allow a more realistic representation of direct path signal obstruction by the ocean surface than is currently implemented.

An investigation of a much wider range of scenarios than that which has been done in this thesis would also be warranted. It would be interesting to investigate several different antenna patterns as well as the results these produce if placed on vessels of various sizes and shapes. Incorporating actual ship superstructures and seeing what kinds of effects this would have on a particular receiving antenna in the presence of

multipath may be interesting. This may be better investigated through some form of physical scale modelling than through numerical techniques, but it would be an interesting undertaking nonetheless.

One final suggestion for future research is the expansion of the model so that it could be used to evaluate more than L-Band data transmission satellite-to-ship systems. With the increase in offshore oil development off the coast of Canada, it may be beneficial to acquire information on oil platform dynamics and investigate the effects that multipath fading may have on communication signals that antennas mounted on these structures receive.

References

[1] Moreland K.W., "Ocean Scatter Propagation Models for Aeronautical and Maritime Satellite Communication Applications", *MEng Thesis*, Carleton University, Ottawa, 1987.

[2] Moreland K.W., "Simulation of Maritime Multipath and Structure Effects", Miller Communications Systems Ltd., Technical Report, MCS File No. 8448, INMARSAT Contract No. INM/84-078, 1985.

[3] Beckmann P. and A. Spizzichino, *The Scattering of Electromagnetic Waves From Rough Surfaces*, The MacMillan Company, New York, 1963.

[4] Cramer H. and A. Leadbetter, *Stationary and Related Stochastic Processes*, John Wiley & Sons Inc., New York, 1967.

[5] Leadbetter L., G. Lindgren, and H. Rootzen, *Extremes and Related Properties of Random Sequences and Processes*, Springer-Verlag, New York, 1983.

[6] Tseung F., "The Multipath Channel Characterization for a Ship/Satellite Communication System", *MSc Thesis*, George Washington University, Washington DC, 1979.

[7] Sobiesk *et al.*, "Sea Surface Scattering Calculations in Maritime Satellite Communications", *IEEE Trans. on Communications*, Vol. 41, No. 10, pp. 1525-1533, October, 1993.

[8] Karasawa Y. and T. Shoikawa, "Characteristics of L-Band Multipath Fading due to Sea Surface Reflection", *IEEE Trans. on Antennas and Propagation*, Vol. 32, No. 1, pp.618-623, January, 1984.

[9] Karasawa Y. and T. Shoikawa, "Fade Duration Statistics of L-Band Multipath due to Sea Surface Reflection", *IEEE Trans. on Antennas and Propagation*, Vol. 35, No. 7, pp.951-956, August, 1987.

[10] Karasawa Y. and T. Shoikawa, "A Simple Prediction Method for L-Band Multipath Fading in Rough Sea Conditions", *IEEE Trans. on Communications*, Vol. 36, No. 10, pp.1098-1104, October, 1988.

[11] Fang *et al.*, "A Low Angle Propagation Measurement of 1.5GHz Satellite Signals in the Gulf of Mexico", *IEEE Trans. on Antennas and Propagation*, Vol. 30, No. 1, pp. 10-15, January, 1982.

[12] Hicks M., "Low Angle L-Band Satellite Signal Strength Measurements Over an Ocean Path", *Canadian Centre for Marine Communications Internal Report*, August, 1993.

[13] "Multipath Fading Effects and Data Transmission for Small Ship Earth Stations (Standard-C)", DFVLR German Aerospace Research Establishment, ESA/ESTEC Contract No. 5323/82/NL/JS, November, 1984.

[14] Clarke R., " A Statistical Theory of Mobile-Radio Reception", *Bell Systems Technical Journal*, July-August, 1968, pp. 957-1000.

[25] Malpole R. and R. Myers, *Probability and Statistics for Engineers and Scientists, Fourth Edition*, MacMillan Publishing Company, New York, 1989.

[26] Haykin S., *Communication Systems, Third Edition*, John Wiley and Sons Inc., New York, 1984.

[27] Rice S.O., "Mathematical Analysis of Random Noise", *Bell Systems Technical Journal*, Vol. 23, pp 282-333, July 1944; Vol. 24, pp. 96-157, January 1945.

[28] Kong J.A., *Electromagnetic Wave Theory*, John Wiley and Sons Inc., New York, 1986.

[29] Collin R.E., *Antennas and Radiowave Propagation*, McGraw-Hill Inc., New York, 1985.

[30] International Telecommunication Union, *Handbook on Satellite Communications (Fixed Satellite Service)*, CCIR International Radio Consultive Committee, Geneva, 1985.

[31] Dagleish D.A., *An Introduction to Satellite Communications*, Peter Perengrinus Ltd., London, 1989.

[32] Hudson J.E., *Adaptive Array Principles*, Peter Perengrinus Ltd., London, 1981.

[33] Stutzman W.L. and G.A. Theile, *Antenna Theory and Design*, John Wiley and Sons Inc., New York, 1981.

[34] *Partnership in Action*, Canadian Centre for Marine Communications Annual Report 1994-1995, St. John's, October 1995.

[35] Cox D.C., "Antenna Diversity Performance in the Mitigating Effects of Portable Radiophone Orientation and Multipath Propagation", *IEEE Trans. on Communications*, Vol. 31, No. 5, May 1983.

[36] Gager D.R., "Signal Fading Characteristics Due to Reflections from the Sea", *Marconi Review*, First Quarter, 1971.

[37] Densmore A.C. and Huang J., "Microstrip Yagi Array Antenna for Mobile Satellite Vehicle Applications", *IEEE Trans. on Antennas and Propagation*, Vol. 39, No. 7, July 1991.

Appendix A

Sea Surface Parameters

The maritime multipath model we have developed makes use of various parameters that characterize the ocean surface distribution of a particular sea state. These parameters include the RMS waveheight and average sea wavelength. The scatter power determination incorporates various conditional density functions relating to the distribution of the ocean surface height, slope, and second derivative. These distributions and parameters are presented in the following sections.

A.1 Sea State Table

The parameters that are used to characterize a specific two dimensional sea surface profile are the RMS deviation in surface waveheight σ_z, and average sea wavelength Λ. Chapter 5 of [17] presents a table comparing sea state, as defined by RMS waveheight, to critical grazing angle of an incident radar signal (the angle below

which specular reflection is insignificant). This comparison is given for various incident signal wavelengths. Using this as a basis, and assuming that the carrier frequency at L-Band is approximately 0.2m, Moreland [1] develops a similar table, part of which is presented here. The significant waveheight H_s is assumed to be $4\sigma_z$.

Table A-1: Sea State Parameters

Sea State Index	Significant Waveheight H_s (m)	RMS Waveheight σ_z (m)	Average Sea Wavelength Λ (m)
1	0.3048	0.0762	6.1
2(i)	0.67	0.1675	12.2
2(ii)	0.884	0.221	16.04
3	1.4	0.35	22.32
4(i)	2.1	0.525	30.75
4(ii)	2.44	0.61	34.26
5(i)	3.048	0.762	41.86
5(ii)	3.658	0.9145	48.77
6(i)	4.572	1.143	57.75
6(ii)	5.49	1.3725	65.82
7(i)	7.925	1.981	87.33
7(ii)	11.28	2.82	116.27

$$f_{z''}(b|z=a, C, d_{\min}) = g_{z,z',z''}(a, m_x, b)\, f_{z''}(b|z=a) \tag{A.3}$$

$$g_{z,z',z''}(a, m_x, b) = \frac{P(d_{\min}|z'=m_x, z''=b)\ \ |b|}{\int_{-\infty}^{\infty} P(d_{\min}|z'=m_x, z''=b)\ \ |b|\ f_{z''}(b|z=a)\, db} \tag{A.4}$$

$$P(d_{\min}|z'=m_x, z''=b) = Q\left(\frac{\frac{-2|b|}{\Delta_{\min}} - K_3 m_x}{\sigma_{m_3}}\right) - Q\left(\frac{\frac{2|b|}{\Delta_{\min}} - K_3 m_x}{\sigma_{m_3}}\right) \tag{A.5}$$

$$f_{z''}(b|z=a) = \frac{1}{\sqrt{2\pi}\sigma_{m_2}} e^{-\frac{1}{2}\frac{(b-K_2 a)^2}{\sigma_{m_2}^2}} \tag{A.6}$$

$$K_2 = -\left(\frac{\sigma_{z'}}{\sigma_z}\right)^2 \tag{A.7}$$

$$K_3 = -\left(\frac{\sigma_{z''}}{\sigma_{z'}}\right)^2 \tag{A.8}$$

$$r_2 = \frac{-\sigma_{z'}^2}{\sigma_{z''}\sigma_z} \tag{A.9}$$

$$r_3 = \frac{-\sigma_{z''}^2}{\sigma_{z''}\sigma_{z'}} \tag{A.10}$$

$$\sigma_{m_2} = \sqrt{1-r_2^2}\ \sigma_{z''} \tag{A.11}$$

$$\sigma_{m_3} = \sqrt{1-r_3^2}\ \sigma_{z'''} \tag{A.12}$$

$$\sigma_{z'}=\frac{2\pi\sigma_z}{\Lambda} \tag{A.13}$$

$$\sigma_{z''}=\sqrt{3}\frac{\sigma_{z'}^2}{\sigma_z} \tag{A.13}$$

$$\sigma_{z'''}=8\sqrt{15}\frac{\sigma_z}{\Lambda^3} \tag{A.15}$$

In the above equations, m_x represents the approximate slope of the surface at a specular scattering point. This is derived in Section 3.1.1. The Q(x) function in (A.5) is equivalent to $0.5\text{erfc}(x/\sqrt{2})$ where erfc(x) is the complimentary error function.

To calculate the expect value of the effective radius of curvature term $E\{R(\beta_1,E_1)\}$, presented in Section 3.5.1, a second conditional density function is used. This function is given as $f_{c2}(z)$. For clarity, the following notation is introduced.

$$f_{cz}(a)=f_z(a|C,d_{\min}) \tag{A.16}$$

Using this representation it can be seen that $f_z(a|C,d_{min})$ is the conditional density function of the sea surface height evaluated at height a given the condition that the minimum distance between specular points is met by satisfying (A.2). Using this and the methods outlined in [1], (A.16) can be expanded as follows.

$$f_z(a|C, d_{\min}) = h_{z,z'}(a, m_x)\, f_z(a) \tag{A.17}$$

$$h_{z,z'}(a, m_x) = \frac{\int_{-\infty}^{\infty} P(d_{\min}|z'=m_x, z''=b)\ |b|\ f_{z''}(b|z=a)\, db}{\int_{-\infty}^{\infty} P(d_{\min}|z'=m_x, z''=b)\ |b|\ f_{z''}(b)\, db} \tag{A.18}$$

$$f_{z''}(b) = \frac{1}{\sqrt{2\pi}\sigma_{z''}} e^{-\frac{1}{2}\left(\frac{b}{\sigma_{z''}}\right)^2} \tag{A.19}$$

$$f_z(a) = \frac{1}{\sqrt{2\pi}\sigma_z} e^{-\frac{1}{2}\left(\frac{a}{\sigma_z}\right)^2} \tag{A.20}$$

Appendix B

Complex Surface Reflection Coefficients

The general Kirchhoff solution for the scattering of electromagnetic waves from rough surfaces presented in [3] does not incorporate the finite conductivity of the reflecting surface in the evaluation of the Helmholtz integral. Beckmann and Spizzichino [3], indicate that by incorporating the refection coefficients into the Helmholtz integral, the solution would become extremely difficult. The Kirchhoff solution is based on approximating the scattered field strength reflected from a point on a rough surface by the field strength that would be scattered from a tangent plane at that point. Because of this, if the surface is of finite conductivity, the reflected field strength can be approximated by the field strength that would be reflected from a perfectly conducting rough surface weighted by the smooth surface reflection coefficient evaluated at the grazing angle of the reflection point.

The complex reflection coefficients (or often termed Fresnal reflection coefficients) for a plane surface are derived by the finding the ratio of the reflected field to the

incident field. If an electromagnetic wave is incident upon a conducting surface at a grazing angle of ψ, then the reflection coefficient $\Gamma(\psi)$ can be written as the following.

$$\Gamma(\psi) = \frac{E_r e^{j\theta_r}}{E_i e^{j\theta_i}} \tag{B.1}$$

The subscripts *r* and *i* stand for reflected and incident respectively. Γ is not only a function of grazing angle but of the permittivity and conductivity of the reflecting medium. Knowing this and using H, V, and RHC to indicate horizontal, vertical, and right-hand-circular polarization respectively, the reflection coefficients can be given by the following expressions which are consistent with many texts on electromagnetics such, as [3], [21], or [24].

$$\Gamma_H(\psi) = \frac{\sin\psi - \sqrt{\varepsilon_r - j60\lambda\sigma - \cos^2\psi}}{\sin\psi + \sqrt{\varepsilon - j60\lambda\sigma - \cos^2\psi}} \tag{B.2}$$

$$\Gamma_V(\psi) = \frac{(\varepsilon_r - j60\lambda\sigma)\sin\psi - \sqrt{\varepsilon_r - j60\lambda\sigma - \cos^2\psi}}{(\varepsilon_r - j60\lambda\sigma)\sin\psi + \sqrt{\varepsilon_r - j60\lambda\sigma - \cos^2\psi}} \tag{B.3}$$

$$\Gamma_{RHC}(\psi) = \frac{\Gamma_H(\psi) + \Gamma_V(\psi)}{2} \tag{B.4}$$

where

ε_r is the relative di-electric constant of the surface,

σ is the surface conductivity in mho/m,

λ is the carrier wavelength (0.2m at L-Band), and

ψ is the surface grazing angle.

Appropriate values of σ and ε_r for L-Band calculations over sea water are σ=4mho/m and ε_r=80 [1]. For first year sea ice these values change to σ=0.02 mho/m and ε_r=3.48.

Appendix C

Numerical Methods and Approximations

For the purpose of providing some sense of validity it is necessary to give a brief overview of some of the techniques used in the numerical modelling of the multipath process. In this appendix some of the methods of integration, as well as approximations that were made to simplify the computing requirements, are described.

C.1 Numerical Integration

The stochastic maritime multipath model involves the evaluation of several complicated integrals. In some cases, these integrals involve several nested integrals and are so complex that the only way to solve them is through numerical methods. The method chosen for this study was a *Simpson's 3/8 Rule Algorithm* [16].

Examples of the complex integrations involved in the multipath model include the integrals that provide values for the mean and effective radius of curvature terms. These integrals depend on conditional forms of the Gaussian density function. Since the integrands in these cases take a form similar to a Gaussian distribution, it can be assumed that their values trail off to zero over a relatively short length. In these expressions, the integral is performed with respect to either the ocean surface height z_s, its derivative z_s', or its second derivative z_s''. In most cases, integration limits from $-6\sigma_z$ to $6\sigma_z$ seemed to be sufficient, where σ_z is the RMS deviation in surface waveheight. Likewise for integrals with respect to z_s' and z_s'', limits of $-6\sigma_{z'}$ to $6\sigma_{z'}$ and $-6\sigma_{z''}$ to $6\sigma_{z''}$ respectively seemed to provide an adequate range. Values of the integrand evaluated outside of these limits were very small and not considered to make a significant contribution to the integral. Integration panel size was determined by dividing the integration range into 32 equally spaced intervals. Decreasing the interval length (or increasing the number of integration panels) beyond this did not lead to a significant improvement. Increasing the number of panels too much leads to the risk of round off errors. Therefore, using 32 intervals was deemed appropriate for these integrals.

For the average scatter power calculation the power density function, $S(\beta)$, is integrated over a range of β_{MIN} to β_{MAX} as shown in Section 3.1.2. From the power density curves of Section 3.5.3 it is seen that the majority of the scatter power comes

from the low reflection angle region. Therefore, the integration of the power density curve is divided into two portions, from β_{MIN} to $\beta_{MAX}/10$ and from $\beta_{MAX}/10$ to β_{MAX}. This allows the use of smaller integration panels in the low reflection angle region and somewhat larger ones in the less sensitive higher reflection angle region.

C.2 Determination of $E\{R(\beta_l,E_l)\}$ Using Interpolation

Because of the number of nested integrations involved in calculating the expected value of the effective radius of curvature term $E\{R(\beta_l,E_l)\}$, the execution time required is quite long even on faster machines. The desired simulation time for the current multipath model was to be relatively short. Therefore, an *initialization run* was included into the model code. After all parameters are put into the model, an initialization routine is called which calculates several values of the $E\{R(\beta_l,E_l)\}$ term and indexes them according to the slope at a specular point m(x) as given by (3.12). These values will then be used as a standardized curve of m(x) versus $E\{R(\beta_l,E_l)\}$. During the simulation, the value of $E\{R(\beta_l,E_l)\}$ at a particular reflection angle with corresponding surface slope m(x) is determined through linear interpolation of the standardized curve constructed during the initialization run. This provided a significant improvement in execution time with minimal loss of accuracy. Figures C-1 to C-8 show the difference between calculating scattered signal power with and

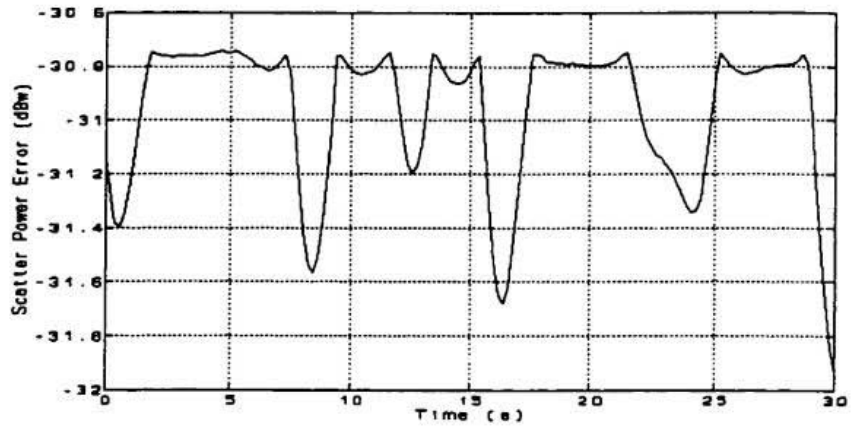

Figure C-2: Error Between Calculations With and Without Interpolation, ss4(ii), E=5°, z_0=20m.

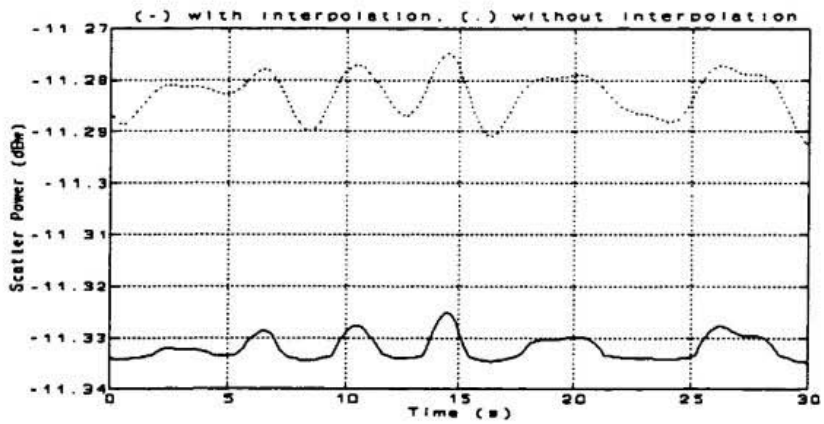

Figure C-3: Difference in Received Scatter Power for Calculations With and Without Interpolation. ss4(ii), E=15°, z_0=20m.

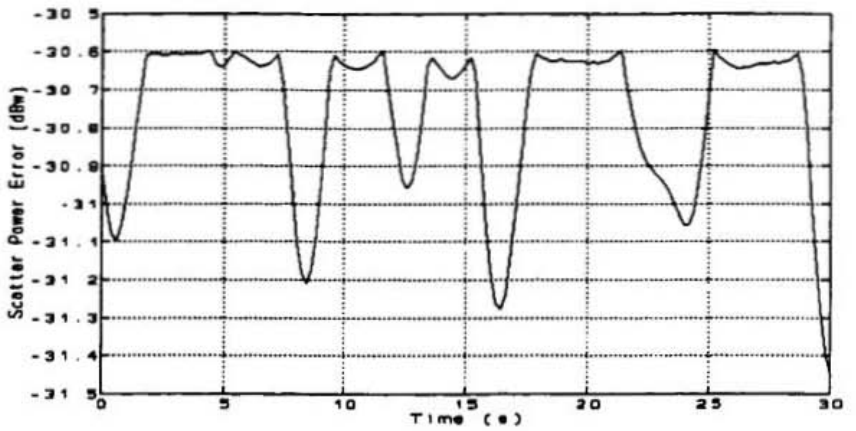

Figure C-4: Error Between Calculations With and Without Interpolation, ss4(ii), E=15°, z_o=20m.

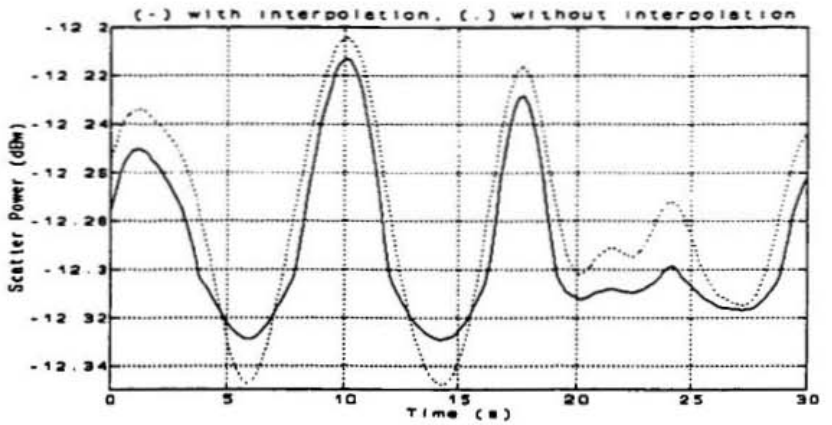

Figure C-5: Difference in Received Scatter Power for Calculations With and Without Interpolation. ss6(ii), E=5°, z_o=20m.

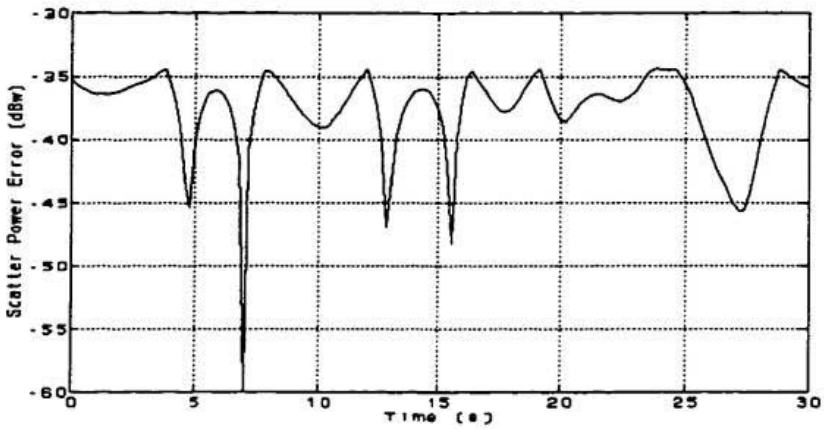

Figure C-6: Error Between Calculations With and Without Interpolation, ss6(ii), E=5°, z_0=20m.

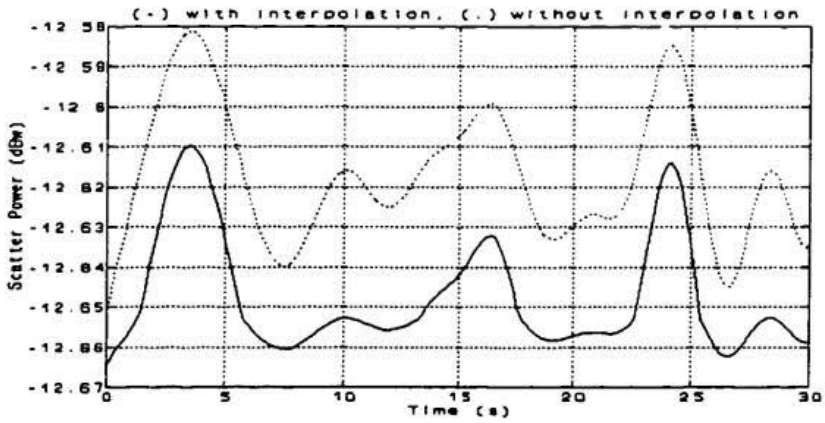

Figure C-7: Difference in Received Scatter Power for Calculations With and Without Interpolation. ss6(ii), E=15°, z_0=20m.

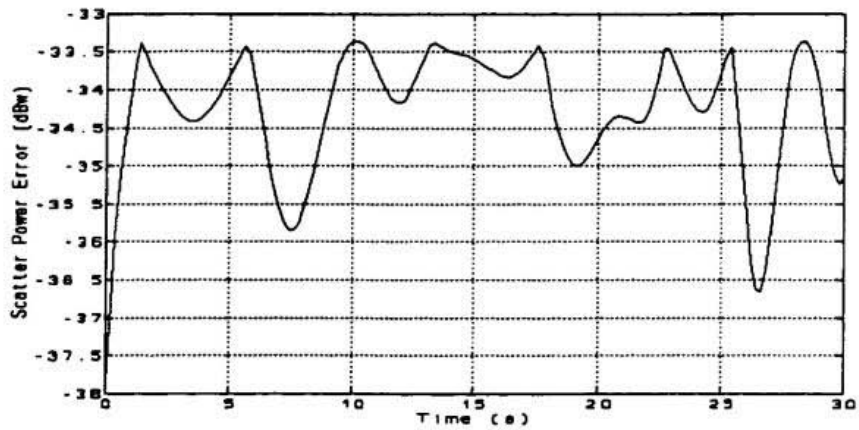

Figure C-8: Error Between Calculations With and Without Interpolation, ss6(ii), E=15°, z_o=20m.

From the above figures it can be seen that the difference between the received power calculated with interpolation and that which is calculated without interpolation is in the range of -30dB or less. This seems like a small enough error to justify the interpolation process.

C.3 The Error Function

The error function and the complimentary error function, as given in the following equations, occur quite frequently in the modelling process.

$$erf(x) = \frac{2}{\sqrt{\pi}}\int_0^x e^{-t^2}dt \tag{C.1}$$

$$erfc(x) = 1-erf(x) = \frac{2}{\sqrt{\pi}}\int_x^\infty e^{-t^2}dt \tag{C.2}$$

Rather than performing the necessary integration each time the error function is used, an algorithm that approximates this function has been utilized. This algorithm is similar to the one outlined in Chapter 40 of [19]. This proved to be an invaluable addition to the model. Since the error function presents itself in many areas of communication theory, the algorithm used is reproduced here in C code.

```
double ERF(double x, double c)
/************************************************
Routine to determine value of:  erf(x)  if c=0
                                erfc(x) if c=1
Value is returned in variable f
************************************************/
{
        double j, f, abx;
        abx = fabs(x);

// Small argument approximation

        if (abx < 0.1 & c== 0.0)
        {
                f = 3.372*x/(3.0+x*x);
        }

// Large argument approximation

        if (x >= 2.7 & c == 1.0)
        {
                f = 1.132*x*exp(-(x*x))/(2.0*x*x+1.0);
        }

// Standard approximations for erf(x), erfc(x)

        else if (abx > 1.5)
        {
                c = c*abx/x;
                j = 3.0+floor(32.0/abx);
                f = 0.0;
                while (j > 0.0)
                {
                        f = 1.0/(f*j +1.14142136*x);
                        j = j-1.0;
                }
                f = f*(c*(c+1.0)-1.0)*0.0079788456*exp(-x*x)+(1.0-c);
        }
        else
        {
                j =3.0+floor(9.0*abx);
                f=1.0;
                while (j > 0.0)
                {
                        f = 1.0+f*x*x*(0.5-j)/(j*(0.5+j));
                        j = j-1.0;
                }
                f = c+f*x*(2.0-4.0*c)/1.7724539;
        }
        return f;
}
```

Appendix D

Notes on the Computer Code

The multipath model has been implemented by using *Borland TurboC V3.0* for DOS. In writing the code, care was taken to ensure that it resembled ANSI C as much as possible so that future investigators wishing to improve or build on the present model using a platform other than DOS could do so. This particular programming language and platform was chosen for its ease and speed in program development and debugging. Many of the programming fundamentals and techniques were taken from [20]. This appendix gives a brief explanation of the various routines that were developed to model the multipath process. It is hoped that this explanation will provide a framework for any future researcher that wishes to continue with the investigation of the maritime multipath process. The code written does not provide a method to perform in-depth analyses. In most cases it creates data files that can be easily imported into various graphical or mathematical analysis packages such as *Matlab*. The code was broken down into the following routines.

MAIN: This routine allows the user to enter all applicable sea, antenna, and vessel parameters. It also calls all other routines that provide portions of the power density curve. It calculates the signal-to-noise ratio at various time instants as well as averages several power spectra of the multipath signal to obtain an estimate of fade duration. It saves all values of signal power, antenna height and orientation, and direct signal power into disk files that can be analyzed through various data analysis packages. The author used Matlab for most of the graphs presented in this document.

INITRUN(β, E, m(x)): This routine performs an initialization run to calculate values of the computationally demanding and time consuming $E\{R(\beta_l,E_l)\}$ term used in the power density calculation. It calculates these values over a wide range of specular point surface slopes. At each update in time of the simulation run, the value of $E\{R(\beta_l,E_l)\}$ is calculated by linear interpolation using the values obtained in the initialization run. To calculate these values *INITRUN* calls the following routines.

> **BLOCSHAD(β_l, E_l, m(x))**: This calculates the blocking and shadowing weighting factors at a particular specular point characterized by slope m(x).
>
> **MRC(β ,E ,m(x))**: This calculates the mean radius of curvature term (M_{RC}) that is used in the divergence attenuation divergence weight.

MOTION(x, t): Uses the superposition of randomly phased sinusoids method to simulate a Gaussian sea surface in order to calculate the ship mounted antenna's position (x_a,z_a) and orientation (θ_{ss}) for a particular time instant.

DBLOCK(x_a, z_a, t, E): If the receiving antenna height falls below twice the RMS surface waveheight, this routine checks to see if the direct path signal is blocked.

DELSPEC(β): Calculates the number of specular points $\lambda(\beta)$, in a particular reflection angle region.

ATERM(β, polarization flag, antenna flag): This routine calculates the polarization dependant term $|a(\beta)|^2$, which takes into account the antenna gain and polarization as well as the surface reflection coefficients. It uses the following routines to achieve this.

> **RCOEFF(β, E, polarization flag)**: calculates the value of reflection coefficients of the sea surface for the incident angle present at a particular scattering point.
>
> **ANTENNA(β, θ_{ss})**: Calculates the gain for the antenna chosen by the user. At present the user has a choice of the four antennas described in Chapter 4.

LININT(m(x)): Determines an approximation for the effective radius of curvature term using values obtained in the *INITRUN* routine.

DIRECT(θ_{ss}, E): Calculates the direct path signal power using the antenna orientation and elevation angle. This makes use of the *ANTENNA* routine as well.

SIMPSON(f(values), number of integration panels, width of panels): Performs a *Simpson's 3/8 Rule* numerical integration on a function by using values of the function in an array. Similar to the algorithm presented in Chapter 4 of [16].

ERF(x, flag): Calculates the value of either the error function erf(x) (flag=0), or the complimentary error function erfc(x) (flag=1). This uses an algorithm similar to the one presented in Chapter 40 of [19].

FADE(S(f), p%): Computes average fade occurance intervals, fade durations, and fade depths for a given p% availability.

Appendix E

Antenna Patterns

The multipath model provides a choice of four antenna patterns. These are an omnidirectional reference antenna, a conical spiral antenna that was implemented in [13] and referred to by the mnemonic *DFVLRC3*, a small backfire antenna, also from [13], referred to as *DFVLRC5*, and a 5-ring adaptive array antenna used in the measurements conducted in [12] which we shall refer to as *CCMCAA*. The latter three of these antennas are described in the following sections.

E.1 DFVLRC3 Antenna

The conical spiral antenna from [13] was modelled by use of the following equation.

$$G(\theta) = \sqrt{\frac{\sin\theta}{\theta}} \left\{ \left(\sin^2\theta + \frac{\cos^2\theta}{6} \right)^2 + \left(\frac{\sin^2\theta}{2} + \cos^2\theta \right)^2 \right\} \qquad \text{(E.1)}$$

Figure E-1 shows the gain pattern achieved by using (E.1) compared to the actual pattern that is reproduce in [1]. The maximum gain has been normalized to unity and

θ is with respect to the vertical axis.

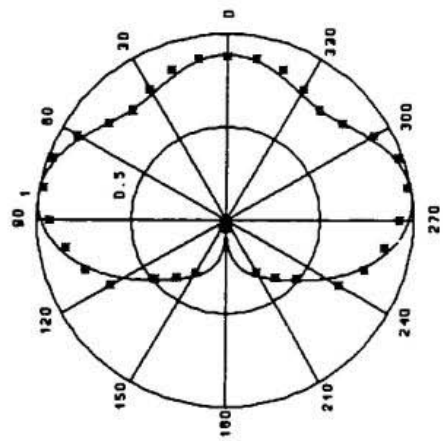

Figure E-1: DFVLRC3 Antenna Pattern, (-) from (E.1), (*) from gain plot in [1].

E.2 DFVLRC5 Antenna

The small backfire antenna from [13] was modelled using the following equation.

$$G(\theta) = \left(\frac{\sin\theta}{\theta}\right)^{1.7} \tag{E.2}$$

Figure E.2 presents the gain pattern obtained by using (E.2) compared to values taken from the actual antenna pattern plot presented in [1]. The maximum gain is

normalized to unity and θ is with respect to the vertical axis.

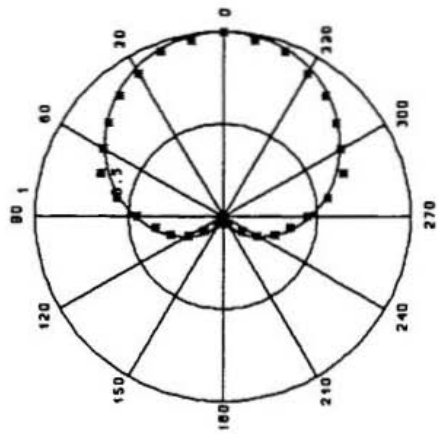

Figure E-2: DFVLRC5 Antenna Pattern, (-) from (E.2), (*) from gain plot in [1].

E.3 CCMCAA Antenna

The 5-ring adaptive antenna array from [12] can be accurately modelled by the following equation.

$$G(\theta) = 21.88\left(10^{-0.00058(\theta-37.88)^2}\right) \tag{E.3}$$

It is pointed out in [12] that (E.3) is only accurate between elevations of 5° and 35°. The validity of this equation for small negative angles of arrival of the multipath

signal may be questionable when it is incorporated into the current model. By using (E.3) the following pattern is realized. Again, the maximum gain has been normalized to unity and unlike the first two antennas, θ is with respect to the horizontal.

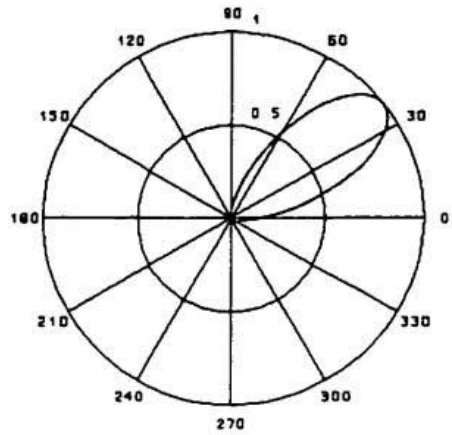

Figure E-3: CCMCAA Antenna Pattern.

E.4 Polarization and Antenna Ellipticity

The antenna patterns given in this appendix assume perfect right-hand-circular (RHC) polarization. In order to incorporate the effects of the surface reflection coefficients, it is necessary to divide the antenna gain into horizontal (H) and vertical (V) polarization components. To do this, it is assumed that the horizontal and vertical polarization are equal and add to give the RHC polarization as follows.

$$G_{RHC} = \frac{G_H + E_R e^{j\theta_m} G_V}{2} \tag{E.4}$$

$$E_R e^{j\theta_m} = \frac{E_V e^{j\theta_V}}{E_H e^{j\theta_H}} \tag{E.5}$$

$E_H e^{j\theta_H}$ is the horizontally polarized field incident upon the antenna and $E_V e^{j\theta_V}$ is the vertically polarized field. The $E_R e^{j\theta_m}$ term is called the polarization ratio of the antenna. This takes into account the ellipticity of the antenna polarization. Most real antennas are not perfectly circularly polarized, but rather elliptically polarized to some degree, depending on the polarization ratio. In the model, E_R is referred to as the gain mismatch of the antenna, and θ_m is the phase mismatch. A detailed discussion of antenna elipticity is presented in Chapter 12 of [21] as well as Appendix D of [1], which follows much the same analysis as [21].

Appendix F

Fade Characteristics

The average signal fade occurrence interval, $\bar{T}_{[p\%}$, as depicted in Figure F-2, can be found by using the power spectrum of the multipath signal. This is accomplished by utilizing the theory presented in Section 14-4 of [23]. In order to use this approach, it is assumed that the changing amplitude of the received signal is a Gaussian process. It is often considered that the variation in received signal *intensity*, at any time instant, due to maritime multipath scatter has a Rician distribution, but for the purpose of finding the average fade interval in a relatively easy manner, it shall be assumed that a Gaussian distribution gives a close enough approximation. This should be adequate when the multipath contribution to the overall received signal magnitude is overwhelming the direct path component. This assumes that the received signal magnitude has an average of 0dB (or unity) and that in the vicinity of this mean, the signal fluctuation appears almost Gaussian, and that the probability of a negative magnitude occurring (as is the case with a Gaussian distribution) is small enough to be considered nonexistent.

Finding the average fade occurrence interval is analogous to finding the average distance between two downward zero-crossings of a zero-mean Gaussian random process. How this is achieved is explained in the following section and the way in which this is applied to finding the signal fade occurrence interval is presented in Section F.2. Section F.3 deals with the estimation of fade depth.

F.1 Average Distance Between Zero-Crossings

Using Figure F-1 as a reference, where X(t) is a zero-mean Gaussian random process, our objective is to find the average distance between two consecutive downward zero-crossings (or alternatively, up-crossings, but since we defined the fade occurrence interval to start and stop on down-crossings in Section 3.6, we shall concern ourselves with down-crossings here as well). In order for this to be linked to fade intervals, we shall refer to the distance between two consecutive down-crossings as $\bar{T}_{I0}$. From Figure F-1, it can be seen that $\bar{T}_{I0}$ is the average interval between downward crossings over a large number of down-crossing interval, T_{I01}, T_{I02},...T_{I0N}. Likewise, $\bar{T}_{D0}$ is the average over a large number of fade durations (*i.e.* durations which the process is beneath its mean value of zero) T_{D01}, T_{D02},...T_{D0N}. Ideally $\bar{T}_{I0}$ and $\bar{T}_{D0}$ would represent averages over the entire process X(t).

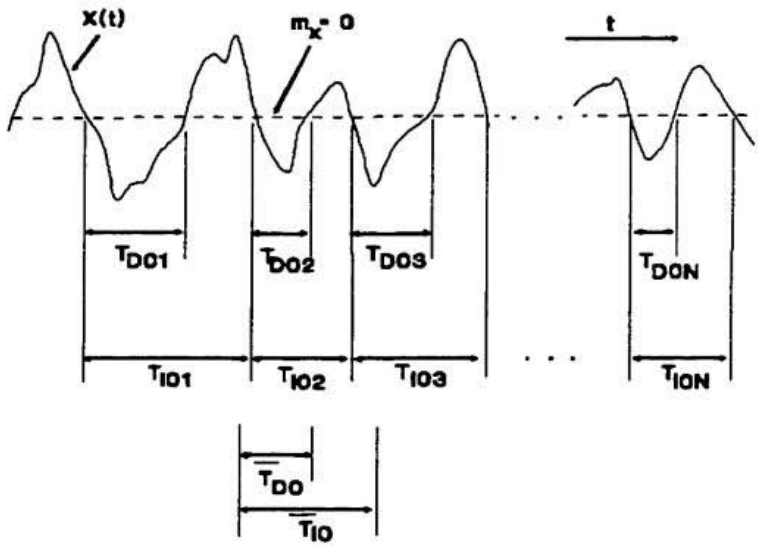

Figure F-1: Definition of the Average Interval Between Zero-Crossings.

In [23] it is shown that the points where a zero-mean Gaussian random process crosses zero forms a Poisson process. With such a process, the probability of having one zero-crossing in a small interval τ is simply the product of the length of the interval and the Poisson parameter λ, which is known as the *density* of zero-crossings. For the zero-crossings of a zero-mean gaussian random process with a power spectrum S(f), λ is given by the (F.1).

$$\lambda = \sqrt{\frac{\int_0^{\infty} f^2 S(f)\, df}{\int_0^{\infty} S(f)\, df}} \qquad \text{(F.1)}$$

Using (F.1), the probability that only one zero-crossing occurs within the small interval τ is given by (F.2).

$$P_{10}(\tau) = \lambda\tau \qquad \text{(F.2)}$$

The objective is to find a length τ that *guarantees* (on average) one zero crossing occurring within that length. From Figure F-1, it can be seen that this length could be approximated by the average distance between two consecutive down-crossings. If such an interval represents the average length between consecutive down-crossings, then in all probability there is an up-crossing in between. Since in all likelihood there is a zero-crossing within this interval, the probability that one zero-crossing occurred can be considered to be almost one (*i.e.* almost 100%). If we refer to this interval as $\bar{T}_{10}$, then by using (F.1) and (F.2), we can write the following expression.

$$\bar{T}_{I0} = \frac{1}{\lambda} = \sqrt{\frac{\int_0^{\infty} S(f)\,df}{\int_0^{\infty} f^2 S(f)\,df}} \qquad \text{(F.3)}$$

Since X(t) is a zero-mean Gaussian random process, it can be safely assumed that 50% of the time X(t) is above zero and 50% of the time it is below zero. Because of this, we can assume that, on average, in the interval between two consecutive downward zero-crossings X(t) is above zero half the time and below zero for the other half. Therefore, we can define an expression $\bar{T}_{D0}$ that represents the average amount of time between the point where X(t) falls below zero to the point where it rises above zero (or the distance between a down-crossing and an adjacent up-crossing). This is analogous to the fade duration, T_D, of Section 3.6. $\bar{T}_{D0}$ is given by (F.4).

$$\bar{T}_{D0} = (1-0.5)\,\bar{T}_{I0} \qquad \text{(F.4)}$$

For the purposes of multipath fading, it will become clear that it is important to find

the average distance between consecutive downward crossings of any arbitrary level and not just for zero. From [23], the probability that a zero-mean Gaussian random process with variance σ^2 crosses some arbitrary level ξ only once in a small interval τ is given by (F.5).

$$P_{1\xi}(\tau) = \lambda\tau e^{-\frac{\xi^2}{2\sigma^2}} = P_{10}(\tau)\, e^{-\frac{\xi^2}{2\sigma^2}} \tag{F.5}$$

For the time being, we are not as concerned with the actual value of ξ as we are with the percentage of time that, on average, X(t) spends above ξ. The actual value of ξ corresponds to the fade depth which is dealt with in Section F.3. For simplification, to specify ξ we shall consider X(t) to possess a standard normal distribution (zero-mean, standard deviation of one). If we define $\xi(p)$ to be the value which X(t) is above, on average, for p percent of the time, then using (F.3) and (F.5) we can write the following expression for the average distance between two consecutive down-crossings of an arbitrary level ξ by a zero-mean Gaussian random process X(t) having a power spectrum S(f).

$$\overline{T}_{Ip\%} = \sqrt{\frac{\int_0^\infty S(f)\, df}{\int_0^\infty f^2 S(f)\, df}}\; e^{\frac{1}{2}\xi^2(p)} \tag{F.6}$$

The value of ξ corresponding to a given p% can be found by extracting values from tables for the standard normal distribution such as those presented in [25]. This involves finding the value of ξ for which the area under the standard normal curve between that value and infinity is p. For example, for a p of 99% ξ is -2.33, for p equal to 99.9% it would be -3.08, and for a p of 99.99% ξ is -3.49. As with the zero-crossing case, if we assume that during the average distance between down-crossings X(t) is, on average, above the threshold value ξ for p% of the time and below this level for the remaining (100-p)% of the time, the average time between when X(t) drops below ξ to when it rises above ξ can be found by using (F.7).

$$\overline{T}_{Dp\%} = \left(1-\frac{p}{100}\right)\overline{T}_{Ip\%} \qquad \text{(F.7)}$$

F.2 Fade Occurrence Interval and Duration

It is possible to apply the theory of the preceding section to the multipath interference phenomenon in order to find average fade occurrence intervals and durations of the received signal. In Figure F-2 we define X(t) to be the received signal intensity, which again is assumed to have a Gaussian distribution. We define a fade depth,

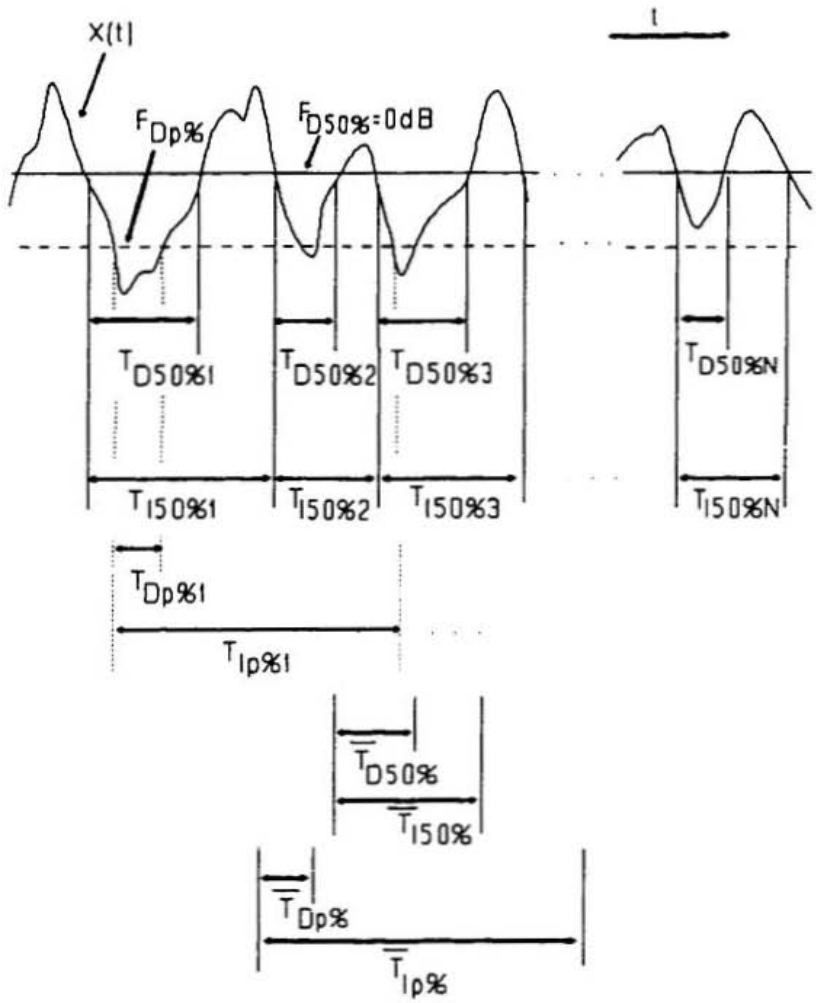

Figure F-2: Signal Fade Characteristics.

$F_{Dp\%}$, to be a value for which the received signal is above for p% of the time and which it is below for the remaining (100-p)% of the time. This corresponds to $\xi(p)$ of the previous section.

For the random signal X(t) shown in Figure F-2, $F_{D50\%}$ is a level for which X(t) is above for 50% of the time (on average). Since X(t) is assumed to be stationary, $F_{D50\%}$ is the mean of X(t). For our purposes, we shall consider this to be 0dB, or the power of the direct path signal, since we can normalize the fading process with respect to the direct path signal. This assumes that the multipath interference adds constructively to the direct path signal for 50% of the time (on average) and destructively for the remaining 50% of the time. If we define the length of time between when X(t) drops below $F_{D50\%}$ and the next point in time where it goes below this value to be a fade interval, then by finding the average distance between two consecutive downward *mean-crossings* (unlike Section F.1, X(t) may not have a zero-mean and therefore we are concerned with where X(t) crosses its mean value which is assumed to be constant at 0db over time as we have normalized the process with respect to the direct path power), we will obtain a value for the average fade occurrence interval $\bar{T}_{I50\%}$. This would correspond to a 50% availability system. This means that system designers would be satisfied with ensuring a detectible signal for only 50% of the time.

To find the average fade occurrence interval for the 50% availability case, we can use the same reasoning that was applied to the zero-crossing case of Section F.1. If S(f) represents the power (or Doppler) spectrum of X(t) (or more specifically, the Doppler spectrum of the multipath signal), then the average fade occurrence interval, $\bar{T}_{I50\%}$, can be given by the following.

$$\overline{T}_{I50\%} = \sqrt{\frac{\int_0^{\infty} S(f)\,df}{\int_0^{\infty} f^2 S(f)\,df}} \tag{F.8}$$

By using similar reasoning to that which was used for the zero-mean case, we can find the average amount of time between when the received signal level drops below the threshold value of $F_{D50\%}$ and when it rises above this value. This is useful to know as it helps predict the amount of time that the signal will be lost during a fade. Referring to this interval as the average fade duration, we can write the following.

$$\overline{T}_{D50\%} = (1-0.5)\,\overline{T}_{I50\%} \tag{F.9}$$

For most practical systems, it is desirable to be able to expect that the received signal is detectable for much more than 50% of the time. Common percentages include 99%, 99.9%, and 99.99% availability. $F_{Dp\%}$ can be defined as the threshold level for

which X(t) can be expected to be above for p% of the time, and below for the remaining (100-p)% of the time, as shown in Figure F-2. For the time being we are not concerned with the actual value of $F_{Dp\%}$. All we know is that for p% of the time, on average, the received signal is above this threshold. Knowing this we can use the same reasoning as (F.6) to find the p% availability (or alternatively the (100-p)% outage) fade interval $\bar{T}_{Ip\%}$.

$$\bar{T}_{Ip\%} = \sqrt{\frac{\int_0^{\infty} S(f)\,df}{\int_0^{\infty} f^2 S(f)\,df}}\; e^{-\frac{1}{2}\xi^2(p)} \qquad \text{(F.10)}$$

$\xi(p)$ is the value for which the area under the standard normal distribution curve from ξ to infinity is p/100. We can use the standard normal curve (even though the received signal will not have a standard normal distribution) due to the fact that, at this point, we are not as concerned with the actual value of ξ as we are with the amount of time the signal spends above this value. By finding the variance of the multipath signal σ_m^2, one could find a value of ξ, say ξ_1, that corresponds to actual distribution of X(t) and replace $\xi^2(p)$ with $\xi_1^2(p)/\sigma_m^2$ in (F.10), but this will lead to the same result. To determine a fade depth value, the variance will have to be incorporated. This is discussed in the Section F.3.

By assuming that during a fade interval, the signal level is above $F_{Dp\%}$ for p% of the time (on average) and below this for the remaining time, then the average fade duration can be calculated from the following.

$$\overline{T}_{Dp\%} = (1-\frac{p}{100})\overline{T}_{Ip\%} \qquad \text{(F.11)}$$

Finding these values is of great importance to system designers as it gives an estimate of how long the received signal may be lost and how often outages may occur. If one has knowledge of this, then appropriate steps can be taken to incorporate appropriate gains into the system that will ensure that the received signal will be detectable for a given percentage of time. Alternatively, if one has access to a receiving system with a particular gain, then the reliability of that system can be estimated by taking the available gain and determining the average fade duration and the expected interval between these instances when the signal is lost.

F.3 Fade Depth

In the previous section, the variation of the received signal intensity was assumed to be a Gaussian distribution. This is not entirely accurate. This assumption was made so that average fade durations and fade intervals could be calculated in a relatively

straightforward manner. Even though this assumption is maintained here so that we can calculate the fade depth $F_{Dp\%}$ (as shown in Figure F-2), it is worth mentioning that in reality, as seen in much of the literature such as [6], [10], [26], and [27], the variation in the received signal level due to multipath interference is said to be a Rician distribution, or more specifically a *Rice-Nakagami* distribution. The next section provides a brief explanation as to why this is the case and in Section F.3.2, we return to the assumption that the received signal intensity is a Gaussian distribution so that we may calculate the fade depth.

F.3.1 Actual Rician Distribution for Fade Depth

For the purposes of this investigation we have considered only an unmodulated L-Band carrier signal propagating between a transmitter and a ship-mounted receiver. This signal arrives at the receiver from a direct path as well as numerous scatter paths arising from the ocean surface. The received scattered signal can be considered to be the phasor sum of all of the multipath components as given by (F.12) and (F.13).

$$V_s = Me^{j\Phi_m} \tag{F.12}$$

$$M = \left| \sum_i M_i e^{j\Phi_i} \right| \tag{F.13}$$

M_i and ϕ_i are independent random variables and ϕ_i is uniformly distributed between $\pm\pi$. Therefore, from [26], the envelope M is a Rayleigh distribution defined by the following.

$$f_M(M) = \frac{M}{\sigma_m^2} e^{-\frac{M}{2\sigma_m^2}} \qquad \text{(F.14)}$$

The variance of the scattered signal, normalized with respect to the direct path component, is given by σ_m^2. This can be approximated by the following equation where P_m and P_D represent the power of the multipath signal and the power of the direct path signal respectively.

$$\sigma_m^2 = \frac{1}{2}\left(\frac{P_m}{P_D}\right) \qquad \text{(F.15)}$$

Since the total received signal is comprised of the sum of the scattered component plus the direct path component, it can be written in a normalized form as follows where F_D is used to represent fade depth.

$$V_r = 1 + Me^{j\phi_m} = F_D e^{j\phi_{fd}} \qquad \text{(F.16)}$$

The fade depth F_D will possess the Rice-Nakagami distribution, which follows from [6] and [10]. This distribution is given by (F.17) where $I_0(x)$ is the modified Bessel

function of the first kind.

$$f_{F_D}(F_D) = \frac{F_D}{\sigma_m^2} e^{-\frac{1+F_D^2}{2\sigma_m^2}} I_0\left(\frac{F_D}{\sigma_m^2}\right) \qquad \text{(F.17)}$$

F.3.2 Gaussian Approximation for Fade Depth

For the purpose of calculating signal fade durations and fade intervals, the assumption was made that the received signal intensity is a Gaussian distribution. In the previous section, it was shown that in reality, the received signal distribution is Rician. However, we shall assume that it is close enough to a normal distribution so that we can continue to assert the Gaussian approximation.

To calculate a value for fade depth, the variance of the received signal is needed. It is desired to normalize the variance with respect to the direct path power. As was seen in the previous section, the normalized variance of the multipath signal can be given by the (F.18) where P_m and P_D represent the average power of the multipath scatter signal and the average power of the direct path signal respectively.

$$\sigma_m^2 = \frac{1}{2}\left(\frac{P_m}{P_D}\right) \qquad \text{(F.18)}$$

By normalizing all values with respect to the direct path signal level, it can be assumed that the average normalized received signal power is unity or 0dB. This would mean that the multipath interference adds destructively to the direct path signal as much as it does constructively. Using this, and the normalized variance of (F.18), the fade depth (in dB) can be found from the following relation.

$$F_{Dpt} = 10\log_{10}[\xi(p)\,\sigma_m + 1] \qquad \text{(F.19)}$$

The value of $\xi(p)$ corresponds to the value for which the area under the standard normal distribution curve between ξ and infinity is p/100. As was seen in the previous sections, typical values for $\xi(p)$ are -2.33 for a p of 99%, -1.645 for a p of 90%, and 2.33 for a p of 1%.